



Barry, Roxanna G. (2020) *Discrete-to-continuum modelling of cells to tissues*. PhD thesis.

<http://theses.gla.ac.uk/81616/>

Copyright and moral rights for this work are retained by the author

A copy can be downloaded for personal non-commercial research or study, without prior permission or charge

This work cannot be reproduced or quoted extensively from without first obtaining permission in writing from the author

The content must not be changed in any way or sold commercially in any format or medium without the formal permission of the author

When referring to this work, full bibliographic details including the author, title, awarding institution and date of the thesis must be given

Enlighten: Theses

<https://theses.gla.ac.uk/>
research-enlighten@glasgow.ac.uk

Discrete-to-Continuum Modelling of Cells to Tissues

Roxanna G Barry

Submitted in fulfilment of the requirements for the
Degree of Doctor of Philosophy

School of Mathematics and Statistics
College of Science and Engineering
University of Glasgow



University
of Glasgow

August 2020

Abstract Constitutive models for the mechanics of soft tissues are typically constructed by fitting phenomenological models to *in vitro* experimental measurements. However, a significant challenge is to construct macroscale soft tissue models which directly encode the properties of the constituent cells and their extracellular matrix in a rational manner. In this work we present a general framework to derive multiscale soft tissue models which incorporate the properties of individual cells without necessarily assuming homogeneity or periodicity at the cell level. The aim of this thesis is to derive a new model for cardiac soft tissue which we approach by forming an individual based model. First, we consider a reduced viscoelastic model for each individual cell and couple this to a network description of a one-dimensional line of cells. We utilise a discrete-to-continuum approach to upscale this array to form new (nonlinear) continuum partial-differential equation (PDE) models for the tissue which allows for gradients in the cell properties along the line. This system is implemented for a test problem inducing a prescribed displacement at one end of the array (while remaining fixed at the other) for both uniform and non-uniform stiffness of cells. A cluster of stiffer cells in the centre of the domain (mimicking a cluster of dead cells in myocardium after an infarction) is investigated and results show that the majority of the deformation is taken on by the more flexible cells while the stiff cells undergo a minimal deformation. We extend this model to include the effects of active contraction, to simulate myocardium behaviour in a periodic domain and we observe a travelling wave of contraction moving through the domain. For all formulations, the discrete and continuum results agree well. For the test problem, these systems also agree well with analytical results of the linearised continuum PDE.

We further extend this model to incorporate cell growth and proliferation to consider the dynamics of a proliferating array, examining how assumptions about cell dissipation translate into different global behaviour. Utilising the theory of morphoelasticity, we introduce cell growth into the system by multiplicative decomposition of the deformation tensor for each cell into an unstressed growth phase and an elastic deformation phase. We investigate stress-driven growth, where a cell grows fastest when it is unstressed and the growth rate reduces under compression (the set up does not allow the cells to be in tension). In order to assess the effect of cell dissipation on the system, we compare two cases: first, that the dissipation is independent of cell surface area; and second, that the dissipation coefficient is linearly proportional to the current cell surface area. We observe that in the latter case, cells pay an extra penalty for enlarging and overall growth of the array is decreased. We further consider cell proliferation in this system, with cells dividing when they reach double their initial size. In this case we can predict changes in the number of cells with time showing that the growth eventually attains a constant rate. Substrate dissipation results in division events becoming localised to the free end of the domain, replicating the behaviour of a proliferating rim. We also observe that cell proliferation generally leads to slower growth of the array (except in cases with very small substrate dissipation).

We then extend the approach to a two-dimensional rectangular array of cells atop a fixed

substrate and the upper boundary of cells parallel to this is subject to zero stress, again utilizing a discrete-to-continuum approach to form new (nonlinear) two-dimensional continuum PDE models. We specify the general formulation where each cell's deformation must (in general) be solved numerically, and then focus on two simpler cases where the cell deformation is approximated as either a uniaxial deformation or a simple shear. For cells undergoing uniaxial deformation, we consider a time-dependent prescribed deformation along one edge of the rectangular domain (while keeping the edge parallel to this fixed) with two different cases for the boundaries normal to the moving edge. First, we consider zero external stress where the resulting deformation is in all three dimensions and the cell area in contact with the substrate decreases. Second, we consider the two boundaries normal to the moving edge to be periodic. In this case, there is no deformation normal to the periodic boundaries, and the prescribed compression on the array is in the out-of-plane direction alone. For a simple shear deformation, we apply a constant shearing force on one edge of the rectangular array (with the opposite edge held fixed) and periodic boundary conditions on the remaining two edges. In this case, we prohibit motion normal to the periodic boundaries, allowing motion only in the direction of the shearing force. Dissipation in the system results in a transient delay in the transmission of the shearing force to all the cells in the array. Cells closer to the sheared boundary move ahead of those closer to the fixed boundary. In this case we show that this deformation can be solved analytically.

We conclude this thesis with an overview of how the approaches developed within can be extended to produce new models of soft tissue mechanics.

Contents

Declaration	xi
1 Introduction	1
1.1 Soft tissue modelling	1
1.2 Continuum models	3
1.2.1 Skin	5
1.2.2 Arterial tissue	5
1.2.3 Cardiovascular tissues	7
1.3 Individual based models	9
1.3.1 Epithelial Models	10
1.4 Upscaling	11
1.4.1 Homogenisation	12
1.4.2 Mixture theory	12
1.4.3 Volume averaging	13
1.4.4 Discrete to continuum asymptotics	13
1.5 Growth	14
1.6 Structure	16
2 Deformation of a Single Array of Cells	18
2.1 Discrete Model	19
2.1.1 Deformation	20
2.1.2 Incompressibility	20
2.1.3 Rheological Model	21
2.1.4 Elastic Stress	21
2.1.5 Viscous Stress	22
2.1.6 Boundary Conditions	22
2.1.7 Substrate Damping	23
2.1.8 Equations of Motion	23
2.1.9 Global Boundary and Initial Conditions	23
2.1.10 Non-dimensional variables	24

2.1.11	Numerical method	26
2.2	Upscaling to continuum model (Incompressible Cells)	27
2.2.1	Neo-Hookean Material	31
2.2.2	Small Displacements in a Neo-Hookean Material	31
2.2.3	Comparison to macroscale static model for a long thin strip	34
2.2.4	Numerical Solutions	36
2.3	Results (Incompressible Cells)	39
2.3.1	Case 1: Prescribed deformation	39
2.3.2	Case 2: Non-uniform shear modulus	43
2.4	Application to cardiac tissue: active contraction	45
2.4.1	Discrete active contraction model	45
2.4.2	Continuum active contraction model	47
2.4.3	Results for the active contraction model	48
2.5	Summary	48
3	Growth and Proliferation of a Single Array of Cells	51
3.1	Discrete Model (Incompressible Cells)	52
3.1.1	Cell Growth	53
3.1.2	Incompressibility	53
3.1.3	Rheological Model	53
3.1.4	Elastic Stress	54
3.1.5	Viscous Stress	54
3.1.6	Boundary Conditions	55
3.1.7	Cell growth rate	55
3.1.8	Cell Division	56
3.1.9	Governing Equations	56
3.1.10	Global Boundary Conditions	57
3.1.11	Initial Conditions	57
3.1.12	Non-dimensional variables	58
3.1.13	Numerical method	59
3.2	Upscaling to Continuum Model (Incompressible Cells)	60
3.2.1	Neo-Hookean Material	63
3.2.2	Numerical Solutions	64
3.3	Results: Cell growth (Incompressible Cells)	65
3.3.1	Case 1: Stress dependent cell growth (no proliferation)	65
3.3.2	Case 2: Stress dependent cell growth with proliferation	67
3.4	Summary	69

4	Two- and Three-Dimensional Discrete-to-Continuum Models	70
4.1	The model	70
4.1.1	Elastic Deformation	72
4.1.2	Elastic Stress	72
4.1.3	Boundary Conditions	72
4.1.4	Governing Equations	73
4.2	Uniaxial deformation	74
4.2.1	Elastic Deformation	75
4.2.2	Incompressibility	75
4.2.3	Elastic Stress	75
4.2.4	Boundary Conditions	76
4.2.5	Discrete governing equations	77
4.2.6	Initial Conditions	77
4.2.7	Discrete global boundary conditions	78
4.2.8	Non-dimensional variables	79
4.2.9	Upscaling to continuum	81
4.2.10	Small displacements in a neo-Hookean material	84
4.2.11	Numerical method	85
4.2.12	Results Case 1: Free boundary condition along $y = w_0$	86
4.2.13	Results Case 2: Periodic boundary condition	88
4.3	Simple shear deformation	88
4.3.1	Elastic deformation	90
4.3.2	Elastic Stress	91
4.3.3	Boundary Conditions	91
4.3.4	Discrete governing equations	91
4.3.5	Initial Conditions	92
4.3.6	Discrete global boundary conditions	92
4.3.7	Angle of shear	93
4.3.8	Non-dimensional variables	93
4.3.9	Upscaling	94
4.3.10	Analytical Solutions	96
4.3.11	Results: Simple Shear	97
4.4	Summary	98
5	Discussion	100
A	Listing of Matlab Codes	105
A.1	Growth	105

List of Figures

1.1	Tissues are composed of large number of cells packed together. Cells comprise of a nucleus, filament networks (e.g. actin), microtubules and a cellular membrane.	2
1.2	(a) Kelvin-Voigt model (spring and dashpot in parallel); (b) Maxwell model (spring and dashpot in series).	4
1.3	The wall of the heart is constructed from predominantly 3 layers; endocardium (inner), myocardium (middle) and pericardium (outer) (left figure from http://stevegallik.org/sites/histologyolm.stevegallik.org/images/heartwall.gif).	7
1.4	Decomposition of the deformation tensor, \mathbb{F} into growth, \mathbf{G} , and elastic, \mathbf{A} , components.	14
2.1	Force diagram of N viscoelastic incompressible 2D cells aligned end-to-end in a single array. The imposed a fixed boundary at $x = 0$ (to investigate the system in a test problem) is represented as a solid wall at the left hand side of the array. The dissipation due to cells attached to the substrate (in the plane of the page) is represented as a dashpot connected to the initial position of the cell centre (displayed on a dashed line above the array of cells here for clarity). See text for more details.	19
2.2	Local reference coordinate system for cell j .	20
2.3	Force balance across boundary between cells j and $j + 1$, summing the individual forces of cell j on cell $j + 1$ and of cell $j + 1$ on cell j .	23
2.4	Stretch of the N -th cell, $\lambda_1^{(N)}$, at $t = 10$. (a) Solutions for relative tolerance values $r_t = 10^{-8}$ to $r_t = 1$; (b) Solutions for absolute tolerance values $a_t = 10^{-8}$ to $a_t = 1$.	27

- 2.5 Solutions for a system of incompressible Neo-Hookean cells aligned in a single array subject to a prescribed displacement (10% decrease in full array length) with substrate dissipation. Solutions for $N = 100$ cells, $\eta = 0$ and uniform shear modulus $\mu = 1$. Discrete solutions (symbols $*$, $+$, \times and \triangle) are displayed with corresponding upscaled continuum solutions (lines) and analytical solutions (symbols \circ , \square , \diamond). (a) Pressure, $p(x, t)$ in the array at $t = 0, 1, 10, 1000$ with $K = 1$; (b) Elastic stretch, $\lambda_1(x, t)$ in the array at $t = 0, 1, 10, 1000$ with $K = 1$; (c) $\max_x(p)$ at $t = 1$ for $K = 10^{-5}, 1, 10$ (inset: $\max_x(p)$ for $t = 10$ for $K = 10^{-5}$ to $K = 1$); (d) $\min_x(\lambda_1)$, at $t = 1$ for $K = 10^{-5}, 1, 10$ (inset: $\min_x(\lambda_1)$ for $t = 10$ for $K = 10^{-5}$ to $K = 1$). 40
- 2.6 Steady state solutions for a system of incompressible Neo-Hookean cells aligned in a single array subject to a prescribed displacement (10% decrease in full array length) with substrate dissipation ($K = 10^{-5}$). Solutions for $N = 100$ cells ($n = 2000$ continuum nodes) and uniform shear modulus $\mu = 1$. Discrete solutions (symbols) are displayed with corresponding upscaled continuum solutions (line with circles) for $t \gg 1$ and static macroscale model solutions (dash line). The profile in x (discrete, continuum), and χ_0 (static macroscale) is displayed against initial position, x_0 41
- 2.7 Solutions for a system of incompressible Neo-Hookean cells aligned in a single array subject to a prescribed displacement (10% decrease in full array length) with substrate dissipation. Solutions for $N = 100$ cells ($n = 101$ continuum nodes) and uniform shear modulus $\mu = 1$. Discrete solutions (symbols) are displayed with corresponding upscaled continuum solutions (lines) and analytical solutions (shapes). (a) Pressure, $p(x, t)$ in the array at $t = 0, 1, 10, 1000$ with $\eta = 1$; (b) Elastic stretch, $\lambda(x, t)$ in the array at $t = 0, 1, 10, 1000$ with $\eta = 1$; (c) $\max_x(p)$ for $t = 0$ to $t = 3$ at $\eta = 10^{-5}, 1, 10$ (inset: $\max_{x,t}(p)$ for $t = 0$ to $t = 10$ for $\eta = 10^{-5}$ to $\eta = 10$); (d) $\min_x(\lambda)$, for $t = 0$ to $t = 2$ at $\eta = 10^{-5}, 1, 10$ (inset: $\min_{x,t}(\lambda)$ for $t = 0$ to $t = 10$ for $\eta = 10^{-5}$ to $\eta = 10$). 42
- 2.8 Solutions for a system of incompressible Neo-Hookean cells aligned in a single array subject to a prescribed displacement (10% decrease in full array length) with substrate damping in the absence of viscous dissipation ($\eta = 0$). The system is considered with a non-uniform $\mu(x)$ as defined in (2.82). (a) $p(x, t)$ over x at $t = 0, 0.5, 1, 10$ for $K = 1$ (inset with the case for $K = 10^{-5}$); (b) $\lambda(x, t)$ over x at $t = 0, 0.5, 1, 10$ for $K = 1$ (inset with the case for $K = 10^{-5}$); (c) $\max_x(p)$ for $t = 0$ to $t = 10$ for $K = 10^{-5}, 1, 10$; (d) $\min_x(\lambda)$ for $t = 0$ to $t = 10$ for $K = 10^{-5}, 1, 10$ 44

- 2.9 Solutions for a system of incompressible Neo-Hookean cells aligned in a single array subject to a prescribed displacement (10% decrease in full array length) with viscous damping in the absence of substrate damping ($K = 0$). The system is considered with a non-uniform $\mu(x)$ as defined in (2.82). (a) $\max_x(p)$ for $t = 0$ to $t = 3$ for $\eta = 10^{-5}, 1, 10$ (inset with $p(x, t)$ over x at $t = 0, 0.5, 1, 10$ for $\eta = 1$); (b) $\min_x(\lambda)$ for $t = 0$ to $t = 3$ for $\eta = 10^{-5}, 1, 10$ (inset with $\lambda(x, t)$ over x at $t = 0, 0.5, 1, 10$ for $\eta = 1$). 45
- 2.10 Solutions for a system of incompressible neo-Hookean cells aligned in a single array in a periodic domain subject to an active contraction force, defined in (2.83) and (2.84), with $\beta = -1$, $\omega = 1/N$, $t_R^{(i)} = 2\pi x_0^{(i)}/N$. The system is considered with a uniform $\mu = 1$ with substrate damping ($K \in [10^{-5}, 10]$), in the absence of viscous dissipation ($\eta = 0$). Both discrete (symbols) and continuum (lines) systems are displayed. (a) internal cell pressure, p , across the domain, x , for $t = 1, 5, 10$ and $K = 10^{-2}$; (b) cell stretch, λ , across the domain, x , for $t = 1, 5, 10$ and $K = 10^{-2}$; (c) The maximum ($\max_{x,t}(p)$ - peaks) and minimum ($\min_{x,t}(p)$ - troughs) internal cell pressure across the domain during $t = 0$ to $t = 100$ for $K = 10^{-5}$ to $K = 10$; (d) The maximum ($\max_{x,t}(\lambda)$ - peaks) and minimum ($\min_{x,t}(\lambda)$ - troughs) cell stretch across the domain during $t = 0$ to $t = 100$ for $K = 10^{-5}$ to $K = 10$; (e) Profiles at $t = 1, 10, 20$, with colour-bars representing internal cell pressure. 49
- 3.1 Solutions for a system of incompressible Neo-Hookean cells aligned in a single array subject to stress-driven growth. Solutions for $N = 100$ cells and uniform shear modulus $\mu = 1$, $\sigma_0 = 0.1$, with $\kappa = 1$. Discrete solutions (symbols) are displayed with corresponding upscaled continuum solutions (lines). (a) Length of the domain for $K = 10^{-5}, 10^{-3}, 10^{-2}, 10^{-1}, 1, \eta = 0$ for $t = 0$ to $t = 100$ (inset: length of the domain at $t = 100$ for $K = 10^{-5}$ to $K = 1$); (b) Stretch, α , at $t = 10$ for $K = 10^{-5}, 10^{-2}, 1$ and $\eta = 0$ (inset: elastic stretch across the domain at $t = 0, 1, 5, 10$ for $K = 10^{-2}$); (c) Length of array for $t = 0$ to $t = 100$ for $\eta = 1$ and $K = 0, 10^{-2}$ (inset: length of array at $t = 100$ for $\eta = 10^{-5}$ to $\eta = 1$ with $K = 0$ or $K = 10^{-2}$); (d) Stretch, α , at $t = 10$ for $\eta = 0.1, 1, 10$ and $K = 10^{-2}$ (inset: maximum compression in the array, $\min_x(\alpha)$, for $\eta = 0.1, 1, 10$ and $K = 10^{-2}$ for $t = 0$ to $t = 20$). 66

3.2 Solutions for a system of incompressible Neo-Hookean cells aligned in a single array subject to stress-driven growth. Solutions for $N = 100$ cells ($n = 101$ continuum nodes) and uniform shear modulus $\mu = 1$ with $\kappa = A(t)$. Discrete solutions ($*$, $+$, \times , \circ) are displayed with corresponding upscaled continuum solutions (solid lines) and discrete (\cdot , \square , \triangleright , \star) and continuum (dash lines) solutions for comparison with $\kappa = 1$. System in the absence of viscous dissipation ($\eta = 0$): (a) Length of the domain for $K = 10^{-5}, 10^{-3}, 10^{-2}, 1$, $\eta = 0$ for $t = 0$ to $t = 100$; (b) Stretch at $t = 0$ for $K = 10^{-5}, 10^{-2}$ and $\eta = 0$ 67

3.3 Solutions for a discrete system of incompressible Neo-Hookean cells aligned in a single array subject to stress-driven growth with substrate dissipation and cell division at $A^{(j)} = 2$. Solutions for $N_0 = 100$ cells and uniform shear modulus $\mu = 1$. (a) Domain length, $L(t)$, against t on a log-log scale for cases with and without proliferation, for $\kappa = 1$ and $\kappa = A(t)$ (inset: the number of cells, N , on a log-log scale for $\kappa = 1$) for $K = 10^{-5}$ for $t = 0$ to $t = 18$; (b) Domain length, $L(t)$, against t on a log-log scale for cases with and without proliferation, for $\kappa = 1$ and $\kappa = A(t)$ (inset: the number of cells, N , on a log-log scale for $\kappa = 1$) for $K = 10^{-2}$ for $t = 0$ to $t = 1000$; (c) Division event location, x_d , relative to current domain length, $L(t)$ for $m = 0$ and $K = 10^{-5}$ for $t = 0$ to $t = 18$; (d) Division event location, x_d , relative to current domain length, $L(t)$ for $m = 0$ and $K = 10^{-2}$ for $t = 0$ to $t = 1000$ 68

4.1 Geometrical set up of a quasi-three dimensional sheet of discrete cells. (a) three-dimensional rectangular cells; (b) vertex-model set up for four-sided cells in the (x,y) plane. 71

4.2 Geometrical set up of M rows of N elastic cells aligned end to end. 74

4.3 Solutions for a discrete system of incompressible Neo-Hookean cells aligned in a two-dimensional array subject to a prescribed displacement at $x = l_0$. Solutions for $N = 10$, $M = 10$, cells and uniform shear modulus $\mu = 1$. (a) The array, with fill-colour representing the internal cell pressure, is displayed for $t = 1, 2, 5, 100$ for $k_1 = 0.1$, $K = 1$ and $\kappa = A$; (b) The maximum pressure in the array, $\max_{x,y}(p)$ for $K = 1$ and $k_1 = 0.01, 0.05, 0.1$ for both dissipative systems, $\kappa = 1, A^{(j)}$; (c) The mean (inset: maximum) error between assumed shared boundary width, $W^{(j+1/2.k)}$, and real shared boundary width, for $K = 1$ and displacement $k_1 = 0.01, 0.05, 0.1, 0.2$; (d) The ratio of the average stretch in the z -direction and the average stretch in the y -direction ($\text{mean}(\lambda_z)/\text{mean}(\lambda_y)$) for $K = 1$ and displacement $k_1 = 0.01, 0.05, 0.1$ 87

- 4.4 Solutions for a discrete system of incompressible neo-Hookean cells aligned in a two-dimensional array subject to a prescribed displacement at $x = l_0$, with a periodic boundary condition at $y = w_0$ ($y = 0$). Solutions for $N = 10$, $M = 10$, cells, $K = 1$ and uniform shear modulus $\mu = 1$. (a) The array, with colour representing cell pressure, for $t = 1, 2, 5, 10$ and $k_1 = 0.5$; (b) The mean height of all cells in the array, $\text{mean}_{x,y}(z)$, for $t = 0$ to $t = 10$ for $k_1 = 0.01, 0.05, 0.1$; (c) The average pressure of all cells in the array, $\text{mean}_{x,y}(p)$, for $t = 0$ to $t = 10$ for $k_1 = 0.01, 0.05, 0.1$ 89
- 4.5 Set up of M elastic cells aligned end to end subject to a shearing force on the outer boundary of cell M . Cell k has shearing angle $\theta^{(j,k)}$, centre of mass position $x_c^{(j,k)}$ and experiences no motion in the y -direction. All cells have uniform, constant length, L_0 , and width, W_0 . The system is subject to substrate dissipation (damping relative to initial position), represented by a dashpot connected to the initial position of the cell centre of mass. 90
- 4.6 Solutions for $M = 10$ cells subject to simple shear. (a) Profiles for $F_A = 1$ at $t = 150$; (b) Maximum difference in shear angle in the array for $F_A = 0.01, 0.1, 1, 10$ (inset: mean shear angle in array); (c) Shear angle of all cells (discrete, dashes) and at discretisation points (continuum, lines) for $t = 0$ to $t = 150$ (inset: displacement); (d) Spatial profile of displacement $t = 1, 10, 50, 100$ for $F = 1$ (discrete, symbols; continuum, lines) (inset: $M = 50$); (e) Spatial profile of shear angle at $t = 1, 10, 50, 100$ for $F = 1$ (discrete, symbols; continuum, lines). . . . 99

Declaration

With the exception of Chapter 1, which contains introductory material, all work in this thesis was carried out by the author unless otherwise explicitly stated. With the exception of a combination of Chapters 2 and 3, which are being submitted as a paper to the Proceedings of the Royal Society A, all work in this thesis has not been submitted elsewhere.

Chapter 1

Introduction

This thesis develops new mechanical models for soft tissue behaviour by constructing rational discrete cell-based models in the form of ordinary-differential equations (ODEs) and, utilising the multiscale asymptotic technique of discrete-to-continuum asymptotics, upscales these discrete systems of ODEs to continuum PDEs. In this chapter, we will introduce the background behind this project, first by discussing soft tissue modelling (Sec. 1.1). We then consider both macroscale continuum models (Sec. 1.2) and the more recent focus on modelling biological systems with discrete formulations (Sec. 1.3). I provide an overview of upscaling and a summary of a few key techniques in Sec. 1.4. In this work, we investigate the role of growth and proliferation in soft tissue behaviour, and summarise relevant research and background in Section 1.5. A summary of the structure of the remainder of this thesis is provided in Sec. 1.6.

1.1 Soft tissue modelling

Physiological systems typically exhibit complicated interaction between tissue and fluid (e.g. blood flowing through arteries and veins, air flow in the lungs, water flows between cells). When applying theoretical models to predict the behaviour of such systems it is necessary to pose constitutive models for the mechanical response of each component. Whilst there are a wide number of accepted constitutive models for physiological fluids (e.g. blood [1–3]) and hard tissues (e.g. bone [4]), models for soft tissues are less well characterised.

Soft tissues range from skin and connective tissues to muscles and organs. To model soft tissues, we must consider the complex structure of the tissue and the cells that form it. Characteristically, these tissues are comprised of large numbers of individual cells, which themselves contain a (stiff) nucleus, intracellular fluid (cytoplasm), a structural cytoskeleton enclosed within a membrane (fluid-like sheet enclosing the cell) and filament networks that maintain cell shape (e.g. actin) [5]; cells are typically deformable but almost perfectly incompressible [6]. The human body alone has over 200 different types of cells. These cells are tightly packed together within a structure called the extracellular matrix (ECM) composed of collagen fibres and other

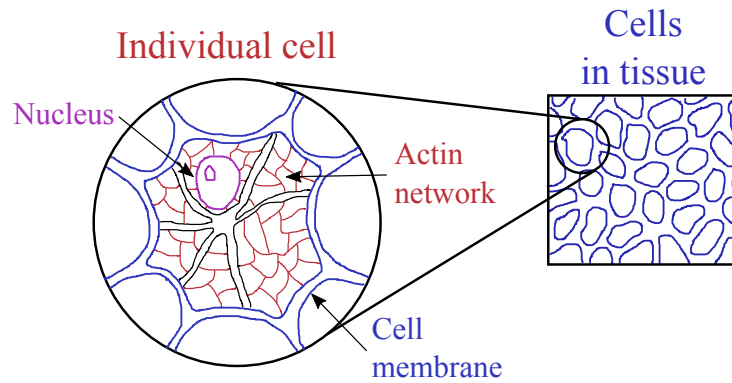


Figure 1.1: Tissues are composed of large number of cells packed together. Cells comprise of a nucleus, filament networks (e.g. actin), microtubules and a cellular membrane.

structural proteins, which provides structural and biochemical support to cells and helps determine their behaviour and shape [7]. The structure described here is outlined in Figure 1.1. Cells bind together via the ECM or by direct attachment to one another at cell junctions [6]. Soft tissues are therefore inherently multiscale.

The behaviour of multiscale materials has been the subject of extensive investigations since the 19th century (e.g. [8] [9]). These theories have been utilised in a diverse range of fields, from biological tissues [10] and biofilms [11], to vascular transport networks [12]. In this wide variety of disciplines, large-scale volumes (e.g. tissue level) contain a large number of media with small-scale (e.g. cell level) heterogeneities. Formulating and validating theoretical mechanical models for soft tissues allows deeper understanding of how these tissues behave and respond to stimuli and is essential in developing computational tools to simulate applications in the medical field (e.g. the design of biocompatible prosthetic devices and implants as in [13]). Mathematical modelling is an important tool in understanding the responses of biological soft tissues and their irreversible deformations or altered morphology e.g. growth of the heart [14], tumors [15] (cancer is a tissue disorder due to mutant cells violating rules of social cell growth) and muscle tissues [4].

Initially, the fields of biomechanics and mechanobiology played an important role in understanding biological form and function, however the focus was on hard tissues. Translating from hard to soft tissues is non-trivial. In contrast to hard tissues, soft tissues undergo larger deformations and the multiphase character of soft tissues plays a critical role [15]. Researchers in biomechanics later laid out a strategy to characterise the living nature of soft tissues which shaped the modelling of the deformation of soft tissues: establish a theory with a testable hypothesis, design experiments, calibrate model parameters (parameters fitted to *in vitro* experimental measurements) and then validate the model [16, 17].

It is often difficult to fully reconcile *in vitro* experiments in relatively small samples to the conditions experienced *in vivo*. Additionally, soft tissues are difficult to preserve, and *ex vivo* responses might vary significantly from *in vivo* behaviour [18]. This difference might be attributed

to residual stress [19–21] or to a pronounced active response [22, 23].

Experimental observations by Fung have shown that soft biological tissues exhibit a highly nonlinear, anisotropic, heterogeneous and large deformation upon physiological loading [24]. The response of soft biological tissues is not only highly non-linear, but time and history dependent and often inelastic [13, 25]. Due to the complexity of the behaviour of soft tissues, there is a challenge to rationally construct macroscale models which encode the properties (e.g. stiffness or fibre orientation) of the cells and matrix which form the tissue. The macroscale models fitted to experimental data can only incorporate a homogenized picture of the entire material, making it difficult to isolate the role of microscale structures and other inhomogeneities. Given these obvious limitations of macroscale models, there is a need for new continuum models for soft materials which encode the microscale behaviour in a rational way.

1.2 Continuum models

Tissues are materials comprised of individual discrete objects (cells) at the micro-scale. In this thesis we consider two ways of constructing tissue models; using an individual-based model (IBM) (discrete) or as a continuum (locally averaged quantities of cell properties) [26]. We will review IBMs in Sec. 1.3, but first we will survey a selection of continuum models of soft tissues in this section. Continuum models are used widely across a variety of soft tissues. In this work, we are interested in working towards a soft tissue model for the human heart.

Effective modelling of the mechanics of soft biological tissues requires the theory of nonlinear continuum mechanics [27]. Modelling a material in the framework of continuum mechanics treats the material as a single body (i.e. continuum). The body is considered to be initially at rest in a reference configuration and material points in the body are described by a position vector relative to some origin, \mathbf{X} . As the body moves and deforms, the material configuration and the position vector describing material points, $\mathbf{x}(\mathbf{X}, t)$, changes with time, t . This new configuration is called the current configuration. The deformation of this material is defined by a deformation tensor, given by

$$\mathbb{F} = \text{Grad}(\mathbf{x}). \quad (1.1)$$

The response of the material is determined by the assumed relationship between strain energy and deformation, that is, from the choice of strain-energy function, denoted \mathcal{W} . This is a scalar valued function relating the strain energy of a material to the deformation gradient, to define hyperelastic (ideally elastic) materials. For example, a popular strain-energy function developed for rubber and applied extensively to soft tissues describes a neo-Hookean material. This strain-energy function has the two-dimensional form

$$\mathcal{W} = \frac{\mu}{2} (\lambda_1^2 + \lambda_2^2 - 2), \quad (1.2)$$

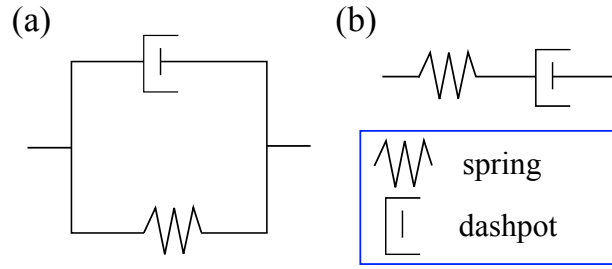


Figure 1.2: (a) Kelvin-Voigt model (spring and dashpot in parallel); (b) Maxwell model (spring and dashpot in series).

where μ is the shear modulus of the material and λ_1 and λ_2 are the principal stretches of the deformation tensor, \mathbb{F} [27]. This model can be used for predicting nonlinear stress-strain behaviour of materials undergoing deformations.

However, materials are not just elastic, but can also have viscous properties as well. Viscoelastic models describe materials that exhibit both viscous (time-dependent resistance) and elastic responses when undergoing deformation. For example, a Kelvin-Voigt material is a viscoelastic material represented by a purely viscous damper and purely elastic spring connected in parallel (Fig. 1.2a). In this system, the total stress, σ_T , and the total strain, ε_T are defined as

$$\sigma_T = \sigma_D + \sigma_S, \quad (1.3)$$

$$\varepsilon_T = \varepsilon_D = \varepsilon_S, \quad (1.4)$$

where the subscript D indicates the stress-strain in the damper, and the subscript S represents the stress-strain in the spring. The stress-strain relationship for a Kelvin-Voigt material is given by

$$\sigma_T = E\varepsilon_T + \eta \frac{d\varepsilon_T}{dt}, \quad (1.5)$$

where E is the elastic modulus and η is the material coefficient of viscosity. If, instead, the dashpot and the spring were connected in series, the system would describe a Maxwell material (Fig. 1.2b). In this system, the total stress, σ_T , and the total strain, ε_T are defined as

$$\sigma_T = \sigma_D = \sigma_S, \quad (1.6)$$

$$\varepsilon_T = \varepsilon_D + \varepsilon_S, \quad (1.7)$$

The stress-strain relationship for a Maxwell material is given by

$$\frac{d\varepsilon_T}{dt} = \frac{\sigma_T}{\eta} + \frac{1}{E} \frac{d\sigma_T}{dt}. \quad (1.8)$$

One advantage of describing soft tissues with continuum models is that techniques for the mathematical analysis of continuum models (e.g. PDEs) are well developed [26], and for numer-

ical solutions using finite element techniques, one can also utilise adaptive meshing techniques, resulting in computational savings. However, existing continuum models fail to resolve cellular or sub-cellular details [28], and hence have limitations in their applications.

1.2.1 Skin

Early continuum models of biomechanical interest include models for skin. For example, Lanir and Fung [29] investigated the two dimensional mechanical properties of rabbit skin by implementing biaxial mechanical tests. This research indicated that the biaxial stress-strain relations were non-linear. These investigations were extended by Fung to develop a pseudo-strain potential, which allowed derivation of a stress-strain relationship for the skin [30]. This pseudo strain potential is defined by

$$\rho_0 \mathcal{W} = f(\alpha, e) + c \exp(F(a, e)), \quad (1.9a)$$

with

$$f(\alpha, e) = \alpha_1 e_{11}^2 + \alpha_2 e_{22}^2 + 2\alpha_4 e_{11} e_{22}, \quad (1.9b)$$

$$F(a, e) = a_1 e_{11}^2 + a_2 e_{22}^2 + a_3 e_{12}^2 + 2a_4 e_1 e_2 + \gamma_0 e_1^3 + \gamma_2 e_2^3 + \gamma_4 e_1^2 e_2 + \gamma_5 e_1 e_2^2, \quad (1.9c)$$

where \mathcal{W} is the strain energy per unit mass, ρ_0 is the density of the material in the initial, undeformed state, e is the Green strain tensor (with i, j -th component e_{ij} and i -th principal strain e_i), and c , α_i , a_i ($i = 1, 2, 3$) and γ are constants (as defined in [30]). This function was fitted to the exponential experimental data for rabbit skin successfully, when linear elasticity models were unable to do so.

Further studies have proposed popular constitutive models of the skin (e.g. Li [31, 32]) and there are numerous theories built in the framework of nonlinear continuum mechanics (e.g. [33–35]). However, constitutive models of skin need to not only include mechanical and viscoelastic effects, but must also account for damage and fracture [31]. For example, constitutive laws have been developed that take into account chemo-mechanobiological modelling for wound healing (e.g. [36, 37]).

1.2.2 Arterial tissue

The arteries are muscular tubes consisting of three layers: the intima (inner layer), the media (muscle layer) and the adventitia (connective tissue). Their job is to deliver oxygenated blood from the heart to tissues around the body. *In vivo*, arteries are pre-stretched under an internal pressure load and if one slices an artery open, the resting state of the tube is an open segment of a circle [38]. Sophisticated models are necessary to take this deformation into account. For example, Ogden [39] developed a model for hyperelastic materials used to describe the nonlinear

stress-strain behaviour of complex materials in the form of the strain-energy function

$$\mathcal{W} = \sum_{p=1}^N \frac{\mu_p}{\alpha_p} \left(\lambda_1^{\alpha_p} + \lambda_2^{\alpha_p} + \lambda_3^{\alpha_p} - 3 \right), \quad (1.10)$$

where N , μ_p and α_p ($p = 1, \dots, N$) are material constants and $\lambda_{1,2,3}$ are the principal stretches of the deformation tensor, \mathbb{F} . This model was developed in relation to the finite deformation of solid and tubular cylinders of incompressible isotropic elastic materials (e.g. arteries). This work was able to predict data from experiments on the torsion and extension of a solid cylinder of natural rubber [39]. In 2000, Holzapfel, Gasser and Ogden [38] presented their breakthrough ‘HGO’ model, in which a constitutive law for the description of passive mechanical response of arterial tissue was presented. The strain-energy-function developed here is given by

$$\mathcal{W} = \frac{c}{2}(\bar{I}_1 - 3) + \frac{k_1}{k_2} \sum_{i=4,6} (\exp(k_2(\bar{I}_i - 1)^2) - 1), \quad (1.11)$$

where $c, k_1, k_2 > 0$ are stress-like material parameters and I_i ($i = 1, 4, 6$) are the invariants of the right Cauchy-Green deformation tensor, $\mathbb{C} = \mathbb{F}^T \mathbb{F}$, defined by

$$I_1 = \lambda_1^2 + \lambda_2^2 + \lambda_3^2, \quad (1.12)$$

$$I_4 = \mathbf{M} \cdot (\mathbf{CM}), \quad (1.13)$$

$$I_6 = \mathbf{M}' \cdot (\mathbf{CM}'), \quad (1.14)$$

where λ_i ($i = 1, 2, 3$) are the principal stretches of \mathbb{F} and \mathbf{M} and \mathbf{M}' are two distinct preferred directions in the reference configuration (e.g. fibre directions). Note that since λ_i ($i = 1, 2, 3$) are the principal stretches, I_1 can be interpreted as half of the area of the surfaces of a deformed unit cube. The strain-energy-function (1.11) consists of the neo-Hookean model for the isotropic response (the term $c(\bar{I}_1 - 3)/2$) and an exponential model of the invariants \bar{I}_4 and \bar{I}_6 which captures the anisotropic response [38]. This work modelled an artery as a thick-walled nonlinearly elastic circular cylindrical tube consisting of two layers, each with embedded fibres. This work emphasised the strong importance of residual stress in the modelling of soft tissues (specifically arteries), previously highlighted by Chuong and Fung [40]. The HGO model accounted for the *in vitro* residual stress by assuming that the unstressed and unstrained configuration of the material corresponded to an open sector of a tube, as observed in experiments. An initial bending is imposed to close the tube, to form a load-free (but stressed) circular cylinder. The HGO model was later extended to reliably predict passive, time-dependent, three-dimensional stress and deformation states of healthy young arterial walls under various loading conditions [41] and to develop the first mathematical model to account for the evolution of the abdominal aortic aneurysm (a bulge or swelling in the main blood vessel that runs from the heart down through the chest) [42].

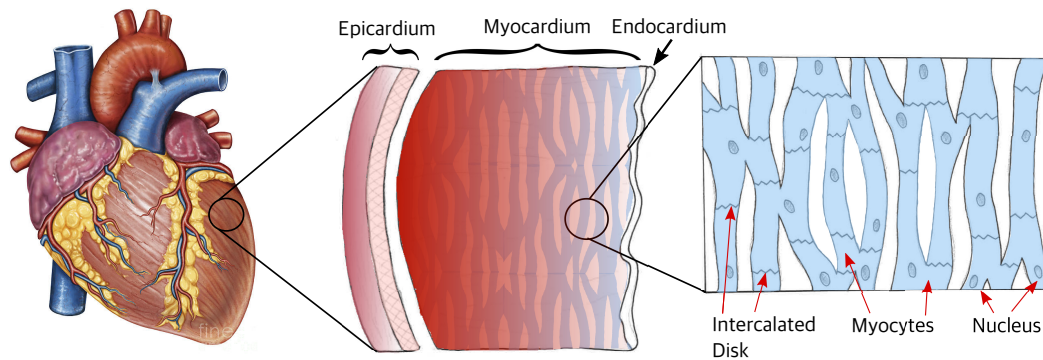


Figure 1.3: The wall of the heart is constructed from predominantly 3 layers; endocardium (inner), myocardium (middle) and pericardium (outer) (left figure from <http://stevegallik.org/sites/histologyolm.stevegallik.org/images/heartwall.gif>)

1.2.3 Cardiovascular tissues

The heart is a muscular organ, the walls of which are made up of three layers: epicardium (outer), myocardium (middle) and endocardium (inner), shown in Fig. 1.3. The myocardium layer, a cardiac muscle, makes up the thickest part of the wall. This is composed of cardiomyocytes (cells), connected end-to-end by intercalated discs. Cardiomyocytes contain myofibrils, a fundamental contractile unit of muscle cells which contract their length during systole (contraction) and relax their length during diastole (relaxation). This ability to contract is critical to the cyclic beating of the heart. Cardiomyocytes form the atria (the chambers where the blood enters the heart) and the ventricles (the chambers where blood is pumped out of the heart). If blood flow supplying the heart wall (coronary circulation) is restricted, such as in myocardial infarction, cardiomyocytes die, which may cause whole portions of myocardium to die. This can cause permanent damage, however research indicates repair may be possible with stem cells [43]. Understanding the behaviour and structure of cardiomyocytes within the tissue (array) can therefore be extremely useful. Modelling of the cardiovascular system includes modelling the heart (myocardium soft tissue) along with the arterial networks. In this section we will outline a selection of relevant studies.

Early models of cardiac muscle mechanics were modified versions of the skeletal muscle models of Hill [44, 45] and have evolved from these studies [46]. Arts *et al.* [47] proposed an early ventricular model to simulate the mechanics of the left ventricle pump function. Here, the left ventricle was simulated by a thick-walled cylinder composed of eight concentric shells, with each cell identified with their own fibre orientation. During a cardiac cycle, the left ventricle twists during systole and untwists during diastole. This twisting motion aids left ventricular ejection (ejecting blood to the arteries) and the untwisting aids relaxation and ventricular filling (taking in blood from the arteries). This work highlighted the importance of twisting in the left ventricle in equalising transmural differences and minimising stress. There are extensive

models for the heart based on a simple cylindrical geometry [47–49]. For example, Hunter [49] presented myocardial constitutive laws for both the passive and active cardiac muscle mechanics. This model was able to describe experimental results on a variety of tissues from various species (mainly rat and ferret). Humphrey and Yin [50] presented a model of myocardium with a thick-walled cylindrical annulus composed of a nonlinear, anisotropic, incompressible material. This work considered finite deformations including inflation, extension, twist and transmural shearing. This model was able to predict transmural variations in stress and strain in comparison with experimental data.

In 2009 Holzapfel and Ogden [51] presented their HO model for passive myocardium. This model was characterised by the strain-energy function

$$\mathcal{W} = \frac{a}{2b} \exp(b(I_1 - 3)) + \sum_{i=f,s} \frac{a_i}{2b_i} (\exp(b_i(I_{4i} - 1)^2) - 1) + \frac{a_{fs}}{2b_{fs}} (\exp(b_{fs}(I_{8fs})^2) - 1), \quad (1.15)$$

where $a, b, a_f, a_s, b_f, b_s, a_{fs}, b_{fs} > 0$ are material constants (with the a parameters having dimension of stress and b parameters being dimensionless), I_1 is the first invariant of the right Cauchy-Green deformation tensor and

$$I_{4f} = \mathbf{f}_0 \cdot (\mathbb{C}\mathbf{f}_0), \quad (1.16)$$

$$I_{4s} = \mathbf{s}_0 \cdot (\mathbb{C}\mathbf{s}_0), \quad (1.17)$$

$$I_{8fs} = \mathbf{f}_0 \cdot (\mathbb{C}\mathbf{s}_0), \quad (1.18)$$

where \mathbf{f}_0 and \mathbf{s}_0 are the basis vectors which coincide with the fibre axis direction and sheet axis direction respectively and \mathbb{C} is the right Cauchy-Green deformation tensor, $\mathbb{C} = \mathbb{F}^T \mathbb{F}$. This model accounts for the fibre direction within myocardium. When applied to simple shear and biaxial deformations, the model was able to successfully fit to existing experimental data. These models have the potential to be useful, noninvasive diagnostic tools, demonstrating their importance in further development.

Fully understanding the human cardiac cycle requires tissue-scale models for the deformation of the heart wall in response to an active stimulus [15], i.e. active contraction. For example, Niederer *et al.* [52] presented the Niederer-Hunter-Smith (NHS) model for active contraction from a biochemical perspective. Calcium levels play a key role in the activation of contraction in myocardium, and this work presented a constitutive model for active contraction derived from a study of calcium activity. Work by Cai *et al.* [53] presented a model in which the HGO constitutive law was utilised to describe the passive myocardial response, coupled with the NHS myofilament model to describe the active tension. These such models provide a foundation to couple the electrophysiology and mechanics in the heart, working towards more accurate cardiac models.

1.3 Individual based models

As discussed in the previous section, continuum models typically fail to resolve cellular or sub-cellular details [28], however, it is straightforward to include these properties along with heterogeneous cell populations within individual-based models (IBMs) [54, 55], providing a natural motivation to construct IBMs. In recent years there has been an increasing focus on biological and physiological IBMs that incorporate a discrete representation of the microscale. These computational models offer a useful means to investigate and test mechanisms (e.g. cell sheet dynamics) and have played a key role in the study of cell-cell interactions [56].

There are multiple discrete approaches developed for modelling cell populations [56]. The simplest discrete models of the mechanical behaviour of tissue are lattice based [57–60], where cells are constrained to lie on a regular grid. These models consist of a lattice on which a parameter is defined in each site. Adjacent sites with the same parameter value define a cell, and the absence of a value represents the medium. Each lattice site can contain at most a single cell, and rules are set up for determining how cells interact, divide and move. However, these models do not treat the mechanics of cellular systems realistically. For example, they can involve moving an entire column or row of cells to accommodate a newborn cell and can therefore contain instantaneous ‘action at a distance’ (whereby cells are moved in the absence of external forces or effects) effects [61]. To overcome this, off-lattice, or cell-centre, models along with vertex models were developed to model cell behaviour in a more realistic fashion.

In cell-centre models, cells are described by a single point (the centre). There are often two vital components to these models. First, a definition of cell-connectivity, defining which cells are in contact, and second, a definition of the force between two cells in contact (cell-cell interaction force) [61]. For example, the overlapping spheres method defined two cells as being in contact if they are within a certain distance of each other. However, cells *in vivo* are not naturally spherical and a model of spherical cells do not pack as closely as cells in reality, hence other methods have been developed, for example, using ellipsoids [62].

In vertex models, each cell is represented as a two-dimensional polygon, with vertices and edges shared between adjacent cells. Cells are defined by a location of a finite set of vertices along with rules defining how any vertex moves based on forces, connecting vertices locations, neighbouring cell areas, etc [63]. The origins of vertex models stem from inorganic structures such as foams [64,65] and grain boundaries [66], however a significant challenge when applying these methods to biological tissues is the ability of cells to grow, divide and die [56].

Work by Fozard *et al.* [26] developed a discrete one-dimensional vertex based IBM of a monolayer of tightly packed cells. In this work, cells were described as a bounded region, defined by the location of their endpoints and had both elastic and viscous mechanical properties. Cells were subject to drag due to adhesion to a substrate and had fixed neighbours, where drag forces were linear functions of the vertex velocities. The evolution of this system was driven by a mechanical free energy, from which force balances on cell vertices were calcu-

lated. Work by Murray *et al.* [67] modelled cells as point masses connected by linear springs in a one-dimensional discrete formulation. These existing models include the forces exerted by cells on each other and their surrounding medium, however this is usually incorporated in a simplistic manner with linear springs (e.g. [67]) or with generic force laws based on Hooke's law (e.g. [68]). These models also incorporate drag on the system due to substrate adhesion, however this is usually proportional to vertex speed with a constant of proportionality. However there is a lack of IBMs of soft tissue cells where forces are derived directly from a continuum mechanical framework. The most extensive application of IBMs in soft tissue is in the modelling of epithelium. This is detailed in Sec. 1.3.1 below.

However, one should note that techniques for the mathematical analysis of continuum models are better developed than those for IBMs [26]. Furthermore, the computational expense of numerical simulations of IBMs depends on the number of cells in the system, whereas for continuum models it depends on the spatial discretisation spacing (dictated by the size of the system relative to the scale on which variations of interest occur) [26]. Additionally, on the global scale, these materials made of discrete objects behave as a continuous medium that can be described by elastic strain, stress and velocity gradients [69], hence is it useful to be able to investigate and consider effects at the macroscale. It is therefore of interest to relate IBMs to continuum models (in a large cell number limit), which are more efficient. This also allows the measurement of cell properties to estimate continuum parameters and vice versa. This relation can be achieved with upscaling techniques (e.g. [26, 67, 68]), which will be discussed in Sec. 1.4.

1.3.1 Epithelial Models

Epithelium is a type of soft tissue which lines the outer surfaces of organs as well as the inner surfaces of cavities in many internal organs. An example is the epidermis, which is the outermost layer of the skin. Epithelial sheets have a highly organised nature and can achieve complex morphogenetic processes through coordinated movement and rearrangement of individual cells. Vertex IBMs (described above) are suitable for tightly packed cell sheets where intercellular space is negligible, as in epithelial tissue cells [56]. Epithelium is widely used in biological modelling literature; this is due to the accessibility of this tissue. They provide a simple experimental framework and are easy to culture in a monolayer, providing ease of access to data for comparisons with mathematical models.

While vertex models were initially developed to study inorganic structures [56], Honda and Eguchi [70] were among the first to use vertex models to study epithelial sheet deformations. In this work, a monolayer of convex polygonal cells with no gaps or overlaps was presented to investigate cell boundary length. These models have since been extensively used to investigate cellular mechanisms and physical mechanics of epithelial monolayer deformations [56], and there are numerous discrete IBMs for epithelium [26, 54, 63, 71–76].

An important resource for vertex modelling of soft tissue is CHASTE (Cancer, Heart and

Soft Tissue Environment), which is an open source C++ simulation package for individual-based modelling of cell populations, specifically applied to soft tissues [61]. For example, Fletcher *et al.* [56] described an approach for implementation of vertex dynamics models within the CHASTE framework. This work investigated the dynamic behaviour of epithelial sheets by comparing two formulations of vertex models within the CHASTE environment. The versatility and generality of this framework has been illustrated using a number of biological examples (e.g. cardiac electro-physiology [77, 78] and intestinal tissue [54]) with the aim of working towards guaranteeing the reproducibility of computational results across the field [56].

Nestor-Bergmann *et al.* [71] used vertex modelling to describe a spatially disordered epithelial monolayer. This work explored the relationship between cell shape and mechanical stress in epithelium, both at the cellular and tissue levels. Here, cellular forces were derived from each cell's own mechanical energy, a similar formulation to previous works (e.g. [63, 70, 75]), including contractile strength. Farhadifar *et al.* [63] (using the CHASTE simulation package) constructed a vertex model to investigate packing geometries and the role of developmental mechanisms in these biophysical properties of cells. In this model, junctional forces were defined in terms an energy function which described the forces due to cell elasticity, active contraction and adhesion (dissipative) molecules. These forces acted to displace the vertices defined in the model.

A review by Fletcher *et al.* [56] summarised how vertex models have been used to provide insight into developmental processes. This work outlined the remarkable progress in experimental studies of epithelial dynamics. Numerous different cell-based modelling approaches have been developed for studying how processes at single cell level influence collective dynamics in epithelial sheets [79, 80]. In particular, the review surmised that cell based vertex models have played an increasingly important role in the study of morphogenesis, particularly in epithelial tissues. However, an important challenge is the computational cost, hence systematic and rational model reduction is critically important [56].

1.4 Upscaling

We have looked at both continuum models and IBMs for soft tissues. We now consider a translation of an IBM into a continuum model. One useful method is to derive continuum models exploiting the separation of spatial scales, which is widely used and central to the development of macroscale theories [81]. The aim of these techniques is to derive equations which govern the behaviour of the system over spatial scales which are much larger than those on which material properties vary. Using such upscaling techniques one can derive continuum macroscale models directly from discrete micro-scale IBMs with appropriate approximations [82, 83].

We will now survey a range of upscaling techniques, which include asymptotic homogenisation (Sec. 1.4.1), mixture theory (Sec. 1.4.2), volume averaging (Sec. 1.4.3) and discrete-to-

continuum asymptotics (Sec. 1.4.4).

1.4.1 Homogenisation

Asymptotic homogenisation is an upscaling technique that substitutes a region (e.g. tissue) formed of a fine grid of discrete heterogeneous items (e.g. cells), with an equivalent homogeneous region, made up of a single coarse-grid item (i.e. a coarse-scale model). For example, one can take known equations describing a small region of the material and use these to describe the entire material, relative to the size of the small region. Homogenisation is typically used in periodic, porous medium [84] and the main advantage of this approach is that it allows a significant reduction of the problem size [85]. Inherent in this method is the compromise between computational cost and the accuracy of the coarse-scale solution, with the most popular upscaling methods working to balance these competing demands [86]. This approach is described as being applicable “to all kinds of processes that occur in periodic media” [87] and has been applied in numerous biological tissues including tumours [88] and bone or tendons [89]. For example, Penta *et al.* [89] developed a model for three-dimensional elastic composite materials using asymptotic homogenisation. This work was able to successfully replicate results from experimental data from bone tissues.

1.4.2 Mixture theory

Mixture theory is used to describe materials composed of multiple different material types and hence is used widely in modelling composites in material science. For example, the heart wall is made up of three layers. To describe the full wall using mixture theory, one can use a weighted sum (or weighted average) of the strain-energy functions describing each individual layer, to derive a strain-energy function describing the full material. This method differs from that of asymptotic homogenisation since the macroscale is a weighted average of heterogeneous materials, instead of describing the full material with a small area of the domain.

This method has been applied to numerous biological tissues. For example, Byrne and Preziosi [90] used the theory of mixtures to develop a multiphase model of the growth of a solid tumour. This model comprised of a solid and liquid phase and results suggested that tumour growth was not only limited by nutrient availability but also by the stress from the surrounding tissue. Work by Lang *et al.* [91] formulated a model for brain tissue, which was considered to be a mixture of solid and liquid components (e.g. extra- and intra-cellular matrices and water), to investigate the swelling of slices of brain tissue.

1.4.3 Volume averaging

Volume averaging is a popular homogenisation technique for multiphase systems [81]. The underlying idea of this method is to develop appropriate macroscopic equations (which hold everywhere in the domain) from microscopic equations which hold at some small point in the domain. This approach has been extensively applied to porous media [92–94]. Whitaker [95] developed a method of using volume averaging with closure to derive macroscale equations. Examples of this homogenisation technique include applications to biological tissues [10], biofilms [11] and transport in vascular networks [12].

1.4.4 Discrete to continuum asymptotics

The methods of multiscale asymptotics include discrete-to-continuum asymptotics [96], and inherent in these methods is the translation of discrete differences into continuum derivatives. Hence these methods are often used to study differential operators (e.g. [97, 98]). These methods involve identifying a discrete (micro-scale) model, then assuming parameters vary in space and time on scales (macro-scales) much larger than the discrete configuration. One can then expand variables as functions of a very small parameter - usually the ratio of micro and macro length scales (it is typical in a multiscale problem that characteristic length scales of individual cells are much smaller than a characteristic length scale of a tissue). If this small parameter is chosen too large, the macro- and micro-scale systems may not agree. These continuum approximations can be obtained by expanding differences in Taylor series [99, 100]. The method of discrete-to-continuum asymptotics will be used in this thesis. This approach does not require a homogeneous problem at the cell level, meaning that cells need not have uniform properties, providing an advantage over most other upscaling techniques.

The method of discrete-to-continuum asymptotics has been utilised in a variety of models. For example, Fozard *et al.* [26] approximated their discrete one-dimensional vertex-based IBM of a monolayer of cells with a continuum PDE model through expanding Taylor series of differences to model heterogeneous cell populations in the limit of a large number of cells. This study found that the error in the continuum approximation was smaller for a system where parameters of neighbouring cells varied slowly in space than in a system that was spatially periodic (and varied faster spatially). This model was therefore applicable for even a modest number of cells if parameters varied slowly in space. Murray *et al.* [67, 68] used discrete-to-continuum asymptotics to construct nonlinear diffusion models for proliferating arrays of large numbers of cells from a discrete IBM consisting of masses and springs. For simulations for a variety of nonlinear force laws in the discrete model and their respective diffusion coefficients in the continuum, excellent agreement is observed between models.

A review by Davit *et al.* [81] investigated the comparison of volume averaging (specifically, the method used by Whitaker [95]) and multiscale asymptotics (specifically periodic multiscale

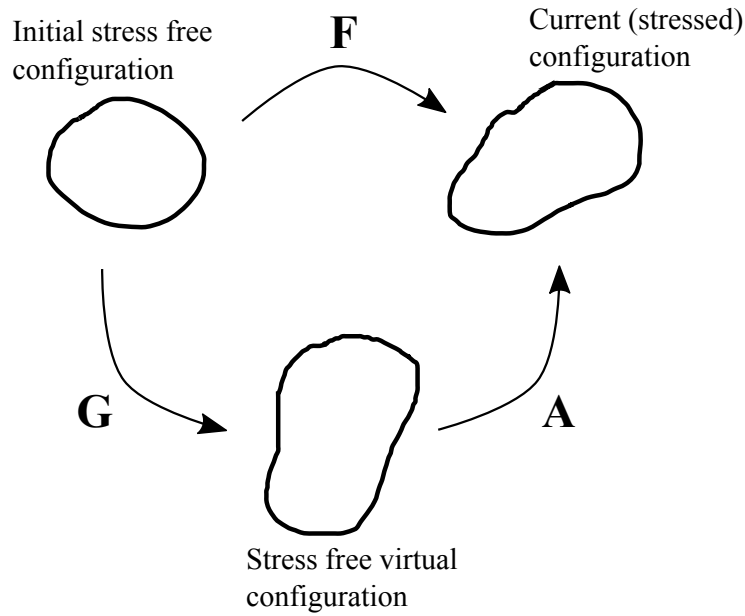


Figure 1.4: Decomposition of the deformation tensor, \mathbb{F} into growth, \mathbf{G} , and elastic, \mathbf{A} , components.

expansions). The work concluded that although they share similar goals, the nature of the approaches are slightly different. However, the main differences lie in the methodologies, the insight provided, the assumptions and algorithms, rather than the results.

1.5 Growth

When modelling any physiological system, including soft tissues, it is a natural to also consider growth and remodelling. Remodelling (and growth) describes changes in properties (e.g. anisotropy, stiffness, strength) resulting from changes in microstructure over time [17]. Biological growth is involved in many fundamental biological processes (e.g. morphogenesis, physiological regulation, pathological disorders) and involves complex interactions across multiple scales [101]. Growth is the process by which a body increases in size through the addition of mass and can be localised or restricted to a certain area [102], for example in a cancerous proliferating rim where growth and proliferation occur only in a localised area [103]. However there is no unified characterisation of growth that is broadly accepted [15]. Volumetric growth (growth throughout the bulk of the body) is common in the growth of hearts [104], arteries [105] and tumours [106].

Continuum mechanics and nonlinear elasticity provides a natural framework to study growth, from which the theory of morphoelasticity was presented [101, 107]. This theory deconstructs the deformation tensor, \mathbb{F} , into a product of two tensors; viscoelastic deformation, \mathbf{A} , and growth, \mathbf{G} . Hence

$$\mathbb{F} = \mathbf{A}\mathbf{G}. \quad (1.19)$$

The deformation is considered to be a two step process. Starting from the initial, stress-free configuration, the material grows to a configuration which is stress free but not compatible with the environment. This configuration is called a virtual configuration. The second step is the elastic response, which can be considered as the problem of fitting the grown material to the environmental constraints. This step introduces stress, mapping the material from the virtual configuration to the current configuration. This is illustrated in Fig. 1.4.

This formulation enabled the modelling of growth in various soft biological tissues and is now commonly used, for example maladaptive cardiac growth [14] or growing tumours [106]. Growth is a key behaviour in cancer, a disorder of tissue renewal due to abnormal growth of mutant cells. Formulating models for growth of soft tissues will therefore provide insight into determining what factors affect the behaviours of these key systems. The majority of models for biological tissue growth focuses on modelling deposition of solid matrix products from a continuum perspective [107–110]. For example, Work by Kida *et al.* [111] developed a continuum mechanical constitutive model of epithelial tissues based in the framework of morphoelasticity, comparing numerical simulations of the model to experimental results. Klisch *et al.* [110] presented a generalised theory of volumetric growth for compressible elastic materials. This work derived a continuum constitutive model for incremental growth.

Biological tissue growth can refer to cell development not only in terms of an increase in volume but also in terms of cell division (proliferation), where a parent cell divides to produce two daughter cells [112]. This process can occur for a number of reasons, such as to preserve a volume-surface area ratio that allows enough nutrients from the environment to pass into the cell to sustain it [113].

Both continuum and discrete models for growth and proliferation of cells have been developed. For example, work by Hywood *et al.* [114] developed a discrete agent-based stochastic model where cells were able to grow and divide within a tissue environment. In this work, discrete cells are able to divide and time between divisions for individual cells were implemented using a probability distribution. The corresponding continuum representation of the proliferating system was derived using discrete-to-continuum upscaling to describe the average behaviour of the stochastic proliferation. A further example is the work by Murray [67], in which proliferation is implemented in the discrete model with cells undergoing division, where cells divide when they reach a certain age. Here, proliferation was accounted for in the continuum model by adding an appropriate source term to the nonlinear diffusion model. Results showed that an appropriate source term could adequately describe the resulting cell population from the discrete model.

1.6 Structure

In this work we present a general framework to derive multiscale models for soft tissues which incorporate the properties of individual cells without assuming homogeneity or periodicity at the cell level. We approach the problem from a viewpoint of rational mechanics rather than cell biology, and consider a reduced mechanical model for individual cells (which can deform, grow and divide) that is grounded in the framework of nonlinear viscoelasticity. We consider rationally derived non-linear forces based on mechanical constitutive models for individual cells and couple these to form a network description of arrays of cells, where each cell has independent material and mechanical properties. Cells exert forces on their neighbours through shared boundaries and we consider the dynamics of these arrays, deriving discrete systems of ODEs. We consider two possible formulations of dissipation due to substrate adhesion. We then utilise a discrete-to-continuum upscaling to derive new (nonlinear) continuum PDE models for the tissue (array) which allows for gradients in cell properties. This approach has been implemented in cell signalling [82, 115] and discrete IBM [26, 67] and we extend its use here to soft tissue mechanics.

In Ch. 2 we consider a single quasi-two-dimensional line of nonlinearly viscoelastic cells (Fig. 2.1 below). In particular the array is constrained so that one end is fixed, but the other is subject to a prescribed displacement. These cells necessarily have a finite size, and exert force on their neighbours along the array, but can also exhibit a force in the transverse direction. Having constructed and solved the discrete model in Sec. 2.1 we then use the methods of discrete-to-continuum upscaling to derive a new PDE model for this system in Sec. 2.2. For static deformation we show that for simple hyperelastic constitutive laws for individual cells (e.g. Neo-Hookean) we recover the corresponding static model at the macroscale. However, this discrete-to-continuum approach informs new time dependent models for these tissues, and we draw comparisons to existing models for viscoelastic tissues. In Sec. 2.3 we illustrate results for test problems, considering the influence of a time-dependent displacement with uniform and non-uniform cell shear modulus, to consider the case where a localised region of tissue has very different mechanical properties, such as in a myocardial infarction. In Sec. 2.4 we extend this formulation to demonstrate a simple application of this approach to models of the deformation of the human heart, incorporating an active mechanical stress into the microscale model, which quantifies macroscale tissue deformation. This allows us to investigate the effect of an active contractive force in a periodic domain, as an approximation to the deformation of a ring of left ventricle tissue.

In Ch. 3 we extend the model from Ch. 2 using the theory of morphoelasticity [116] to include growth in one dimension. The array is constrained so that one end is fixed, but the other end is subject to zero external stress. We construct the discrete model in Sec. 3.1 and upscale to derive the corresponding PDE model for this system in Sec. 3.2. In Sec. 3.3.1 we investigate the role of dissipation in the system, comparing two different dissipative functions

and the effect they have on the behaviour of the system in terms of the length of the growing array. In Sec. 3.3.2 we couple cell proliferation with cell growth, implementing a division event when cells grow to double their initial area. We examine how dissipation translates into different macroscale deformations, for example, a proliferating rim.

In Ch. 4 we consider a quasi-three-dimensional sheet of nonlinearly viscoelastic cells. We first consider the discrete formulation for a general deformation in Sec. 4.1 and outline the challenges of maintaining generality. We then specify the system for two types of deformation: uniaxial deformation and simple shear. In Sec. 4.2 we consider each cell undergoing a uniaxial deformation and derive the corresponding upscaled system in Sec. 4.2.9. For a static deformation we show that for simple hyperelastic constitutive laws for individual cells we recover the corresponding static model at the macroscale. In this system, one edge of the sheet is fixed and the parallel edge is subject to a prescribed deformation. We consider two cases for the remaining boundary conditions. First, in Sec. 4.2.12, that one is fixed and the other is subject to zero external stress. Second, in Sec. 4.2.13, we implement periodic boundary conditions on the remaining two boundaries. In Sec. 4.3 we then consider each cell undergoes a simple shear deformation and derive the corresponding upscaled PDE model in Sec. 4.3.9. In this system, we enforce periodicity in one dimension and consider uniformity in cell parameters in this direction, allowing us to reduce the system to consider a single array of cells. We fix one end of the array and implement a shearing force at the parallel edge. We enforce no motion perpendicular to the applied shearing force. In Sec. 4.3.11 we investigate the response of the system subject to forces of different magnitudes.

Finally, in Ch. 5 we conclude with a summary of the results and findings and consider some extensions to the work.

Chapter 2

Deformation of a Single Array of Cells

In this chapter we consider the dynamic deformation of a single array of nonlinearly viscoelastic cells of constant density that are arranged end-to-end along a single line atop a rigid substrate, as shown in Fig. 2.1. For simplicity the cells are assumed to be of uniform thickness, H (measured in the direction normal to the substrate, parametrised by the coordinate z), and we assume there is no deformation in this direction, reducing the three-dimensional system to a two-dimensional one. The midline of this two-dimensional array is parameterised by the coordinate x (shown as a dashed line in Fig. 2.1), while the tangential direction (in the plane of the page) is parametrised by the coordinate y . These cells are assumed to be in contact along their shared edges where stress can be transmitted. All cells are assumed to be incompressible, which allows us to model the two-dimensional system with one-dimensional ODEs. We assume the outer edge of the cell at one end is adhered to a fixed impermeable boundary at $x = 0$. At the other end of the array, we denote the location of the outer edge at $x = l(t)$, where we apply a boundary condition of either prescribed displacement, prescribed force, or periodicity. In the lateral y -direction, we assume boundary conditions of zero normal and tangential stress on external interfaces. In practice, the difference in external pressures on soft tissues can be non-zero, but we assume here that the pressure difference between adjacent layers of constituent cells at the microscale will be small, and for the purposes of this study is assumed negligible. The system is subject to substrate dissipation (damping relative to initial position) and Kelvin dissipation (damping relative to internal viscosity). Although idealised, this model system elucidates the competition between local elastic deformation at the single cell level to the global mechanical deformation and expansion of the entire array.

We construct the geometry of N cells, aligned end to end, and first construct discrete IBMs in Sec. 2.1. This discrete model is upscaled to form a new macroscale PDE model in Sec. 2.2, where we consider the case of small displacements and also draw comparisons to a static system derived from an equivalent macroscale model. We investigate this system by considering the effects of a prescribed deformation at one end of the array in Sec. 2.3 and then extending this passive formulation to incorporate effects of active contraction in Sec. 2.4.

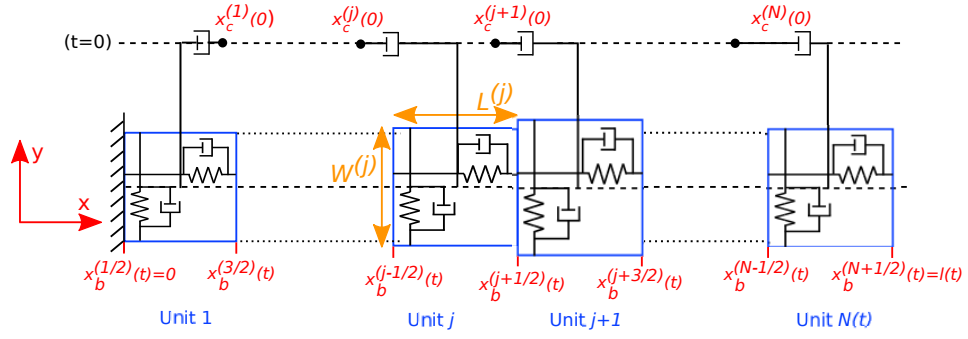


Figure 2.1: Force diagram of N viscoelastic incompressible 2D cells aligned end-to-end in a single array. The imposed a fixed boundary at $x = 0$ (to investigate the system in a test problem) is represented as a solid wall at the left hand side of the array. The dissipation due to cells attached to the substrate (in the plane of the page) is represented as a dashpot connected to the initial position of the cell centre (displayed on a dashed line above the array of cells here for clarity). See text for more details.

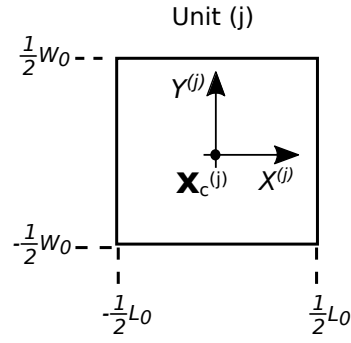
2.1 Discrete Model

We consider a single line of N discrete cells, as shown in Fig. 2.1. These cells are indexed by the coordinate j ($j = 1, \dots, N$) and the properties of cell j are labelled with a superscript (j) . In general these individual cells can have complicated shapes and are embedded within an extracellular matrix. For simplicity in this study, we assume that each constituent cell can be modelled as a cuboid which deforms in a way such that the cell remains cuboidal. Since the out-of-plane thickness remains constant, each cell is characterised by a length in the x -direction (along unit vector $\hat{\mathbf{x}}$), denoted by $L^{(j)}(t)$ (with initial value $L_0^{(j)}$), and width in the y -direction (along unit vector $\hat{\mathbf{y}}$), denoted by $W^{(j)}(t)$ (with initial value $W_0^{(j)}$) for $j = 1, \dots, N$. As mentioned above, the system is assumed to have no displacement or growth in the out-of-plane direction and so the deformation can be treated as entirely planar; for simplicity in the analysis below we ignore the out-of-plane direction entirely and present the tensors for stress and strain as two-dimensional. Denoting the total length of the line of cells as $l(t)$ (which may be either prescribed or solved for, with initial total length l_0), we assume there are no voids and must have

$$l(t) = \sum_{j=1}^N L^{(j)}(t), \quad l(0) = l_0 = \sum_{j=1}^N L_0^{(j)}. \quad (2.1)$$

We assume the cells have uniform density $\rho^{(j)}$ ($j = 1, \dots, N$), and characterise cells by the position of their centre of mass (which coincides with their geometric centre since the density is uniform) denoted by $\mathbf{x}_c^{(j)} = (x_c^{(j)}(t), 0)$, for $j = 1, \dots, N$ and the position of their boundaries, denoted by $\mathbf{x}_b^{(j)} = (x_b^{(j-1/2)}(t), 0)$, for $j = 1, \dots, N+1$, where the index $j-1/2$ denotes the boundary between cells $j-1$ and $j+1$ (while the index $1/2$ denotes the outer boundary of cell 1 and the index $N+1/2$ denotes the outer boundary of cell N).

We assume each cell can undergo a nonlinear viscoelastic deformation relative to its geo-

Figure 2.2: Local reference coordinate system for cell j .

metric centre, while this geometric centre moves according to a global force balance. The local reference coordinate system for cells (Fig. 2.2) is $\mathbf{X}^{(j)} = (X^{(j)}, Y^{(j)}) = (x - x_c^{(j)}(0), y)$ so that $-\frac{1}{2}L_0^{(j)} \leq X^{(j)} \leq \frac{1}{2}L_0^{(j)}$ and $-\frac{1}{2}W_0^{(j)} \leq Y^{(j)} \leq \frac{1}{2}W_0^{(j)}$. In the current configuration, the coordinate system for cells is defined by $\mathbf{x}^{(j)} = \boldsymbol{\chi}^{(j)}(\mathbf{X}^{(j)}, t)$. The mapping $\boldsymbol{\chi}$ defines the deformation from the reference to the current configuration. The corresponding deformation gradient tensor is $\mathbb{F}^{(j)} = \text{Grad}(\mathbf{x}^{(j)})$, where the gradient operator is defined in the reference coordinate system $\mathbf{X}^{(j)}$.

2.1.1 Deformation

The deformation gradient tensor $\mathbb{F}^{(j)}(t)$ for the deformation of a single cell is

$$\mathbb{F}^{(j)}(t) = \begin{bmatrix} \lambda_1^{(j)}(t) & 0 \\ 0 & \lambda_2^{(j)}(t) \end{bmatrix}, \quad (2.2)$$

where $\lambda_1^{(j)}(t)$ and $\lambda_2^{(j)}(t)$ are the principal stretches of cell j ($j = 1, \dots, N$), and

$$\lambda_1^{(j)}(t) = \frac{x_b^{(j+1/2)}(t) - x_b^{(j-1/2)}(t)}{L_0^{(j)}}. \quad (2.3)$$

In all models we consider a uniaxial deformation, that is, applied deformation is applied in one direction only.

2.1.2 Incompressibility

The constraint of incompressibility on the deformation implies that $\det(\mathbb{F}^{(j)}) = \lambda_1^{(j)}\lambda_2^{(j)} = 1$, ($j = 1, \dots, N$). Hence $\lambda_2^{(j)} = (\lambda_1^{(j)})^{-1}$.

2.1.3 Rheological Model

We assume that each cell is composed of an elastic component in parallel with a viscous dashpot, the Kelvin-Voigt rheological model, which has previously been used to model cells (e.g. [117]) (Fig. 2.1).

Since the two components are arranged in parallel, this results in an additive decomposition of the total Cauchy stress i.e.

$$\boldsymbol{\sigma}^{(j)} = \boldsymbol{\sigma}_e^{(j)} + \boldsymbol{\sigma}_v^{(j)}, \quad (j = 1, \dots, N), \quad (2.4)$$

where $\boldsymbol{\sigma}_e^{(j)}$ and $\boldsymbol{\sigma}_v^{(j)}$ represent the elastic and viscous components of the Cauchy stress, respectively.

2.1.4 Elastic Stress

The hyperelastic component of the cell deformation follows from an incompressible strain energy functional,

$$\mathcal{W}_e^{(j)} = \mathcal{W}_e^{(j)}(\lambda_1^{(j)}, \lambda_2^{(j)}), \quad (j = 1, \dots, N), \quad (2.5)$$

where the function $\mathcal{W}_e^{(j)}$ is chosen to satisfy objectivity requirements [118]. We characterise the elasticity of individual cells by their shear modulus, denoted $\mu^{(j)}$ ($j = 1, \dots, N$) and denote μ_0 as a typical shear modulus for each cell (for example, the mean value for a healthy cell and in this chapter we use $\mu_0 = 1$). We preserve generality when specifying the model, but show results below for the incompressible neo-Hookean strain energy functional

$$\mathcal{W}_e^{(j)} = \frac{1}{2}\mu^{(j)} \left((\lambda_1^{(j)})^2 + (\lambda_2^{(j)})^2 - 2 \right), \quad (j = 1, \dots, N), \quad (2.6)$$

which is often used for modelling biological soft tissues (e.g. [119, 120]).

The corresponding Cauchy stress tensor for cell j is then given by,

$$\boldsymbol{\sigma}_e^{(j)} = \mathbb{F}^{(j)} \frac{\partial \mathcal{W}_e^{(j)}}{\partial \mathbb{F}^{(j)}} - p^{(j)} \mathbb{I}, \quad (j = 1, \dots, N), \quad (2.7)$$

where $p^{(j)}$ is a Lagrange multiplier interpreted as the elastic pressure j ($j = 1, \dots, N$) [102] and \mathbb{I} is the identity tensor. Since we assume a rectangular deformation for each cell this results in a diagonal Cauchy stress tensor of the form

$$\boldsymbol{\sigma}_e^{(j)} = \begin{bmatrix} \lambda_1^{(j)} \mathcal{W}_1^{(j)} - p^{(j)} & 0 \\ 0 & \lambda_2^{(j)} \mathcal{W}_2^{(j)} - p^{(j)} \end{bmatrix}, \quad \mathcal{W}_{1,2}^{(j)} = \frac{\partial \mathcal{W}_e^{(j)}}{\partial \lambda_{1,2}^{(j)}}, \quad (j = 1, \dots, N). \quad (2.8)$$

2.1.5 Viscous Stress

Since the deformation is such that cells remain cuboidal, the velocity of deformation is the time derivative of the stretches in the principal directions, which are spatially uniform across the cell, denoted by $\dot{\lambda}_1^{(j)}$ and $\dot{\lambda}_2^{(j)}$ ($j = 1, \dots, N$), where the dot notation denotes the time derivative. Hence the viscous Cauchy stress is

$$\boldsymbol{\sigma}_v^{(j)} = \begin{bmatrix} 2\eta^{(j)}\dot{\lambda}_1^{(j)} & 0 \\ 0 & 2\eta^{(j)}\dot{\lambda}_2^{(j)} \end{bmatrix}, \quad (j = 1, \dots, N), \quad (2.9)$$

where $\eta^{(j)}$ ($j = 1, \dots, N$) is the internal cell viscosity.

2.1.6 Boundary Conditions

The pressure $p^{(j)}$ ($j = 1, \dots, N$) within each cell is determined by applying the boundary condition of no lateral force on the unconfined edges (parallel to $\hat{\mathbf{x}}$), which gives

$$p^{(j)} = \lambda_2^{(j)}\mathcal{W}_2^{(j)} + 2\eta^{(j)}\dot{\lambda}_2^{(j)}, \quad (j = 1, \dots, N). \quad (2.10)$$

Using (2.10), the total force on the shared boundary (force per unit length) exerted by an individual cell on its neighbours (Fig. 2.3) then takes the form

$$\begin{aligned} \mathbf{F}_{\pm}^{(j)} &= F_{\pm}^{(j)}\hat{\mathbf{x}} = \int_{-\frac{1}{2}W^{(j+1/2)}}^{\frac{1}{2}W^{(j+1/2)}} \boldsymbol{\sigma}^{(j)} \cdot (\mp\hat{\mathbf{x}}) \, dy \\ &= \mp\hat{\mathbf{x}}W^{(j+1/2)} \left(\lambda_1^{(j)}\mathcal{W}_1^{(j)} - \lambda_2^{(j)}\mathcal{W}_2^{(j)} + 2\eta^{(j)} \left(\dot{\lambda}_1^{(j)} - \dot{\lambda}_2^{(j)} \right) \right), \quad (j = 1, \dots, N), \end{aligned} \quad (2.11)$$

where $W^{(j+1/2)}$ is the length of the shared boundary between cells j and $j \pm 1$, $\min(W^{(j)}, W^{(j+1)})$ (the minimum value of the widths of cells j and $j + 1$). However, it is not straightforward to carry this term through the upscaling for the continuum model, and so we approximate this by the mean of the cell widths

$$W^{(j+1/2)} = \frac{1}{2} \left(W^{(j+1)} + W^{(j)} \right), \quad (2.12)$$

where $W^{(j)} = W_0\lambda_2^{(j)}$. The resultant force at the boundary between cells j and $j + 1$ is

$$F_b^{(j+1/2)} = F_+^{(j)} + F_-^{(j+1)}, \quad (j = 1, \dots, N - 1). \quad (2.13)$$

This net force drives motion and deformation of the line of cells.

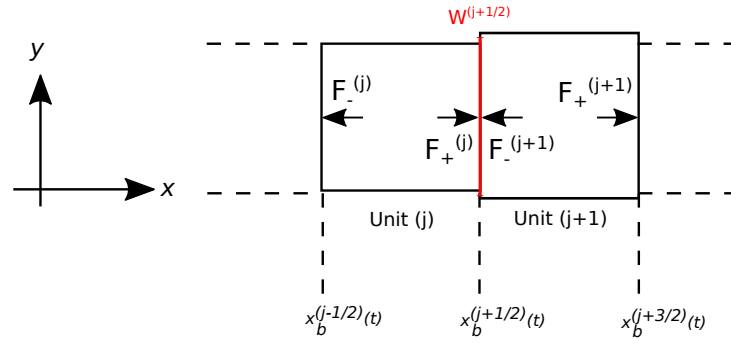


Figure 2.3: Force balance across boundary between cells j and $j + 1$, summing the individual forces of cell j on cell $j + 1$ and of cell $j + 1$ on cell j .

2.1.7 Substrate Damping

We consider the additional possibility that the cells are binding and unbinding to a substrate that is fixed in the plane of the page; the resulting force is assumed proportional to the rate of change of the position of the centre of mass of the cell relative to the substrate, with constant of proportionality $K^{(j)}$, ($j = 1, \dots, N$). The damping is reminiscent of a Stokes drag on a sedimenting sphere in fluid mechanics, and is attributed to friction due to the ECM [7]. This is equivalent to each cell having a dashpot connected to a reference point (Fig. 2.1).

2.1.8 Equations of Motion

We apply Newton's second law to each internal cell. To simplify the equation, we approximate the motion as being over-damped, since cells usually move in relatively dissipative environments (e.g. [67, 74, 121, 122]). Hence we neglect inertial effects and the global force balance can be expressed as

$$K^{(j)} \frac{dx_c^{(j)}}{dt} = F_b^{(j-1/2)} + F_b^{(j+1/2)}, \quad (j = 1, \dots, N). \quad (2.14)$$

The cell's centre of mass is the mean of its boundary positions,

$$x_c^{(j)} = \frac{1}{2} \left(x_b^{(j-1/2)} + x_b^{(j+1/2)} \right), \quad (j = 1, \dots, N). \quad (2.15)$$

2.1.9 Global Boundary and Initial Conditions

To complete the system, we define boundary conditions on the outer boundaries. We investigate the system by first considering a test problem with simple boundary conditions. For all systems outlined here, the boundary of cell $j = 1$ at $x = 0$ remains fixed and we prescribe the total length of the line, $l(t)$, so that

$$x_b^{(1/2)}(t) = 0, \quad x_b^{(N+1/2)} = l(t), \quad \text{for } t \geq 0. \quad (2.16)$$

In general, initially the cell boundaries are located at

$$x_b^{(j-1/2)} = \sum_{i=0}^j L_0^{(i)}, \quad (j = 1, \dots, N+1), \quad (2.17)$$

with $x_b^{(1/2)} = 0$; however, in the simulations below we assume all cells are initially the same length $L_0^{(j)} = L_0$ and width $W_0^{(j)} = W_0$ ($j = 1, \dots, N$). This is not a necessary assumption but significantly simplifies the specification of the model and the upscaling to a continuum model for Sec. 2.2. In this case, (2.17) reduces to

$$x_b^{(j-1/2)} = L_0 j, \quad (j = 1, \dots, N+1). \quad (2.18)$$

2.1.10 Non-dimensional variables

It is useful to consider the system in terms of non-dimensional variables (denoted with an overbar). We consider that the damping parameters are uniform across the array, hence $K^{(j)} = K$ and $\eta^{(j)} = \eta$ ($j = 1, \dots, N$). We scale time on a pertinent timescale t_0 (defined below by the boundary conditions which, in the case of prescribed displacement this is the rate of the applied deformation), lengths on L_0 , pressures on μ_0 and forces on $\mu_0 L_0^2$ so that

$$(x, L^{(j)}, W^{(j)}) = L_0(\bar{x}, \bar{L}^{(j)}, \bar{W}^{(j)}), \quad \mu^{(j)} = \mu_0 \bar{\mu}^{(j)}, \quad t = t_0 \bar{t}, \quad (j = 1, \dots, N). \quad (2.19)$$

This results in the following dimensionless groups

$$\bar{\gamma}_0 = \frac{W_0}{L_0}, \quad \bar{\eta} = \frac{2\eta}{\mu_0 t_0}, \quad \bar{K} = \frac{K}{2t_0 \mu_0} \quad (2.20)$$

representing the planar aspect ratio of the cells, and the dimensionless viscous and substrate damping coefficients respectively. We further define the dimensionless domain length, intracellular force across the shared boundary width (force per unit length), cell width, strain-energy function and cell pressure:

$$l(t) = L_0 \bar{l}(\bar{t}), \quad F_b(t) = \mu_0 L_0 \bar{F}_b(\bar{t}), \quad \bar{W}^{(j)}(t) = \frac{\bar{\gamma}_0}{\lambda_1^{(j)}(\bar{t})}, \quad \mathcal{W}^{(j)} = \mu_0 \bar{\mathcal{W}}^{(j)}, \quad p^{(j)} = \mu_0 \bar{p}^{(j)}. \quad (2.21)$$

The non-dimensional system (2.14) takes the form

$$2\bar{K} \frac{d\bar{x}_c^{(j)}}{d\bar{t}} = -\bar{W}^{(j+1/2)} \left(\bar{\sigma}_1^{(j)} - \bar{\sigma}_1^{(j+1)} \right) - \bar{W}^{(j-1/2)} \left(\bar{\sigma}_1^{(j-1)} - \bar{\sigma}_1^{(j)} \right), \quad (j = 2, \dots, N-1) \quad (2.22a)$$

where

$$\bar{W}^{(j\pm 1/2)} = \gamma_0 \left(\lambda_2^{(j\pm 1)} + \lambda_2^{(j)} \right), \quad (2.22b)$$

$$\bar{\sigma}_1^{(j)} = \lambda_1^{(j)} \mathcal{W}_1^{(j)} - \lambda_2^{(j)} \mathcal{W}_2^{(j)} + \bar{\eta} \left(\dot{\lambda}_1^{(j)} - \dot{\lambda}_2^{(j)} \right), \quad (2.22c)$$

$$\lambda_1^{(j)} = \bar{x}_b^{(j+1/2)} - \bar{x}_b^{(j-1/2)} \text{ and} \quad (2.22d)$$

$$\lambda_2^{(j)} = \frac{1}{\lambda_1^{(j)}}. \quad (2.22e)$$

The cell centre of mass in terms of cell boundary locations (2.15) in non-dimensional variables is

$$\bar{x}_c^{(j)} = \frac{1}{2} \left(\bar{x}_b^{(j-1/2)} + \bar{x}_b^{(j+1/2)} \right). \quad (2.22f)$$

The cell pressure from (2.10) is

$$\bar{p}^{(j)} = \lambda_2^{(j)} \mathcal{W}_2^{(j)} + \bar{\eta} \dot{\lambda}_2^{(j)}. \quad (2.22g)$$

Substituting (2.15) into (2.14) and considering the fixed boundary condition at $x = 0$ yields

$$\bar{K} \frac{d\bar{x}_b^{(j+1/2)}}{d\bar{t}} = \bar{W}^{(j+1/2)} \left(\bar{\sigma}_1^{(j+1)} - \bar{\sigma}_1^{(j)} \right), \quad (j = 1, \dots, N-1). \quad (2.22h)$$

This form of the governing equations is used in numerical solutions of the discrete model.

The boundary conditions for prescribed displacement are

$$\bar{x}_b^{(1/2)} = 0, \quad \bar{x}_b^{(N+1/2)} = \bar{l}(\bar{t}), \quad (2.22i)$$

or with a free boundary at one end of the line

$$\bar{x}_b^{(1/2)} = 0, \quad \bar{K} \frac{d\bar{x}_b^{(N+1/2)}}{d\bar{t}} = -\bar{W}^{(N)} \sigma_1^{(N)} \quad (2.22j)$$

where

$$\bar{W}^{(N)} = \gamma_0 \lambda_2^{(N)}. \quad (2.22k)$$

The initial condition is $\bar{x}_b^{(j-1/2)}(0) = j - 1$, ($j = 1, \dots, N + 1$).

Henceforth, we drop over-bars for notational convenience and consider only non-dimensional variables in the simulations below.

2.1.11 Numerical method

The discrete system (2.22) is a closed system of ODEs which is solved numerically using MATLAB solver `ode15s` with the prescribed displacement boundary condition (2.22i) implemented as an algebraic constraint. The code to solve this system can be derived from the code in Appendix A.1 when the growth rate is set to zero (no growth) and the boundary condition at $x = l_0$ for a prescribed displacement is implemented. In simulations throughout we consider a neo-Hookean material. Due to the additional time-derivative terms in the viscous stress formulation, we formulate a matrix problem within the solver, such that

$$\mathbf{M}_b \frac{d\mathbf{x}_b}{dt} = \mathbf{f}_b, \quad (2.23)$$

where \mathbf{x}_b which has entries $x_b^{(j-1/2)}$ ($j = 1, \dots, N+1$), \mathbf{M}_b is the $N+1 \times N+1$ matrix with first and last diagonal entries equal to one (to implement the boundary conditions, where the prescribed displacement at the end of the array is implemented as $x_b^{(N+1/2)} = l(t)$ where $l(t)$ is the prescribed deformation) and, for $j = 2, \dots, N$, the coefficients of $\frac{dx_b^{(j+1/2)}}{dt}$ terms from the viscous part of the Cauchy stress (2.9) and the cell pressure (2.10), which take the form

$$\mathbf{M}_b(j, j-1) = -\eta W^{(j-1/2)} \left(1 + \left(\lambda_1^{(j-1)} \right)^{-2} \right) \quad (2.24a)$$

$$\mathbf{M}_b(j, j) = K + \eta W^{(j-1/2)} \left(2 + \left(\lambda_1^{(j-1)} \right)^{-2} + \left(\lambda_1^{(j)} \right)^{-2} \right) \quad (2.24b)$$

$$\mathbf{M}_b(j, j+1) = -\eta W^{(j-1/2)} \left(1 + \left(\lambda_1^{(j)} \right)^{-2} \right), \quad (2.24c)$$

for $j = 2, \dots, N$ and \mathbf{f}_b , the vector with components

$$\mathbf{f}_b(1) = 0 \quad (2.24d)$$

$$\begin{aligned} \mathbf{f}_b(j) = & -W^{(j+1/2)} \left(\mu^{(j)} \left(\left(\lambda_1^{(j)} \right)^2 - \left(\lambda_1^{(j)} \right)^{-2} \right) \right. \\ & \left. - \mu^{(j+1)} \left(\left(\lambda_1^{(j+1)} \right)^2 - \left(\lambda_1^{(j+1)} \right)^{-2} \right) \right), \quad (j = 2, \dots, N), \end{aligned} \quad (2.24e)$$

$$\mathbf{f}_b(N) = -W^{(N)} \mu^{(N)} \left(\left(\lambda_1^{(N)} \right)^2 - \left(\lambda_1^{(N)} \right)^{-2} \right). \quad (2.24f)$$

This matrix problem is then solved for using the in-built matrix division (backslash) in MATLAB to solve for $d\mathbf{x}_b/dt$.

The MATLAB solver `ode15s` is a solver for stiff differential algebraic equations (DAEs) and uses a variable-step, variable-order solver. A study of the solver `ode15s` can be found in [123]. In simulations below, the standard absolute, a_t , and relative error tolerances, r_t , were used (10^{-6}). For larger tolerances ($a_t \geq 10^{-2}$, $r_t \geq 10^{-2}$) the solutions diverge, however for

$a_t < 10^{-2}$ and $r_t < 10^{-2}$, the solutions converge (Figure 2.4).

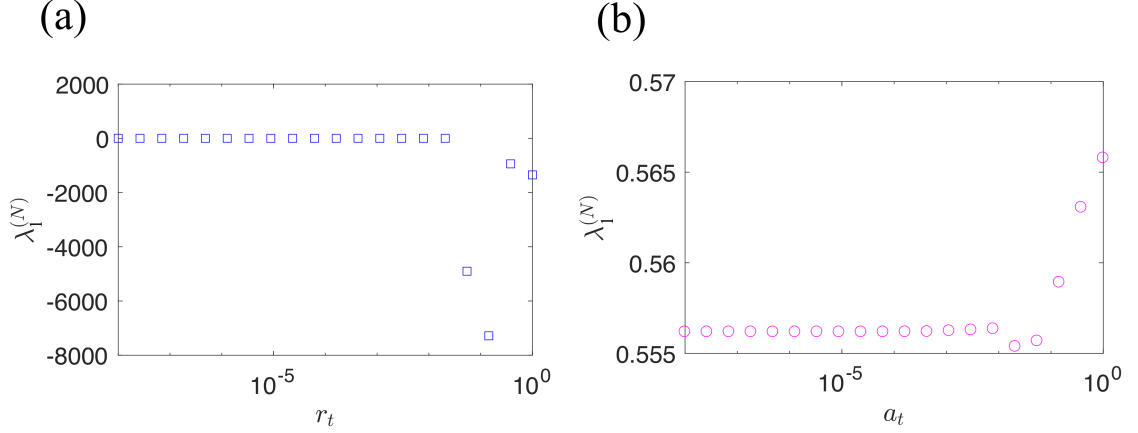


Figure 2.4: Stretch of the N -th cell, $\lambda_1^{(N)}$, at $t = 10$. (a) Solutions for relative tolerance values $r_t = 10^{-8}$ to $r_t = 1$; (b) Solutions for absolute tolerance values $a_t = 10^{-8}$ to $a_t = 1$.

Numerical solutions of this IBM are discussed in Sec. 2.3 below. This discrete formulation does not require any regularity or smoothness of material properties, which can be sampled randomly from an appropriate distribution. However, to construct a continuum (PDE) model of this arrangement of cells, we must assume that the material properties vary smoothly along the array over a prescribed lengthscale.

2.2 Upscaling to continuum model (Incompressible Cells)

We now derive a (PDE) continuum model description of the discrete model of Sec. 2.1. In this approach we utilise discrete-to-continuum upscaling to map the discrete equations (2.22) to a PDE [82, 115].

We assume the initial number of cells, N , is large and introduce a small parameter $\varepsilon = N^{-1} \ll 1$. We are working with non-dimensional variables and lengths have been scaled on L_0 , the typical length of a cell (Sec. 2.1.10). Thus we assume that the lengthscale of a typical deformation is long ($\mathcal{O}(\varepsilon^{-1})$) compared to that of an individual cell ($\mathcal{O}(1)$). The discrete-to-continuum approach uses Taylor expansions local to each cell to transform discrete differences to derivatives, which requires that the properties of the individual cells (e.g. $\mu^{(j)}$) vary smoothly across the entire length of the array (i.e. spatial derivatives are $\mathcal{O}(1)$). We define a long wavelength rescaling of the independent variables in the form

$$X = \varepsilon x, \quad T = \varepsilon t, \quad (2.25a)$$

so that $0 \leq X \leq 1$. Note that this choice is not unique, but we make this assumption as it maintains an $\mathcal{O}(1)$ cell velocity and hence this term is retained in the dominant balance. Other

choices would lead to a different dominant balance (for example, one could choose a different scaling for t that would leave the viscous terms out of the dominant balance) however these choices were not considered in this work. In accordance with this rescaling we then express the cell boundary positions as

$$\tilde{x}_b^{(j+1/2)}(T) = \varepsilon x_b^{(j+1/2)}(t), \quad (j = 0, \dots, N), \quad (2.25b)$$

where tilded variables are functions of rescaled time, T . Furthermore, we rescale the time-dependent descriptors of an individual cell in the form,

$$\left(\tilde{W}^{(j)}, \tilde{L}^{(j)}, \tilde{\lambda}^{(j)}, \tilde{\mathcal{W}}_{1,2}^{(j)} \right) = \left(W^{(j)}, \varepsilon L^{(j)}, \lambda^{(j)}, \mathcal{W}_{1,2}^{(j)} \right), \quad (j = 1, \dots, N). \quad (2.25c)$$

We further rescale the two dimensionless damping parameters as $K = \varepsilon \tilde{K}$ and $\eta = \varepsilon^{-1} \tilde{\eta}$ to ensure a dominant balance. We discretise the continuous variable X into N equally sized intervals, so that $X_j = j/N = \varepsilon j$, ($j = 0, \dots, N$), so the rescaled initial positions of the cell centre of mass and cell boundaries can be expressed as $\tilde{x}_b^{(1/2)}(0) = 0$ with

$$\tilde{x}_b^{(j+1/2)}(0) = X_j, \quad \tilde{x}_c^{(j)}(T) = X_{j-1/2} = \frac{1}{2}(X_{j-1} + X_j), \quad (j = 1, \dots, N). \quad (2.26)$$

We then express the cell boundary and centre of mass positions as a single continuum function $\check{x}(X, T)$ such that $\tilde{x}_b^{(1/2)}(T) = \check{x}(0, T) = 0$ and

$$\tilde{x}_b^{(j+1/2)} = \check{x}(X_j, T), \quad \tilde{x}_c^{(j)} = \check{x}(X_{j-1/2}, T), \quad (j = 1, \dots, N), \quad (2.27a)$$

as well as continuum representations of the other dependent variables in the model, in the form

$$\tilde{W}^{(j)}(t) = \check{W}(X_{j-1/2}, T), \quad \tilde{\lambda}_1^{(j)}(t) = \check{\lambda}_1(X_{j-1/2}, T), \quad (2.27b)$$

$$\tilde{\lambda}_2^{(j)}(t) = \check{\lambda}_2(X_{j-1/2}, T), \quad \tilde{\mathcal{W}}_{1,2}^{(j)}(T) = \check{\mathcal{W}}_{1,2}(X_{j-1/2}, T), \quad (j = 1, \dots, N). \quad (2.27c)$$

In this case differences in discrete variables can be mapped to derivatives of these continuum functions using Taylor expansions in the limit as $\varepsilon \rightarrow 0$ ($N \rightarrow \infty$). From (2.22h), the governing equation for the continuum strain energy functional $\check{\mathcal{W}}$ is expanded at $X_j = j\varepsilon$ in the form

$$\begin{aligned} \varepsilon \tilde{K} \frac{\partial \check{x}(j\varepsilon, T)}{\partial T} = & -\check{W}(j\varepsilon, T) \left(\check{\lambda}_1\left(\left(j + \frac{1}{2}\right)\varepsilon, T\right) \check{\mathcal{W}}_1\left(\left(j + \frac{1}{2}\right)\varepsilon, T\right) - \check{\lambda}_2\left(\left(j + \frac{1}{2}\right)\varepsilon, T\right) \check{\mathcal{W}}_2\left(\left(j + \frac{1}{2}\right)\varepsilon, T\right) \right. \\ & + \tilde{\eta} \frac{\partial}{\partial T} \left(\check{\lambda}_1\left(\left(j + \frac{1}{2}\right)\varepsilon, T\right) - \check{\lambda}_2\left(\left(j + \frac{1}{2}\right)\varepsilon, T\right) \right) \\ & - \check{\lambda}_1\left(\left(j + \frac{3}{2}\right)\varepsilon, T\right) \check{\mathcal{W}}_1\left(\left(j + \frac{3}{2}\right)\varepsilon, T\right) + \check{\lambda}_2\left(\left(j + \frac{3}{2}\right)\varepsilon, T\right) \check{\mathcal{W}}_2\left(\left(j + \frac{3}{2}\right)\varepsilon, T\right) \\ & \left. - \tilde{\eta} \frac{\partial}{\partial T} \left(\check{\lambda}_1\left(\left(j + \frac{3}{2}\right)\varepsilon, T\right) - \check{\lambda}_2\left(\left(j + \frac{3}{2}\right)\varepsilon, T\right) \right) \right). \end{aligned} \quad (2.28a)$$

Taylor expanding the variables about the point $X = j\varepsilon$ and evaluating the resulting expressions at $X = j + \varepsilon/2$ and $X = j + 3\varepsilon/2$, we obtain

$$\check{\lambda}_{1,2}((j + \frac{1}{2})\varepsilon, T) = \check{\lambda}_{1,2}(j\varepsilon, T) + \frac{\varepsilon}{2} \frac{\partial \check{\lambda}_{1,2}(j\varepsilon, T)}{\partial X} + \mathcal{O}(\varepsilon^2), \quad (2.28b)$$

$$\check{\lambda}_{1,2}((j + \frac{3}{2})\varepsilon, T) = \check{\lambda}_{1,2}(j\varepsilon, T) + \frac{3\varepsilon}{2} \frac{\partial \check{\lambda}_{1,2}(j\varepsilon, T)}{\partial X} + \mathcal{O}(\varepsilon^2), \quad (2.28c)$$

$$\check{\mathcal{W}}_{1,2}((j + \frac{1}{2})\varepsilon, T) = \check{\mathcal{W}}_{1,2}(j\varepsilon, T) + \frac{\varepsilon}{2} \frac{\partial \check{\mathcal{W}}_{1,2}(j\varepsilon, T)}{\partial X} + \mathcal{O}(\varepsilon^2), \quad (2.28d)$$

$$\check{\mathcal{W}}_{1,2}((j + \frac{3}{2})\varepsilon, T) = \check{\mathcal{W}}_{1,2}(j\varepsilon, T) + \frac{3\varepsilon}{2} \frac{\partial \check{\mathcal{W}}_{1,2}(j\varepsilon, T)}{\partial X} + \mathcal{O}(\varepsilon^2), \quad (2.28e)$$

Substituting (2.28b)-(2.28e) into (2.28a) yields

$$\begin{aligned} \varepsilon \tilde{K} \frac{\partial \check{x}(j\varepsilon, T)}{\partial T} = & -\check{W}(j\varepsilon, T) \left(\left(\check{\lambda}_1(j\varepsilon, T) + \frac{\varepsilon}{2} \frac{\partial \check{\lambda}_1(j\varepsilon, T)}{\partial X} \right) \left(\check{\mathcal{W}}_1(j\varepsilon, T) + \frac{\varepsilon}{2} \frac{\partial \check{\mathcal{W}}_1(j\varepsilon, T)}{\partial X} \right) \right. \\ & - \left(\check{\lambda}_2(j\varepsilon, T) + \frac{\varepsilon}{2} \frac{\partial \check{\lambda}_2(j\varepsilon, T)}{\partial X} \right) \left(\check{\mathcal{W}}_2(j\varepsilon, T) + \frac{\varepsilon}{2} \frac{\partial \check{\mathcal{W}}_2(j\varepsilon, T)}{\partial X} \right) \\ & + \check{\eta} \left(\frac{\partial \check{\lambda}_1(j\varepsilon, T)}{\partial T} + \frac{\varepsilon}{2} \frac{\partial^2 \check{\lambda}_1(j\varepsilon, T)}{\partial X \partial T} - \frac{\partial \check{\lambda}_2(j\varepsilon, T)}{\partial T} - \frac{\varepsilon}{2} \frac{\partial^2 \check{\lambda}_2(j\varepsilon, T)}{\partial X \partial T} \right) \\ & - \left(\check{\lambda}_1(j\varepsilon, T) + \frac{3\varepsilon}{2} \frac{\partial \check{\lambda}_1(j\varepsilon, T)}{\partial X} \right) \left(\check{\mathcal{W}}_1(j\varepsilon, T) + \frac{3\varepsilon}{2} \frac{\partial \check{\mathcal{W}}_1(j\varepsilon, T)}{\partial X} \right) \\ & + \left(\check{\lambda}_2(j\varepsilon, T) + \frac{\varepsilon}{2} \frac{\partial \check{\lambda}_2(j\varepsilon, T)}{\partial X} \right) \left(\check{\mathcal{W}}_2(j\varepsilon, T) + \frac{\varepsilon}{2} \frac{\partial \check{\mathcal{W}}_2(j\varepsilon, T)}{\partial X} \right) \\ & \left. - \check{\eta} \left(\frac{\partial \check{\lambda}_1(j\varepsilon, T)}{\partial T} + \frac{3\varepsilon}{2} \frac{\partial^2 \check{\lambda}_1(j\varepsilon, T)}{\partial X \partial T} - \frac{\partial \check{\lambda}_2(j\varepsilon, T)}{\partial T} - \frac{3\varepsilon}{2} \frac{\partial^2 \check{\lambda}_2(j\varepsilon, T)}{\partial X \partial T} \right) \right), \end{aligned} \quad (2.28f)$$

which, upon neglecting $\mathcal{O}(\varepsilon^2)$ terms reduces to and so

$$\begin{aligned} \varepsilon \tilde{K} \frac{\partial \check{x}(j\varepsilon, T)}{\partial T} = & -\varepsilon \check{W}(j\varepsilon, T) \left(-\frac{\partial \check{\lambda}_1(j\varepsilon, T)}{\partial X} \check{\mathcal{W}}_1(j\varepsilon, T) - \check{\lambda}_1(j\varepsilon, T) \frac{\partial \check{\mathcal{W}}_1(j\varepsilon, T)}{\partial X} \right. \\ & + \frac{\partial \check{\lambda}_2(j\varepsilon, T)}{\partial X} \check{\mathcal{W}}_2(j\varepsilon, T) + \check{\lambda}_2(j\varepsilon, T) \frac{\partial \check{\mathcal{W}}_2(j\varepsilon, T)}{\partial X} \\ & \left. - \check{\eta} \left(\frac{\partial^2 \check{\lambda}_1(j\varepsilon, T)}{\partial X \partial T} - \frac{\partial^2 \check{\lambda}_2(j\varepsilon, T)}{\partial X \partial T} \right) \right). \end{aligned} \quad (2.28g)$$

This can be simplified to give the governing equation

$$\tilde{K} \frac{\partial \check{x}_b}{\partial T} = \tilde{W} \frac{\partial}{\partial X} \left(\check{\lambda}_1 \check{\mathcal{W}}_1 - \check{\lambda}_2 \check{\mathcal{W}}_2 + \tilde{\eta} \frac{\partial}{\partial T} (\check{\lambda}_1 - \check{\lambda}_2) \right). \quad (2.28h)$$

Furthermore, we can rescale the continuum independent variables (X, T) back to the original parametrisation of the domain using $x = \varepsilon^{-1}X$, $t = \varepsilon^{-1}T$, $K = \varepsilon \tilde{K}$ and $\eta = \varepsilon^{-1} \tilde{\eta}$. We denote functions of these variables with the hat notation. We then define

$$\begin{aligned} \check{\lambda}_{1,2}(X, T) &= \hat{\lambda}_{1,2}(x, t) & \check{\mathcal{W}}(X, T) &= \hat{\mathcal{W}}(x, t) \\ \check{x}(X, T) &= \varepsilon \hat{x}(x, t), & \check{W}(X, T) &= \hat{W}(x, t). \end{aligned} \quad (2.29)$$

In this formulation, the principal stretch in the x -direction is

$$\hat{\lambda}_1(x, t) = \frac{\partial \hat{x}}{\partial x}, \quad (0 \leq x \leq l_0), \quad (2.30)$$

while incompressibility requires that

$$\hat{\lambda}_2(x, t) = \frac{1}{\hat{\lambda}_1}, \quad \hat{W}(x, t) = \gamma_0 \hat{\lambda}_2, \quad (0 \leq x \leq l_0). \quad (2.31)$$

Using (2.22g) total pressure takes the continuum form

$$\hat{p}(x, t) = \hat{\lambda}_2 \hat{\mathcal{W}}_2 + \eta \frac{\partial \hat{\lambda}_2}{\partial t}, \quad (0 \leq x \leq l_0). \quad (2.32)$$

From (2.28h), the governing equations for the continuum strain energy functional $\hat{\mathcal{W}}$ become

$$\hat{K} \frac{\partial \hat{x}}{\partial t} = \gamma_0 \hat{\lambda}_1^{-1} \frac{\partial}{\partial x} \left(\hat{\lambda}_1 \hat{\mathcal{W}}_1 - \hat{\lambda}_2 \hat{\mathcal{W}}_2 + \eta \frac{\partial}{\partial t} (\hat{\lambda}_1 - \hat{\lambda}_2) \right), \quad (0 < x < l_0). \quad (2.33a)$$

For the fixed boundary at $x = 0$, we set

$$\hat{x}(0, t) = 0, \quad (2.33b)$$

and for a prescribed displacement, the boundary condition (2.16) becomes

$$\hat{x}(l_0, t) = l(t), \quad (2.33c)$$

where $l(t)$ is prescribed in (2.22i).

2.2.1 Neo-Hookean Material

For a Neo-Hookean material with cell-level strain-energy function (2.6), we have

$$\hat{\mathcal{W}}_1 = \hat{\mu} \hat{\lambda}_1, \quad \hat{\mathcal{W}}_2 = \hat{\mu} \hat{\lambda}_2 = \hat{\mu} \hat{\lambda}_1^{-1}, \quad (0 \leq x \leq l_0), \quad (2.34)$$

where $\hat{\mu}$ is the continuum shear modulus and we obtain the continuum PDE

$$K \frac{\partial \hat{x}}{\partial t} = \gamma_0 \hat{\lambda}_1^{-1} \frac{\partial}{\partial x} \left(\hat{\mu} \left(\hat{\lambda}_1^2 - \hat{\lambda}_1^{-2} \right) + \eta \frac{\partial}{\partial t} \left(\hat{\lambda}_1 - \hat{\lambda}_1^{-1} \right) \right), \quad (0 < x < l_0), \quad (2.35a)$$

with boundary conditions (2.33b) and (2.33c) where

$$\hat{\lambda}_1 = \frac{\partial \hat{x}}{\partial x}, \quad \hat{p} = \hat{\mu} \hat{\lambda}_1^{-2} - \eta \frac{\partial \hat{\lambda}_1}{\partial t} \hat{\lambda}_1^{-2}, \quad 0 \leq x \leq l_0. \quad (2.35b)$$

2.2.2 Small Displacements in a Neo-Hookean Material

We consider small displacements of amplitude, $0 < k_1 \ll l_0$ of the form

$$\hat{x} = x + k_1 \hat{d}(x, t), \quad (2.36)$$

where $k_1 \hat{d}(x, t)$ is the displacement from the initial position. For this analytical investigation, we set $\hat{\mu} = \mu$ constant and uniform in the array. Substituting this in to (2.35a) gives

$$\begin{aligned} K k_1 \frac{\partial \hat{d}}{\partial t} = & \gamma_0 \left(1 + k_1 \frac{\partial \hat{d}}{\partial x} \right)^{-1} \frac{\partial}{\partial x} \left\{ \mu \left(\left(1 + k_1 \frac{\partial \hat{d}}{\partial x} \right)^2 - \left(1 + k_1 \frac{\partial \hat{d}}{\partial x} \right)^{-2} \right) \right. \\ & \left. + \eta k_1 \frac{\partial \hat{d}}{\partial t} \left(1 + \left(1 + k_1 \frac{\partial \hat{d}}{\partial x} \right)^{-2} \right) \right\} \end{aligned} \quad (2.37)$$

which, to leading order is

$$\frac{K}{4\gamma_0\mu} \frac{\partial \hat{d}}{\partial t} = \frac{\partial^2 \hat{d}}{\partial x^2} + \frac{\eta}{2\mu} \left(\frac{\partial^3 \hat{d}}{\partial x^2 \partial t} \right). \quad (2.38)$$

Neglecting terms of $\mathcal{O}(k_1^2)$, (2.37) reduces to the linearised PDE

$$t_s \frac{\partial \hat{d}}{\partial t} = \left(1 + t_k \frac{\partial}{\partial t} \right) \frac{\partial^2 \hat{d}}{\partial x^2}, \quad (0 < x < \hat{l}_0), \quad (2.39)$$

where $t_s = K/4\gamma_0\mu$ and $t_k = \eta/2\mu$ are characteristic relaxation times related to the substrate and internal viscosity respectively. A similar mechanical model was used by Gracheva and Othmer

[117] as a model for the motility of a single cell described as a one-dimensional element. In the limit $t_s = 0$ (no substrate damping), this PDE is reminiscent of the classical linear Kelvin–Voigt viscoelasticity [124]. Conversely, the limit $t_k = 0$ gives the diffusion equation. We can solve this system analytically. Substituting the ansatz (2.36) into the pressure in (2.35b) gives

$$\hat{p} = \mu \left(1 - 2k_1 \frac{\partial \hat{d}}{\partial x} \right) - \eta k_1 \frac{\partial^2 \hat{d}}{\partial t \partial x} + \mathcal{O}(k_1^2). \quad (2.40)$$

Firstly, for comparison to both the fully nonlinear discrete and continuum results below (Sec. 2.3.1), we consider a system with substrate damping but no viscous effects ($t_k = 0$). Noting that $\hat{x} = (1 - k_1)x$ is a steady-state solution of (2.39) satisfying $\hat{x}(l_0) = (1 - k_1)l_0$, we again assume small displacements of typical amplitude $0 < k_1 \ll l_0$, but now take $\hat{x}(x, t) = (1 - k_1)x + k_1 \check{d}(x, t)$, where $\check{d}(x, t)$ is the *displacement from the final steady-state solution*, thus $\hat{d}(x, t) = \check{d}(x, t) - x$. The PDE (2.39) becomes

$$t_s \frac{\partial \check{d}}{\partial t} = \frac{\partial^2 \check{d}}{\partial x^2}. \quad (2.41)$$

The boundary conditions of the prescribed displacement (2.33b) and (2.33c) are

$$\check{d}(0, t) = 0, \quad \check{d}(l_0, t) = l_0 \exp(-t), \quad (2.42)$$

where the prescribed deformation boundary condition is chosen to prescribe a smooth exponential shortening of the domain length for that allows for analytical solutions to be derived easily (rather than representing any realistic applications). The equivalent function is also used in the boundary conditions for the discrete and continuum simulations below to allow for comparisons. The initial condition is

$$\check{d}(x, 0) = x. \quad (2.43)$$

Using separation of variables, the boundary condition at $x = 0$ yields

$$\check{d}(x, t) = c \sin(x\sqrt{P}) \exp\left(-\frac{P}{t_s}t\right), \quad (2.44)$$

where c and P are constants. For compatibility with the prescribed boundary conditions at $x = l_0$, we require $P = t_s$ and $c = l_0 / \sin(l_0\sqrt{t_s})$, and the solution takes the form

$$\check{d}(x, t) = \frac{l_0 \sin(x\sqrt{t_s}) \exp(-t)}{\sin(l_0\sqrt{t_s})}. \quad (2.45)$$

Initially this function takes the form

$$\check{d}(x, 0) = \frac{l_0 \sin(x\sqrt{t_s})}{\sin(l_0\sqrt{t_s})}, \quad (2.46)$$

which, for small values of $\sqrt{t_s}$, becomes

$$\check{d}(x, 0) \approx x. \quad (2.47)$$

Hence the solution (2.45) is only valid in the limit of small t_s (and hence, small amounts of substrate dissipation, K). The pressure (2.40) with (2.45) becomes

$$\check{p}(x, t) = \mu + k_1(\eta - 2\mu) \frac{\sqrt{t_s} l_0 \cos(x\sqrt{t_s}) \exp(-t)}{\sin(l_0\sqrt{t_s})} + \mathcal{O}(k_1^2). \quad (2.48)$$

Secondly, the linearised PDE for the Kelvin dissipation system with no substrate damping is obtained from (2.39) with $t_s = 0$. The PDE (2.39) becomes

$$t_k \frac{\partial^3 \hat{d}}{\partial t \partial x^2} + \frac{\partial^2 \hat{d}}{\partial x^2} = 0. \quad (2.49)$$

For the boundary conditions (2.33b) and (2.33c), we take the linearised form

$$\hat{d}(0, t) = 0, \quad \text{and} \quad \hat{d}(l_0, t) = \begin{cases} -l_0(3t^2 - 2t^3), & (0 \leq t \leq 1), \\ -l_0, & (t > 1). \end{cases} \quad (2.50)$$

The boundary condition at $x = l_0$ is chosen to give a smooth decrease in domain length for $0 \leq t \leq 1$ with continuous derivatives at $t = 0$ and $t = 1$ to allow for analytical solutions to be derived easily (rather than representing any realistic applications). The equivalent function is also used in the boundary conditions for the discrete and continuum simulations below.

Integrating the linear PDE twice with respect to x yields

$$\frac{\partial \hat{d}}{\partial t} + \frac{1}{t_k} \hat{d} = f_1(t)x + f_2(t), \quad (2.51)$$

where $f_1(t)$ and $f_2(t)$ are functions of integration, independent of x . At $x = 0$, the boundary condition requires $f_2(t) = 0$. Applying the boundary condition at $x = \hat{l}_0$, (2.51) takes the form

$$\frac{\partial \hat{d}}{\partial t} + \frac{1}{t_k} \hat{d} = f_1(t)l_0 = \begin{cases} 6(t^2 - t) + (2t^3 - 3t^2)/t_k, & (0 \leq t \leq 1), \\ -1/t_k, & (t > 1). \end{cases} \quad (2.52)$$

Using an integrating factor for both cases and integrating, we obtain the analytical solution

$$\hat{d}(x,t) = \begin{cases} -x(3t^2 - 2t^3), & (0 \leq t \leq 1), \\ -x, & (t > 1). \end{cases} \quad (2.53)$$

The pressure (2.40) with (2.53) yields

$$\check{p}(x,t) = \begin{cases} \mu(1 + 2k_1)(3t^2 - 2t^3) - 6\eta k_1(t^2 - t), & (0 \leq t \leq 1), \\ \mu(1 + 2k_1), & (t > 1). \end{cases} \quad (2.54)$$

These analytical solutions are compared to predictions of the full nonlinear discrete and continuum systems in Sec. 2.3.1 below.

2.2.3 Comparison to macroscale static model for a long thin strip

We wish to compare the upscaled macroscale continuum tissue model derived in Sec. 2.2.1 with a model derived directly from a continuum framework. We consider a long, thin strip of continuous, incompressible, hyperelastic material of length l_0 and width W_0 , with constant, uniform shear modulus, μ . We describe the strip using reference coordinates $\mathbf{x} = (x, y)$ with x along the strip ($0 \leq x \leq l_0$) and y perpendicular ($-\frac{1}{2}W_0 \leq y \leq \frac{1}{2}W_0$). The deformations in the x - and y - directions are $\chi(x, y)$ and $\psi(x, y)$ respectively, and the incompressible deformation gradient is

$$\mathbb{F} = \begin{bmatrix} \frac{\partial \chi}{\partial x} & \frac{\partial \chi}{\partial y} \\ \frac{\partial \psi}{\partial x} & \frac{\partial \psi}{\partial y} \end{bmatrix} \quad (2.55)$$

We assume this material has strain-energy functional \mathscr{W} and Cauchy stress tensor

$$\boldsymbol{\sigma} = \mathbb{F} \frac{\partial \mathscr{W}}{\partial \mathbb{F}} - p(x, y) \mathbb{I}, \quad (2.56)$$

where p is a Lagrange multiplier analogous to the pressure.

For a long and thin strip, we assume that the strip width, W_0 , is much less than the length, l_0 . Hence

$$\gamma = \frac{\gamma_0}{N} = \frac{W_0}{NL_0} = \frac{W_0}{l_0} \ll 1. \quad (2.57)$$

We take $x, \chi \sim \mathcal{O}(1)$ and rescale $y = \gamma \tilde{y}$, $\psi = \gamma \tilde{\psi}$, where $\tilde{y}, \tilde{\psi} \sim \mathcal{O}(1)$ and assume the expansions

$$\begin{aligned} (\tilde{\chi}, \tilde{p}) &= (\chi_0(x, \tilde{y}), p_0(x, \tilde{y})) + \gamma^2 (\chi_2(x, \tilde{y}), p_2(x, \tilde{y})) + \mathcal{O}(\gamma^4), \\ \tilde{\psi} &= \gamma \psi_1(x, \tilde{y}) + \gamma^3 \psi_3(x, \tilde{y}) + \mathcal{O}(\gamma^5). \end{aligned} \quad (2.58)$$

We assume this form of expansions to capture the asymmetry of the system. Due to the long thin approximation, lengths in the x -direction are of order 1, while lengths in the y -direction are

of order γ , hence we expand χ in even powers of γ and ψ in odd powers of γ . We have,

$$\mathbb{F} = \begin{bmatrix} \frac{\partial \chi_0}{\partial x} & \frac{1}{\gamma_0} \frac{\partial \chi_0}{\partial \bar{y}} + \gamma_0 \frac{\partial \chi_2}{\partial y} \\ \gamma_0 \frac{\partial \psi_1}{\partial x} & \frac{\partial \psi_1}{\partial \bar{y}} \end{bmatrix} + \mathcal{O}(\gamma_0^2), \quad (2.59)$$

$$\boldsymbol{\sigma} = \begin{bmatrix} \frac{1}{\gamma_0} \frac{\partial \chi_0}{\partial y} \mathscr{W}_{21} + \frac{\partial \chi_0}{\partial x} \mathscr{W}_{11} - p_0 & \frac{1}{\gamma_0} \frac{\partial \chi_0}{\partial \bar{y}} \mathscr{W}_{22} + \frac{\partial \chi_0}{\partial x} \mathscr{W}_{12} \\ \gamma_0 \frac{\partial \psi_1}{\partial x} \mathscr{W}_{21} & \frac{\partial \psi_1}{\partial \bar{y}} \mathscr{W}_{22} - p_0, \end{bmatrix} + \mathcal{O}(\gamma_0), \quad (2.60)$$

where $\mathscr{W}_{ij} = \partial \mathscr{W} / \partial \mathbb{F}_{ji}$ are $\mathcal{O}(1)$. The incompressibility condition, $\det(\mathbb{F}) = 1$ requires, to leading order,

$$\frac{\partial \chi_0}{\partial x} \frac{\partial \psi_1}{\partial y} - \frac{\partial \chi_0}{\partial y} \frac{\partial \psi_1}{\partial x} = 1. \quad (2.61)$$

We apply the condition of no lateral forcing on the long edges of the strip,

$$\boldsymbol{\sigma} \cdot \mathbf{e}_2 = \mathbf{0}, \quad (2.62)$$

which requires, at $\mathcal{O}(\gamma_0^{-1})$

$$\frac{\partial \chi_0}{\partial \bar{y}} = 0, \quad (2.63)$$

and at $\mathcal{O}(1)$, requires

$$p_0 = \frac{\partial \psi_1}{\partial \bar{y}} \mathscr{W}_{22}, \quad (2.64)$$

to leading order, using (2.59). The incompressibility condition then takes the form

$$\frac{\partial \psi_1}{\partial y} = \left(\frac{\partial \chi_0}{\partial x} \right)^{-1}. \quad (2.65)$$

We consider the equilibrium equation

$$\nabla \cdot \boldsymbol{\sigma} = 0, \quad (2.66)$$

where $\nabla = (\frac{\partial}{\partial x}, \gamma^{-1} \frac{\partial}{\partial \bar{y}})$. To leading order, this yields the nonlinear ODE

$$0 = \frac{\partial}{\partial x} \left(\mathscr{W}_{11} \frac{\partial \chi_0}{\partial x} - \mathscr{W}_{22} \left(\frac{\partial \chi_0}{\partial x} \right)^{-1} \right), \quad (2.67)$$

which describes the steady solution of the fully non-linear macroscale continuum PDE system.

Neo-Hookean material

In the particular case of a neo-Hookean material, with a uniaxial deformation, we have

$$\mathcal{W}_{11} = \mu \frac{\partial \chi_0}{\partial x}, \quad \mathcal{W}_{22} = \mu \frac{\partial \psi_1}{\partial y}. \quad (2.68)$$

The condition of no normal stress along the long edges of the material, (2.64) with (2.65), becomes

$$p_0 = \mu \left(\frac{\partial \chi_0}{\partial x} \right)^{-2}. \quad (2.69)$$

Expanding the equilibrium equations to the leading order and substituting for ψ_1 and p_0 we obtain

$$0 = \mu \frac{\partial^2 \chi_0}{\partial x^2} \left(1 + \left(\frac{\partial \chi_0}{\partial x} \right)^{-4} \right). \quad (2.70)$$

This ODE can be integrated once, giving

$$\mu \left(\left(\frac{\partial \chi_0}{\partial x} \right)^2 - \left(\frac{\partial \chi_0}{\partial x} \right)^{-2} \right) = C \quad (2.71)$$

where C is an integration constant. Applying boundary conditions of fixed displacement $\chi_0(x=0) = 0$ and $\chi_0(x=l_0) = l$, this system has a solution of linear displacement

$$\chi_0(x) = x \sqrt{\frac{l^4 - l_0^4}{2l^2 l_0^2} + \sqrt{\left(\frac{l_0^4 - l^4}{2l^2 l_0^2} \right)^2 + 1}} = \frac{l}{l_0} x, \quad (2.72)$$

since $l, l_0 > 0$, which is compared to the time-dependent predictions of the discrete and continuum simulations below.

For a prescribed deformed length of $l = l_0(1 - k_1)$, where k_1 represents the fractional decrease in length of the array, (2.72) becomes

$$\chi_0(x) = x(1 - k_1), \quad (2.73)$$

where we have considered only the positive square roots (to avoid negative or imaginary solutions).

2.2.4 Numerical Solutions

The continuum PDE system for Neo-Hookean cells (2.35a) is solved numerically using the MATLAB solver `ode15s` along with a spatial discretisation scheme. Note that for specific choices

of finite difference stencils and number of discretisation points, one can revert back to the discrete formulation, however we do not use these specific stencils here (as we wish to use higher order stencils). The spatial domain ($0 \leq x \leq l_0$) is divided into n equally sized spatial intervals. We use a second order centered-finite-difference scheme for the mid-points,

$$\frac{\partial \hat{x}^{(i)}}{\partial x} = \frac{1}{2dX} \left(\hat{x}^{(i+1)} - \hat{x}^{(i-1)} \right) + \mathcal{O}(dX^2) \quad (i = 2, \dots, n-1), \quad (2.74a)$$

$$\frac{\partial^2 \hat{x}^{(i)}}{\partial x^2} = \frac{1}{dX^2} \left(\hat{x}^{(i-1)} - 2\hat{x}^{(i)} + \hat{x}^{(i+1)} \right) + \mathcal{O}(dX^2) \quad (i = 2, \dots, n-1), \quad (2.74b)$$

where $dX = l_0/n$ is the step size and $\hat{x}^{(i)}$ is a discretisation point in the domain ($i = 1, \dots, n$). For the boundary conditions, we use a second order forward or backward finite-difference scheme,

$$\frac{\partial \hat{x}^{(1)}}{\partial x} = \frac{1}{2dX} \left(-3\hat{x}^{(1)} + 4\hat{x}^{(2)} - \hat{x}^{(3)} \right) + \mathcal{O}(dX^2), \quad (2.74c)$$

$$\frac{\partial \hat{x}^{(n)}}{\partial x} = \frac{1}{2dX} \left(3\hat{x}^{(n)} - 4\hat{x}^{(n-1)} + \hat{x}^{(n-2)} \right) + \mathcal{O}(dX^2). \quad (2.74d)$$

Since variations occur over the lengthscale l_0 , not the lengthscale $O(1)$, the step-size dX need not be fine, but rather $dX \ll l_0$. In simulations below, for small K , $dX = 1$. However, for larger K , we use more stencil points due to the boundary layer that forms in the system from the high levels of dissipation. Hence, variations occur over a smaller boundary lengthscale and in this system we use $dX = 0.05$. Convergence for a variety of choices of discretisation points (and hence, step-size) are discussed below.

Due to the additional time-derivative terms in the viscous stress formulation, we must rearrange (2.35a) to be compatible with the solver. Note that this equation expands to the form

$$\begin{aligned} K \frac{\partial \hat{x}}{\partial t} - \eta \left(\frac{\partial^3 \hat{x}}{\partial x^2 \partial t} \left(\frac{\partial \hat{x}}{\partial x} \right)^{-1} \left(1 + \left(\frac{\partial \hat{x}}{\partial x} \right)^{-2} \right) - 2 \frac{\partial^2 \hat{x}}{\partial x^2} \left(\frac{\partial \hat{x}}{\partial x} \right)^{-3} \frac{\partial^2 \hat{x}}{\partial x \partial t} \right) \\ = \gamma_0 \left(2 \frac{\partial^2 \hat{x}}{\partial x^2} \hat{\mu} \left(1 - \left(\frac{\partial \hat{x}}{\partial x} \right)^{-4} \right) \right), \quad (0 < x < l_0). \end{aligned} \quad (2.75)$$

Applying the stencils (2.74a), this can be written as

$$\begin{aligned}
& \left\{ K + \frac{2\eta}{dX^2} \left(\left(\frac{\partial x_n^{(i)}}{\partial x} \right)^{-1} + \left(\frac{\partial x_n^{(i)}}{\partial x} \right)^{-3} \right) \right\} \frac{\partial \hat{x}_n^{(i)}}{\partial t} \\
& + \eta \left\{ \frac{1}{dX} \frac{\partial^2 x_n^{(i)}}{\partial x^2} \left(\frac{\partial x_n^{(i)}}{\partial x} \right)^{-4} - \frac{1}{dX^2} \left(\left(\frac{\partial x_n^{(i)}}{\partial x} \right)^{-1} + \left(\frac{\partial x_n^{(i)}}{\partial x} \right)^{-3} \right) \right\} \frac{\partial \hat{x}_n^{(i+1)}}{\partial t} \\
& + \eta \left\{ -\frac{1}{dX} \frac{\partial^2 x_n^{(i)}}{\partial x^2} \left(\frac{\partial x_n^{(i)}}{\partial x} \right)^{-4} - \frac{1}{dX^2} \left(\left(\frac{\partial x_n^{(i)}}{\partial x} \right)^{-1} + \left(\frac{\partial x_n^{(i)}}{\partial x} \right)^{-3} \right) \right\} \frac{\partial \hat{x}_n^{(i-1)}}{\partial t} \\
& = 2\gamma_0\mu \frac{\partial^2 x_n^{(i)}}{\partial x^2} \left(1 + \left(\frac{\partial x_n^{(i)}}{\partial x} \right)^{-4} \right), \quad (0 < x < l_0).
\end{aligned} \tag{2.76}$$

We can then define this system within the ODE solver as the matrix problem

$$\mathbf{M}_n \frac{d\mathbf{X}}{dt} = \mathbf{f}_n, \tag{2.77}$$

where \mathbf{X} has entries of the spatial discretisation points $x^{(i)}$ ($i = 1, \dots, n$), \mathbf{M}_n is the $n \times n$ matrix with first and last entries equal to one and, for $i = 2, \dots, n-1$

$$\mathbf{M}_n(i, i-1) = \eta \left\{ -\frac{1}{dX} \frac{\partial^2 x_n^{(i)}}{\partial x^2} \left(\frac{\partial x_n^{(i)}}{\partial x} \right)^{-4} - \frac{1}{dX^2} \left(\left(\frac{\partial x_n^{(i)}}{\partial x} \right)^{-1} + \left(\frac{\partial x_n^{(i)}}{\partial x} \right)^{-3} \right) \right\}, \tag{2.78a}$$

$$\mathbf{M}_n(i, i) = \left\{ K + \frac{2\eta}{dX^2} \left(\left(\frac{\partial x_n^{(i)}}{\partial x} \right)^{-1} + \left(\frac{\partial x_n^{(i)}}{\partial x} \right)^{-3} \right) \right\}, \tag{2.78b}$$

$$\mathbf{M}_n(i, i+1) = \eta \left\{ \frac{1}{dX} \frac{\partial^2 x_n^{(i)}}{\partial x^2} \left(\frac{\partial x_n^{(i)}}{\partial x} \right)^{-4} - \frac{1}{dX^2} \left(\left(\frac{\partial x_n^{(i)}}{\partial x} \right)^{-1} + \left(\frac{\partial x_n^{(i)}}{\partial x} \right)^{-3} \right) \right\}. \tag{2.78c}$$

and \mathbf{f}_n is the vector

$$\mathbf{f}_n = \begin{bmatrix} 0 \\ \vdots \\ 2\gamma_0\mu \frac{\partial^2 x_n^{(i)}}{\partial x^2} \left(1 - \left(\frac{\partial x_n^{(i)}}{\partial x} \right)^{-4} \right) \\ \vdots \\ \gamma_0\mu \left(\left(\frac{\partial x_n^{(n)}}{\partial x} \right) - \left(\frac{\partial x_n^{(n)}}{\partial x} \right)^{-3} \right) \end{bmatrix}. \tag{2.79}$$

	$a_t = 10^{-8}$ to $a_t = 1$
$n = 10$	29.436232
$n = 50$	14.750124
$n = 100$	14.080681
$n = 200$	13.953633
$n = 500$	13.920982
$n = 1000$	13.916439
$n = 2000$	13.915242

Table 2.1: Values of \hat{p} (to 6 d.p.) at the last discretisation point (n) at $t = 10$ for values of the absolute tolerance, a_t (with $r_t = 10^{-6}$) for different numbers of discretisation points, n . Note that these values are identical for identical values of r_t with $a_t = 10^{-6}$.

The MATLAB solver `ode15s` chooses temporal step-sizes based on the absolute, a_t , and relative, r_t tolerances chosen. The error in this system is dominated by the error from the stencil and spatial discretisation step-size, dX . The numerical scheme outlined in this section converges to a fixed solution for values from $n = 10$ to $n = 150$ for values of absolute tolerances from $a_t = 10^{-8}$ to $a_t = 1$ (Table 2.1) and for relative tolerances from $r_t = 10^{-8}$ to $r_t = 1$ (values identical for Table 2.1 with $a_t = 10^{-6}$, hence not duplicated) when considering the pressure, \hat{p} at the prescribed deformation (the end point in the domain). In the results below, we show the agreement with both the analytical solutions to the linearised equations from Sec. 2.2.2 and the discrete system.

Since there is no need for this number of intervals to be the same as the number of discrete cells in the IBM, this continuum PDE approach can result in a significant computational saving compared to the IBM when the number of discrete cells is large.

In the results below we compute the continuum pressure (2.31) and stretch (2.32), which are compared to the discrete simulations.

2.3 Results (Incompressible Cells)

We numerically solve the discrete and continuum systems with $\gamma_0 = 1$ and $\mu = 1$. We use $N = 100$ cells in the discrete systems and $n = 100$ grid points in the continuum model, unless otherwise stated.

2.3.1 Case 1: Prescribed deformation

To benchmark our model we consider the case of prescribed displacement at one end of the array with no growth. The discrete system of cells aligned in a single array is defined by (2.22h), subject to boundary conditions (2.22i), defining a fixed boundary at $x = 0$ and a prescribed displacement at the other end of the domain. The continuum system is defined by (2.35a) with

boundary conditions (2.33b) and (2.33c).

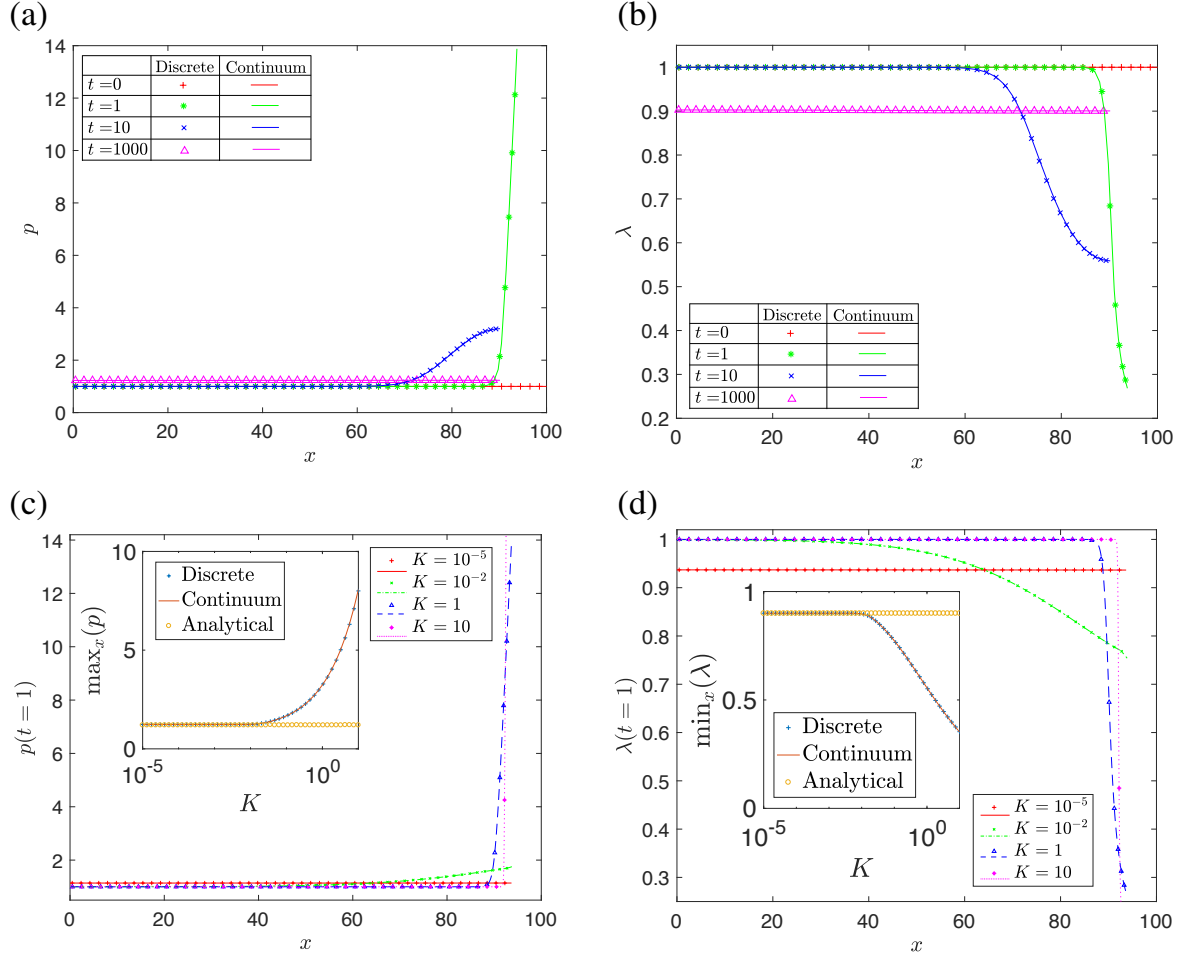


Figure 2.5: Solutions for a system of incompressible Neo-Hookean cells aligned in a single array subject to a prescribed displacement (10% decrease in full array length) with substrate dissipation. Solutions for $N = 100$ cells, $\eta = 0$ and uniform shear modulus $\mu = 1$. Discrete solutions (symbols $*$, $+$, \times and \triangle) are displayed with corresponding upscaled continuum solutions (lines) and analytical solutions (symbols \circ , \square , \diamond). (a) Pressure, $p(x, t)$ in the array at $t = 0, 1, 10, 1000$ with $K = 1$; (b) Elastic stretch, $\lambda_1(x, t)$ in the array at $t = 0, 1, 10, 1000$ with $K = 1$; (c) $\max_x(p)$ at $t = 1$ for $K = 10^{-5}, 1, 10$ (inset: $\max_x(p)$ for $t = 10$ for $K = 10^{-5}$ to $K = 1$); (d) $\min_x(\lambda_1)$, at $t = 1$ for $K = 10^{-5}, 1, 10$ (inset: $\min_x(\lambda_1)$ for $t = 10$ for $K = 10^{-5}$ to $K = 1$).

First we consider the system with substrate dissipation only (no viscoelasticity, $\eta = 0$), for various values of K . The length of the domain is prescribed as a saturating function of time,

$$l(t) = l_0(1 - k_1) + k_1 l_0 \exp\left(-\frac{t_0}{t_{\text{ramp}}}t\right), \quad (2.80)$$

where t_{ramp} is the rate of ramping of the prescribed displacement and k_1 (constant) represents the fractional decrease in length of the array. In simulations we choose $k_1 = 0.1$, corresponding to a 10% strain in the final state and we choose $t_{\text{ramp}} = t_0$ to simplify (2.80). We compare the

numerical solutions to the analytical solution in (2.45).

In order to assess the dynamic response of the system, Fig. 2.5 illustrates solutions with $K = 1$, showing spatial profiles of pressure (Fig. 2.5a) and stretch (Fig. 2.5b) at various times. Initially, cells towards the displaced end of the array undergo a large deformation, becoming compressed with increased pressure (Fig. 2.5a), while those at the fixed end remain relatively unstressed. Once the prescribed deformation has saturated, the system then relaxes toward equilibrium with cells at the fixed end becoming increasingly compressed and cells at the displaced end relaxing to the new equilibrium (Fig. 2.5b). The maximal pressure observed across the array at a fixed time increases with increasing K (Fig. 2.5c), also reflected in the maximum compression of the array at that time, which decreases with increasing K (Fig. 2.5d). Note that in all cases, the discrete and continuum solutions agree extremely well, though the analytical solutions, (2.45), do not agree well for large K as the analytical solution is only valid for small K (see discussion in Sec. 2.2.2). For example, for large enough K ($K > 10^{-2}$) the maximum pressure in the array diverges from numerical solutions (Fig. 2.5c), while the minimum stretch profiles for $K > 10^{-2}$ appear to oscillate (or wiggle) around the value for $K < 10^{-2}$ (Fig. 2.5d). In summary, this figure demonstrates the damping effect of K , outlining the delay of cell response to a prescribed displacement.

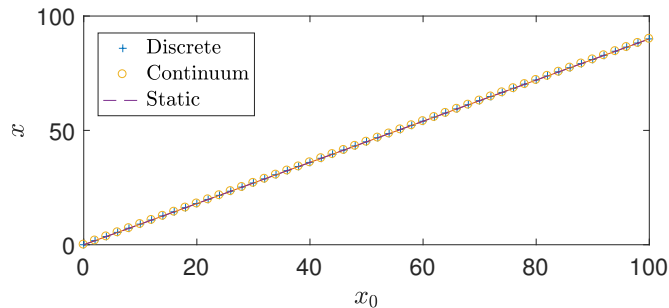


Figure 2.6: Steady state solutions for a system of incompressible Neo-Hookean cells aligned in a single array subject to a prescribed displacement (10% decrease in full array length) with substrate dissipation ($K = 10^{-5}$). Solutions for $N = 100$ cells ($n = 2000$ continuum nodes) and uniform shear modulus $\mu = 1$. Discrete solutions (symbols) are displayed with corresponding upscaled continuum solutions (line with circles) for $t \gg 1$ and static macroscale model solutions (dash line). The profile in x (discrete, continuum), and x_0 (static macroscale) is displayed against initial position, x_0 .

We also compare solutions to this system with the static macroscale model derived in Sec. 2.2.3. For $K = 10^{-5}$, the system has saturated by $t = 10$, and so we compare the spatial profile to that of the steady solution (2.73). These solutions are displayed in Fig. 2.6 and show an excellent agreement, with all solutions showing a linear profile in x (since the cells have uniform shear modulus).

Alternatively, we consider the system with Kelvin viscoelasticity but no substrate dissipation

($K = 0$). To facilitate comparison with analytical solutions (Sec. 2.2.2), the prescribed length of the domain is defined by the smooth polynomial function with continuous first derivative

$$l(t) = \begin{cases} l_0 (1 - k_1 (3t^2 - 2t^3)), & (0 \leq t \leq \frac{t_{\text{ramp}}}{t_0}), \\ l_0 (1 - k_1), & (t > \frac{t_{\text{ramp}}}{t_0}), \end{cases} \quad (2.81)$$

where the constant k_1 represents the fractional decrease in length of the array. In simulations we choose $k_1 = 0.1$ and $t_{\text{ramp}} = t_0$ (the ramping time). We solve the IBM and PDE models for various values of η and compare the results with the predictions of the analytical model (2.53).

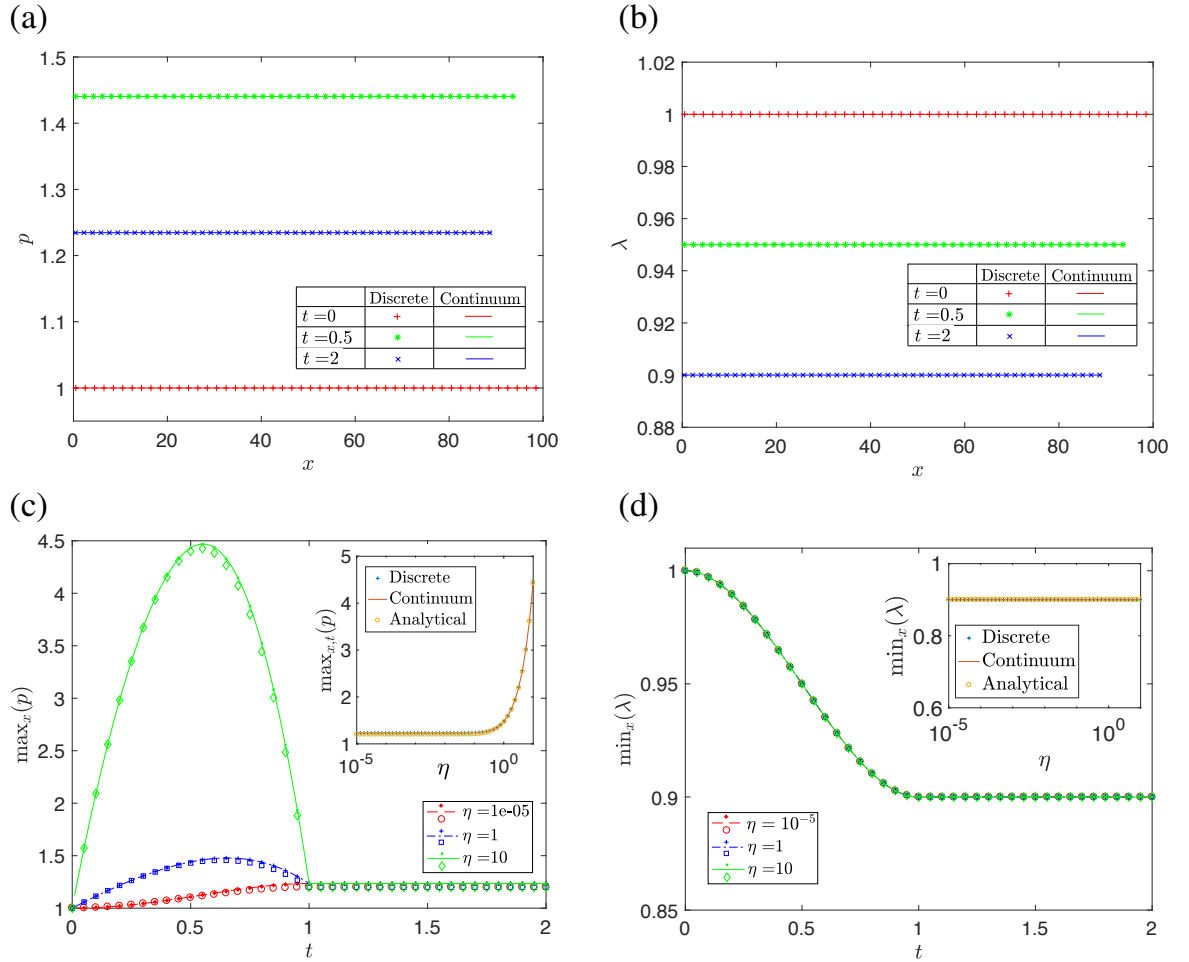


Figure 2.7: Solutions for a system of incompressible Neo-Hookean cells aligned in a single array subject to a prescribed displacement (10% decrease in full array length) with substrate dissipation. Solutions for $N = 100$ cells ($n = 101$ continuum nodes) and uniform shear modulus $\mu = 1$. Discrete solutions (symbols) are displayed with corresponding upscaled continuum solutions (lines) and analytical solutions (shapes). (a) Pressure, $p(x, t)$ in the array at $t = 0, 1, 10, 1000$ with $\eta = 1$; (b) Elastic stretch, $\lambda(x, t)$ in the array at $t = 0, 1, 10, 1000$ with $\eta = 1$; (c) $\max_x(p)$ for $t = 0$ to $t = 3$ at $\eta = 10^{-5}, 1, 10$ (inset: $\max_{x,t}(p)$ for $t = 0$ to $t = 10$ for $\eta = 10^{-5}$ to $\eta = 10$); (d) $\min_x(\lambda)$, for $t = 0$ to $t = 2$ at $\eta = 10^{-5}, 1, 10$ (inset: $\min_{x,t}(\lambda)$ for $t = 0$ to $t = 10$ for $\eta = 10^{-5}$ to $\eta = 10$).

Figure 2.7 illustrates solutions with $\eta = 10^{-2}$, including the pressure (Fig. 2.7a) and the stretch (Fig. 2.7b). Across all these approaches, the system responds in a spatially uniform manner (Fig. 2.7a,b). Over time, we observe that the maximum pressure across the array, $\max_x(p)$ (Fig. 2.7c), initially increases, reaching a maximum before decreasing again toward equilibrium beyond $t > 1$. This maximum pressure over the entire simulation increases as η increases (Fig. 2.7c). Also, the temporal profiles in Fig. 2.7c indicate that as η increases, the time where the maximum occurs approaches the time where the rate of change in length is greatest ($t = 0.5$ in this case). Similarly, for all values of η the maximal compression across the array, $\min_x(\lambda)$, (Fig. 2.7d) decreases towards equilibrium.

The results demonstrate an excellent agreement between discrete, continuum and analytical models in all cases. In summary, this figure demonstrates that, while the visual response of the systems are identical and spatially uniform, the viscous parameter η affects the internal pressure of cells. The analytical solutions for this system (derived in Sec 2.2.2) for displacement (2.53) and pressure (2.54) indicate solutions of stretch and pressure being uniform in x .

2.3.2 Case 2: Non-uniform shear modulus

We consider the prescribed displacement defined in 2.80 with $k_1 = 0.1$. However, we now consider a non-uniform shear modulus, μ , to consider inhomogeneous cells. We choose a shear modulus in the form of a normal distribution. Most cells have $\mu \approx 1$, however a cluster of cells have a higher shear modulus, $\mu > 1$, to represent a cluster of stiffer cells in the array (e.g. dead or dying cells following a myocardial infarction, as these cells tend to be stiffer during the first few weeks following an infarction [125]). The shear modulus takes the form

$$\mu(x) = 1 + \exp\left(-\frac{(x_0 - b)^2}{2c^2}\right) \quad (2.82)$$

where b and c are the location of the centre of the peak and the standard deviation of the normal distribution respectively. In simulations, we choose $b = l_0/2$ and $c = l_0/10$.

In the absence of internal viscous dissipation ($\eta = 0$) for $K = 1$ we observe increased pressure in the cells at the moving boundary as in the case with uniform shear modulus (due to the dissipation in the system resulting in a lag in force transmission along the array), however we now observe an increased pressure at the middle of the array, where the cluster of cells with an increased shear modulus are located (Fig. 2.8a). For smaller values of K , the boundary layer at the prescribed deformation disappears and the inhomogeneity in the array pressure arises solely from the inhomogeneity in the shear modulus (Fig. 2.8a inset). For $K = 1$ the elastic stretch of the cells is, for early times, shows compression in the cells at the deformed boundary, while for smaller K we observe that cells with a higher shear modulus undergo less compression (Fig. 2.8b). Note that for longer times for $K = 1$ the system relaxes to the equilibrium configuration shown in the case for $K = 10^{-5}$, with a cluster of cells at the centre less compressed than

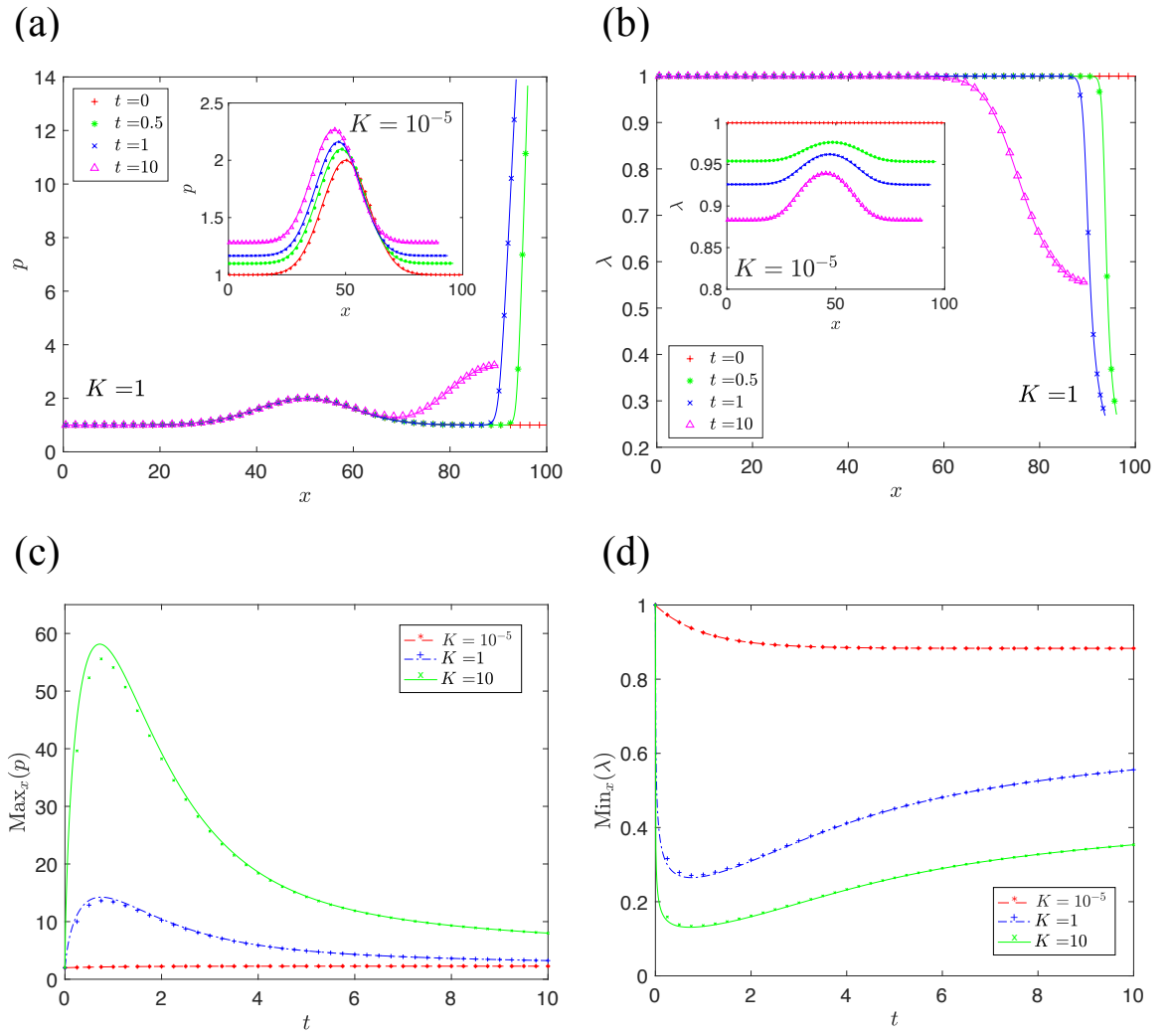


Figure 2.8: Solutions for a system of incompressible Neo-Hookean cells aligned in a single array subject to a prescribed displacement (10% decrease in full array length) with substrate damping in the absence of viscous dissipation ($\eta = 0$). The system is considered with a non-uniform $\mu(x)$ as defined in (2.82). (a) $p(x,t)$ over x at $t = 0, 0.5, 1, 10$ for $K = 1$ (inset with the case for $K = 10^{-5}$); (b) $\lambda(x,t)$ over x at $t = 0, 0.5, 1, 10$ for $K = 1$ (inset with the case for $K = 10^{-5}$); (c) $\max_x(p)$ for $t = 0$ to $t = 10$ for $K = 10^{-5}, 1, 10$; (d) $\min_x(\lambda)$ for $t = 0$ to $t = 10$ for $K = 10^{-5}, 1, 10$.

those towards the boundaries of the array. The maximum pressure (Fig. 2.8c) and the maximum compression (Fig. 2.8d) in the array are larger for larger K .

In the absence of substrate dissipation ($K = 0$), we observe the pressure profile reflects the profile of the shear modulus (as was the case for uniform shear modulus) and that for larger η , the maximum pressure in the array is larger. However, the pressure in the array saturates to an equilibrium configuration for $t > 1$ (Fig. 2.9a). We note that the value of this saturation ($\max_x(p) \approx 2.267$ for large t) is larger than the system with uniform μ ($\max_x(p) \approx 1.235$ for large t), as are the ‘peaks’ of $\max_x(p)$. The maximum compression in the array saturates to a

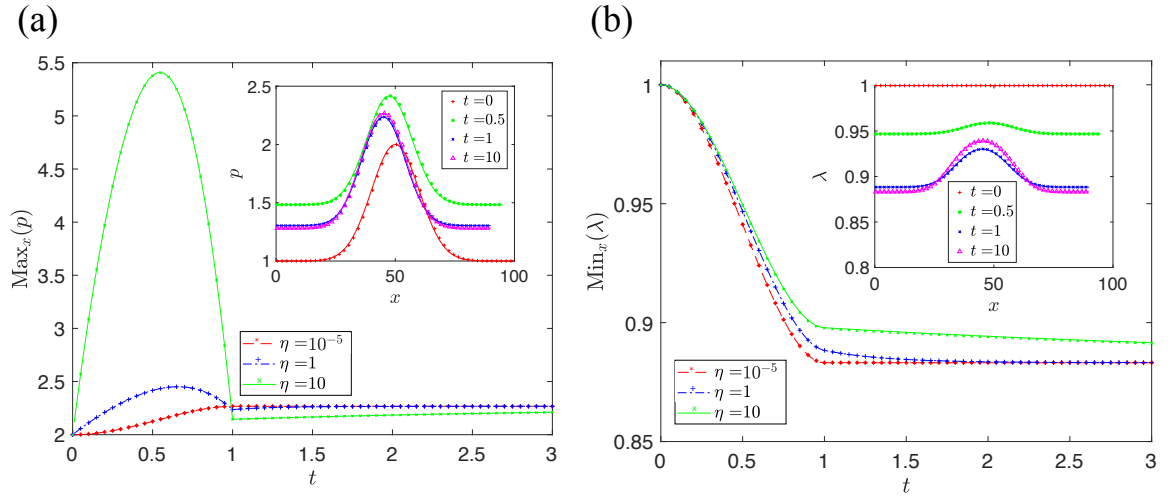


Figure 2.9: Solutions for a system of incompressible Neo-Hookean cells aligned in a single array subject to a prescribed displacement (10% decrease in full array length) with viscous damping in the absence of substrate damping ($K = 0$). The system is considered with a non-uniform $\mu(x)$ as defined in (2.82). (a) $\text{max}_x(p)$ for $t = 0$ to $t = 3$ for $\eta = 10^{-5}, 1, 10$ (inset with $p(x, t)$ over x at $t = 0, 0.5, 1, 10$ for $\eta = 1$); (b) $\text{min}_x(\lambda)$ for $t = 0$ to $t = 3$ for $\eta = 10^{-5}, 1, 10$ (inset with $\lambda(x, t)$ over x at $t = 0, 0.5, 1, 10$ for $\eta = 1$).

lower value ($\text{min}_x(\lambda) \approx 0.88$ for large t) than the uniform μ ($\text{min}_x(\lambda) = 0.9$ for large t) in this system since the cells at the centre with the larger shear modulus are stiffer, and undergo less compression, hence neighbouring cells must compress more to accommodate the prescribed deformation (Fig. 2.9b). All systems show an excellent agreement between discrete and continuum solutions.

2.4 Application to cardiac tissue: active contraction

We now apply the one-dimensional modelling framework presented in Sec. 2.1 to model a cardiac myofibre, the constituent tissue of the human heart. In this framework we ignore the influence of growth and cell division, which will occur on much longer timescales than an individual heartbeat. In addition, we now apply periodic boundary conditions to mimic a ring of myocardium. However, this approximation neglects the curvature effects that would arise in a ring and is only valid when the resting cell length is much smaller than the circumference (length of the array), i.e. for a large number of cells.

2.4.1 Discrete active contraction model

To incorporate active contraction of individual cells into the discrete model of Sec. 2.1 we modify the Cauchy stress to include an active contraction component (following [53]) of the

form

$$C_a^{(j)} = b^{(j)}(t) \left(1 + \frac{\beta}{2} (\lambda^{(j)} - 1) \right), \quad (2.83)$$

where $b^{(j)}(t)$ is a time-dependent function driven by the underlying electrical signalling and β is a constant. In particular, we choose the functional form

$$b^{(j)}(t) = 1 + \sin \left(2\pi\omega t - t_R^{(j)} \right), \quad (2.84)$$

where ω is the frequency and $t_R^{(j)} = 2\pi(j-1)$ is the discrete phase ($j = 1, \dots, N$). This form defines a periodic contractile force propagating across the domain.

The Cauchy stress is given by

$$\boldsymbol{\sigma}^{(j)} = \boldsymbol{\sigma}_e^{(j)} + \boldsymbol{\sigma}_v^{(j)} + C_a^{(j)} \hat{\mathbf{x}} \otimes \hat{\mathbf{x}}, \quad (2.85)$$

where $\boldsymbol{\sigma}_e^{(j)}$ is the elastic stress component in (2.8) and $\boldsymbol{\sigma}_v^{(j)}$ is the viscous stress component in (2.9), $\hat{\mathbf{x}}$ is the unit vector in the x -direction and \otimes is the tensor product (the contractive force is implemented purely in the x -direction).

The forcing now takes the form

$$\begin{aligned} \mathbf{F}_{\pm}^{(j)} &= F_{\pm}^{(j)} \hat{\mathbf{x}} = \mp \hat{\mathbf{x}} \int_{-\frac{1}{2}W^{(j\pm 1/2)}}^{\frac{1}{2}W^{(j\pm 1/2)}} \left(\lambda_1^{(j)} \mathcal{W}_1^{(j)} - \lambda_2^{(j)} \mathcal{W}_2^{(j)} + C_a^{(j)} \right) dy, \\ &= \mp \hat{\mathbf{x}} W^{(j\pm 1/2)} \left(\lambda_1^{(j)} \mathcal{W}_2^{(j)} - \lambda_2^{(j)} \mathcal{W}_2^{(j)} + C_a^{(j)} \right) \quad (j = 1, \dots, N), \end{aligned} \quad (2.86)$$

and the non-dimensional system becomes

$$\begin{aligned} K \frac{dx_b^{(j+1/2)}}{dt} &= W^{(j+1/2)} \left(\left(\lambda_1^{(j+1)} \mathcal{W}_1^{(j+1)} - \lambda_1^{(j)} \mathcal{W}_1^{(j)} \right) - \left(\lambda_2^{(j+1)} \mathcal{W}_2^{(j+1)} - \lambda_2^{(j)} \mathcal{W}_2^{(j)} \right) \right) \\ &\quad + \eta^{(j+1)} \left(\dot{\lambda}_1^{(j+1)} - \dot{\lambda}_2^{(j+1)} \right) - \eta^{(j)} \left(\dot{\lambda}_1^{(j)} - \dot{\lambda}_2^{(j)} \right) + C_a^{(j+1)} - C_a^{(j)} \end{aligned} \quad (2.87a)$$

for $j = 2, \dots, N$. For all systems, we implement a periodic domain, hence we have

$$x_b^{(N+1/2)} = x_b^{(1/2)}(t) + l_0. \quad (2.87b)$$

Neo-Hookean Material

For a Neo-Hookean material with cell-level strain-energy function (2.6), the non-dimensional system is defined by

$$\begin{aligned} K \frac{dx_b^{(j+1/2)}}{dt} = & W^{(j+1/2)} \left(\mu^{(j+1)} \left(\left(\lambda_1^{(j+1)} \right)^2 - \left(\lambda_1^{(j+1)} \right)^{-2} \right) - \mu^{(j)} \left(\left(\lambda_1^{(j)} \right)^2 - \left(\lambda_1^{(j)} \right)^{-2} \right) \right. \\ & \left. + \eta^{(j+1)} \lambda_1^{(j+1)} \left(1 - \left(\lambda_1^{(j+1)} \right)^{-2} \right) - \bar{\eta}^{(j)} \lambda_1^{(j)} \left(1 - \left(\lambda_1^{(j)} \right)^{-2} \right) + C_a^{(j+1)} - C_a^{(j)} \right) \end{aligned} \quad (2.88a)$$

for $j = 2, \dots, N$, with boundary condition (2.87b).

2.4.2 Continuum active contraction model

To derive the corresponding continuum equation we take the scalings (2.25)-(3.35) and Taylor expand (2.87a) around $j\varepsilon$. We obtain the leading order continuum PDE,

$$\tilde{K} \frac{\partial \hat{x}}{\partial t} = \hat{W} \frac{\partial}{\partial x} \left(\hat{\lambda}_1 \mathscr{W}_1 - \hat{\lambda}_2 \mathscr{W}_2 + \eta \frac{\partial}{\partial t} (\hat{\lambda}_1 - \hat{\lambda}_2) + \hat{b} \left(1 + \frac{\beta}{2} \left(\frac{\partial \hat{x}}{\partial x} - 1 \right) \right) \right), \quad (2.89)$$

where \hat{b} is the upscaled function

$$\hat{b} = 1 + \sin(2\pi\omega t - \hat{t}_R), \quad (2.90)$$

with $\hat{t}_R = 2\pi x$.

We implement a periodic domain and periodic boundary conditions corresponding to (2.87b), by defining

$$\hat{x} \Big|_{X=0} = \hat{x} \Big|_{X=1} + l_0. \quad (2.91)$$

Neo-Hookean Material

For a Neo-Hookean material with cell-level strain-energy function (2.6), we obtain the continuum PDE

$$\begin{aligned} \hat{K} \frac{\partial \hat{x}}{\partial t} = & \gamma_0 \left(\frac{\partial \hat{x}}{\partial x} \right)^{-1} \frac{\partial}{\partial x} \left(\hat{\mu} \left(\left(\frac{\partial \hat{x}}{\partial x} \right)^2 - \left(\frac{\partial \hat{x}}{\partial x} \right)^{-2} \right) + \hat{\eta} \frac{\partial}{\partial t} \left(\frac{\partial \hat{x}}{\partial x} - \left(\frac{\partial \hat{x}}{\partial x} \right)^{-1} \right) \right. \\ & \left. + \hat{b} \left(1 + \frac{\beta}{2} \left(\frac{\partial \hat{x}}{\partial x} - 1 \right) \right) \right), \quad (0 < x < \hat{l}_0), \end{aligned} \quad (2.92)$$

with boundary conditions (2.91)

2.4.3 Results for the active contraction model

The discrete system (2.88a) with boundary condition (2.87b) was solved for $N = 100$ cells and active contraction parameter $t_R^{(i)} = \pi x_0^{(i)} / N$ for a Neo-Hookean material. The continuum system (2.92) with boundary condition (2.91) was solved for $n = 50$ nodes and $\hat{t}_R = \pi \hat{x}_0 / N$. For all simulations we took $\gamma_0 = 1$, $\mu = 1$, $\beta = -1$ and $\omega = 1/l_0$. Both systems were solved for values from $K = 10^{-5}$ to $K = 10$.

For $K = 10^{-2}$ we observe a travelling wave passing along the array for pressure (Fig. 2.10a) and elastic stretch (Fig. 2.10b). As the active contraction component forces cells to contract their length, they compress ($\lambda < 1$), resulting in an increased internal pressure (Fig. 2.10a). When this occurs, the remaining cells in the domain expand ($\lambda > 1$) to account for the length lost due to contraction, resulting in a decreased internal pressure (Fig. 2.10b). Initially ($t < 5$), the system adjusts from the equilibrium configuration, reacting to the new contraction force. This small lag is due to the dissipation from the substrate. Further investigation The system then reaches a travelling wave with constant magnitudes of peaks and troughs, however we note that a lag between the contractive force and the cells contraction persists (but becomes constant) after these initial transients have disappeared. The dissipation in the system causes a delay in the cells response to the active forcing. The magnitude of the peaks and troughs of the pressure (Fig. 2.10c) and stretch (Fig. 2.10d) waves decrease as K increases. The differences between the peaks and troughs are due to the spatial profile of the contraction. A small cluster of cells contract and the remaining cells (a larger number than that which are contracting) stretch to account for this, however this stretch is spread between a larger number of cells. The active contraction forcing results in a travelling wave of compressed cells with heightened pressure moving through the domain, with remaining cells in a relaxed or stretched state. This is observed as a bulge in the domain (with colour representing internal cell pressure) in Fig. 2.10e. All results show an excellent agreement between discrete and continuum systems.

2.5 Summary

In this chapter we have constructed an IBM for a single array of incompressible viscoelastic cells both with and without active contraction, and derived the corresponding upscaled continuum PDE equations using discrete-to-continuum asymptotics. To benchmark the system, we considered the passive response of an applied deformation, demonstrating that increased substrate dissipation delays force transmission along the line, resulting in larger deformation towards the end at which the deformation is applied before the system settles to equilibrium. In the absence of substrate dissipation, a higher viscosity of cells results in heightened pressure during the same prescribed deformation, however the system is always spatially uniform. For the case of a cluster of stiffer cells in the centre of the domain, the majority of the deformation is taken on by the softer cells and the array has a larger average internal cell pressure. We then considered a system

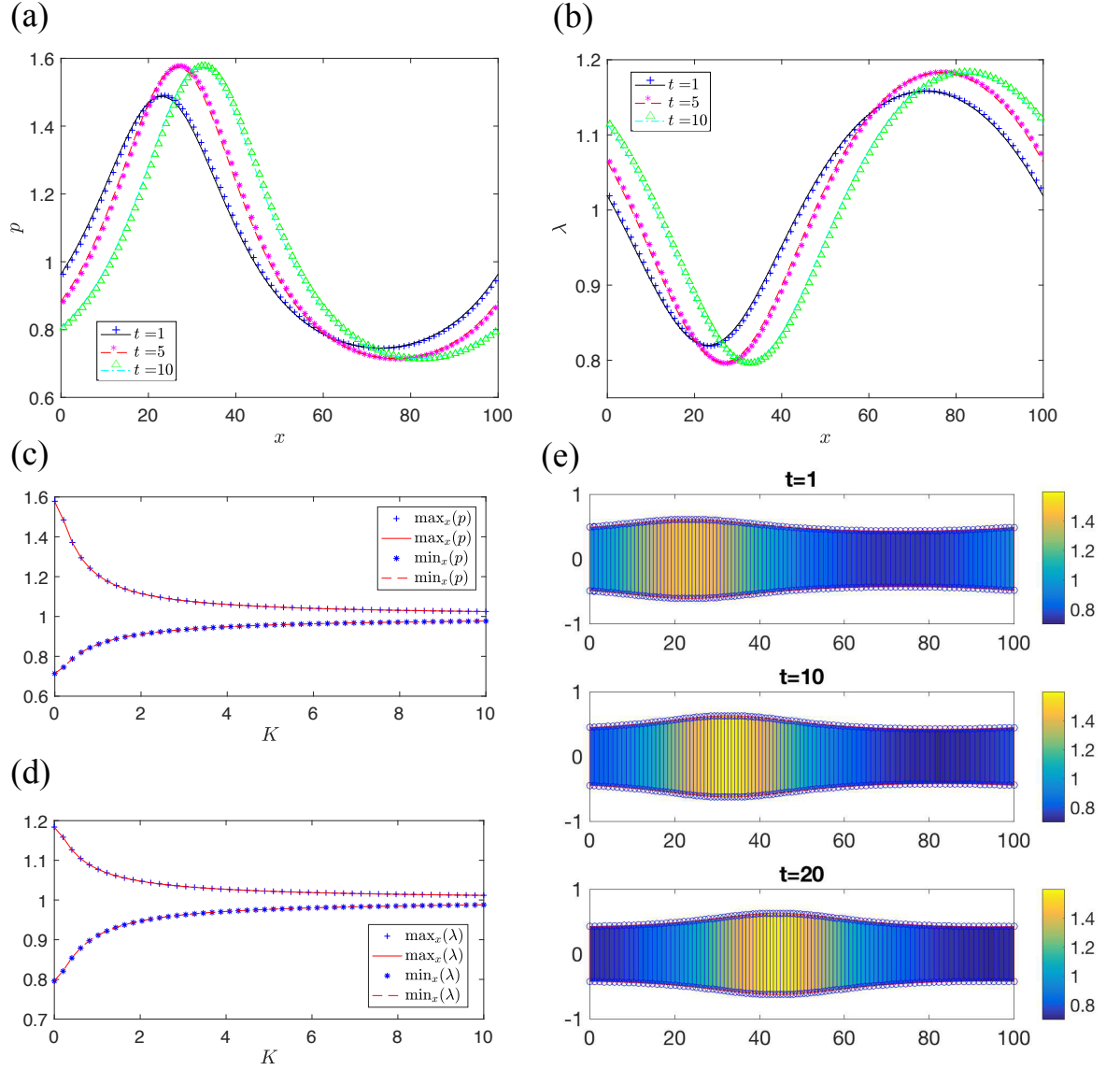


Figure 2.10: Solutions for a system of incompressible neo-Hookean cells aligned in a single array in a periodic domain subject to an active contraction force, defined in (2.83) and (2.84), with $\beta = -1$, $\omega = 1/N$, $t_R^{(i)} = 2\pi x_0^{(i)}/N$. The system is considered with a uniform $\mu = 1$ with substrate damping ($K \in [10^{-5}, 10]$), in the absence of viscous dissipation ($\eta = 0$). Both discrete (symbols) and continuum (lines) systems are displayed. (a) internal cell pressure, p , across the domain, x , for $t = 1, 5, 10$ and $K = 10^{-2}$; (b) cell stretch, λ , across the domain, x , for $t = 1, 5, 10$ and $K = 10^{-2}$; (c) The maximum ($\max_{x,t}(p)$ - peaks) and minimum ($\min_{x,t}(p)$ - troughs) internal cell pressure across the domain during $t = 0$ to $t = 100$ for $K = 10^{-5}$ to $K = 10$; (d) The maximum ($\max_{x,t}(\lambda)$ - peaks) and minimum ($\min_{x,t}(\lambda)$ - troughs) cell stretch across the domain during $t = 0$ to $t = 100$ for $K = 10^{-5}$ to $K = 10$; (e) Profiles at $t = 1, 10, 20$, with colour-bars representing internal cell pressure.

with an active contraction component. In simulations, a wave of contraction passes through the periodic domain in the form of a travelling wave. For all formulations, we observe excellent agreement between both discrete and continuum systems.

Chapter 3

Growth and Proliferation of a Single Array of Cells

In this chapter we extend the single array of nonlinearly viscoelastic cells in Chapter 2 to include cell growth and proliferation. We again consider cells of constant density and uniform thickness, H (measured in the direction normal to the substrate, parametrised by the coordinate z), atop a rigid substrate in a state of plane strain, shown in Fig. 2.1. The midline of this quasi-two-dimensional array is parameterised by the coordinate x (shown as dashed line in Fig. 2.1), while the tangential direction (in the plane of the page) is parametrised by the coordinate y . These cells are assumed to be in contact along their shared edges where stress can be transmitted. All cells are assumed to be incompressible, but may grow in response to an abundant nutrient in the surrounding fluid medium ($z > H$). This is replicated with a stress-dependent growth rate for each cell, such that if a cell is very compressed, it will stop growing, and if a cell is under extension, it will grow at a maximum rate. If a particular cell becomes too large (for example a cell may have difficulty moving enough nutrients and waste across its membrane to cater for its volume [113]), it is assumed to divide into two daughter cells according to a prescribed law. To maintain the one-dimensional array we assume the cells divide along their midline parallel to the y -direction. Although idealised, this model system elucidates the competition between local growth, proliferation and elastic deformation at the single cell level to the global mechanical deformation and expansion of the entire array.

For simplicity, at one end of the array we assume the outer edge of the cell is adhered to an impermeable boundary located along $x = 0$. At the other end of the array we denote the location of the outer edge as $x = l(t)$, where we apply a boundary condition of zero external forces. In the lateral (y -)direction we assume boundary conditions of zero normal and tangential stress on external interfaces. Although the difference in external pressures can be large, the pressure difference between adjacent layers of constituent cells will be significantly smaller and for the purposes of this study is assumed negligible.

We now formulate both (discrete) individual-based (Sec. 3.1) and continuum PDE models

(Sec. 3.2) for this single line of cells.

3.1 Discrete Model (Incompressible Cells)

We consider a single line of discrete cells, as shown in Fig. 2.1. The number of cells may increase over time, t , due to cell division, so the current number of cells is denoted $N(t)$, with an initial number N_0 . These cells are indexed by j ($j = 1, \dots, N$) and the properties of cell j are labelled with a superscript (j) . In general these individual cells can have complicated shapes and are embedded within an extracellular matrix. For simplicity in this study, we assume that each constituent cell can be modelled as a cuboid which deforms subject to a uniaxial deformation (but deforms in two-dimensions). Hence, since the out of plane thickness remains constant, each cell is characterised by a length in the x -direction (along unit vector $\hat{\mathbf{x}}$), denoted $L^{(j)}$ (with initial value $L_0^{(j)}$), and width in the y -direction (along unit vector $\hat{\mathbf{y}}$), denoted $W^{(j)}$ (with initial value $W_0^{(j)}$) for $j = 1, \dots, N$. As mentioned above, the system is assumed to have no displacement or growth in the out-of-plane (z) direction and so the deformation can be treated as entirely planar; for simplicity in the analysis below we ignore the out-of-plane direction entirely and present the tensors for stress and strain as two-dimensional. Denoting the total length of the line of cells as $l(t)$ (which may be either prescribed or solved for, with initial total length l_0), we assume there are no voids and must have

$$l(t) = \sum_{j=1}^N L^{(j)}(t), \quad l(0) = l_0 = \sum_{j=1}^N L_0^{(j)}. \quad (3.1)$$

We assume the cells have uniform density $\rho^{(j)}$ ($j = 1, \dots, N$), and characterise cells by the position of their centre of mass (which coincides with their geometric centre since the density is assumed uniform) denoted $\mathbf{x}_c^{(j)} = (x_c^{(j)}(t), 0)$, for $j = 1, \dots, N$. We also use the index $j + 1/2$ to denote the boundary between cells j and $j + 1$.

We assume each cell can undergo a nonlinear viscoelastic deformation relative to its geometric centre, while this geometric centre moves according to a global force balance. The (local) reference coordinate system for cells is denoted $\mathbf{X}^{(j)} = (X^{(j)}, Y^{(j)})$ where $X^{(j)} = x - x_c^{(j)}$ and $Y^{(j)} = y$ so that $-\frac{1}{2}L_0^{(j)} \leq X^{(j)} \leq \frac{1}{2}L_0^{(j)}$ and $-\frac{1}{2}W_0^{(j)} \leq Y^{(j)} \leq \frac{1}{2}W_0^{(j)}$. In the current configuration, the coordinate system for cells is defined by $\mathbf{x}^{(j)} = \boldsymbol{\chi}^{(j)}(\mathbf{X}^{(j)}, t)$. The mapping $\boldsymbol{\chi}$ defines the deformation from the reference to the current configuration. Hence, the corresponding deformation gradient tensor is defined by $\mathbb{F}^{(j)} = \text{Grad}(\mathbf{x}^{(j)})$, where the gradient operator for each cell is measured with respect to the reference coordinate system $\mathbf{X}^{(j)}$.

3.1.1 Cell Growth

We allow for morphological growth of each constituent cell according to a growth tensor $\mathbf{G}^{(j)}$ ($j = 1, \dots, N$). For simplicity, we assume this tensor is diagonal $\mathbf{G}^{(j)} = \text{diag}(g_1^{(j)}, g_2^{(j)})$, where $g_1^{(j)}$ and $g_2^{(j)}$ are functions we construct below. In accordance with many similar studies of morphological growth [107, 116] we assume a multiplicative decomposition of the deformation gradient tensor, $\mathbb{F}^{(j)}$, which can be interpreted as splitting the full deformation into an unconstrained growth phase (to a stress free configuration) followed by a viscoelastic rearrangement phase to fit the boundary conditions (which can generate residual stress), in the form

$$\mathbb{F}^{(j)} = \mathbf{A}^{(j)} \mathbf{G}^{(j)}, \quad (j = 1, \dots, N), \quad (3.2)$$

where $\mathbf{A}^{(j)}$ is a tensor describing the viscoelastic deformation of cell j , ($j = 1, \dots, N$). Since (by assumptions) the deformation is always rectangular, the tensors $\mathbb{F}^{(j)}$ and $\mathbf{A}^{(j)}$ are diagonal and can be written in the form

$$\mathbf{A}^{(j)} = \begin{bmatrix} \alpha_1^{(j)} & 0 \\ 0 & \alpha_2^{(j)} \end{bmatrix}, \quad \mathbb{F}^{(j)} = \begin{bmatrix} \lambda_1^{(j)} & 0 \\ 0 & \lambda_2^{(j)} \end{bmatrix} = \begin{bmatrix} g_1^{(j)} \alpha_1^{(j)} & 0 \\ 0 & g_2^{(j)} \alpha_2^{(j)} \end{bmatrix}, \quad (3.3)$$

where $\alpha_1^{(j)}$ and $\alpha_2^{(j)}$ ($\lambda_1^{(j)}$ and $\lambda_2^{(j)}$) are the viscoelastic (full) principal stretches of cell j ($j = 1, \dots, N$), where

$$\lambda_1^{(j)} = \frac{x_b^{(j+1/2)} - x_b^{(j-1/2)}}{L_0^{(j)}}. \quad (3.4)$$

These principal stretches must be calculated using a rheological model, as described in Sec. 3.1.3.

3.1.2 Incompressibility

The constraint of incompressibility on the viscoelastic part of the deformation implies that $\det(\mathbf{A}^{(j)}) = \alpha_1^{(j)} \alpha_2^{(j)} = 1$, ($j = 1, \dots, N$). Hence $\alpha_2^{(j)} = (\alpha_1^{(j)})^{-1}$.

3.1.3 Rheological Model

We assume that each cell is composed of an elastic component in parallel with a viscous dashpot, the Kelvin–Voigt rheological model which has previously been used to model cells (e.g. [117]). Since the two components are arranged in parallel, this results in an additive decomposition of the total Cauchy stress for each cell in the form

$$\boldsymbol{\sigma}^{(j)} = \boldsymbol{\sigma}_e^{(j)} + \boldsymbol{\sigma}_v^{(j)}, \quad (j = 1, \dots, N), \quad (3.5)$$

where $\boldsymbol{\sigma}_e^{(j)}$ and $\boldsymbol{\sigma}_v^{(j)}$ represent the elastic and viscous components of the Cauchy stress, respectively.

3.1.4 Elastic Stress

The elastic component of the cell deformation follows from an incompressible strain energy functional,

$$\mathcal{W}_e^{(j)} = \mathcal{W}_e^{(j)}(\alpha_1^{(j)}, \alpha_2^{(j)}), \quad (j = 1, \dots, N), \quad (3.6)$$

where the function $\mathcal{W}_e^{(j)}$ is chosen to satisfy objectivity requirements [118]. We characterise the elasticity of individual cells by their shear modulus, denoted $\mu^{(j)}$ ($j = 1, \dots, N$) and denote μ_0 as a typical shear modulus for each cell. We preserve generality when specifying the model, but show results below for the incompressible neo-Hookean strain energy functional

$$\mathcal{W}_e^{(j)} = \frac{1}{2}\mu^{(j)} \left((\alpha_1^{(j)})^2 + (\alpha_2^{(j)})^2 - 2 \right), \quad (j = 1, \dots, N), \quad (3.7)$$

which is often used for modelling biological soft tissues (e.g. [119, 120]).

The corresponding Cauchy stress tensor for cell j is then given by,

$$\boldsymbol{\sigma}_e^{(j)} = \mathbf{A}^{(j)} \frac{\partial \mathcal{W}_e^{(j)}}{\partial \mathbf{A}^{(j)}} - p^{(j)} \mathbb{I}, \quad (j = 1, \dots, N), \quad (3.8)$$

where $p^{(j)}$ is a Lagrange multiplier interpreted as the elastic pressure j ($j = 1, \dots, N$) [102]. Since we assume a rectangular deformation for each cell this results in a diagonal Cauchy stress tensor in the form

$$\boldsymbol{\sigma}_e^{(j)} = \begin{bmatrix} \alpha_1^{(j)} \mathcal{W}_1^{(j)} - p^{(j)} & 0 \\ 0 & \alpha_2^{(j)} \mathcal{W}_2^{(j)} - p^{(j)} \end{bmatrix}, \quad \mathcal{W}_{1,2}^{(j)} = \frac{\partial \mathcal{W}_e^{(j)}}{\partial \alpha_{1,2}^{(j)}}, \quad (j = 1, \dots, N). \quad (3.9)$$

3.1.5 Viscous Stress

Since the deformation is rectangular, we approximate the velocity of deformation by the time derivative of the stretch in the principal directions, which are spatially uniform across the cell, denoted $\dot{\alpha}_1^{(j)}$ and $\dot{\alpha}_2^{(j)}$ ($j = 1, \dots, N$). Hence the viscous Cauchy stress is given by

$$\boldsymbol{\sigma}_v = \begin{bmatrix} 2\eta^{(j)} \dot{\alpha}_1^{(j)} & 0 \\ 0 & 2\eta^{(j)} \dot{\alpha}_2^{(j)} \end{bmatrix}, \quad (j = 1, \dots, N), \quad (3.10)$$

where $\eta^{(j)}$ is the internal cell viscosity ($j = 1, \dots, N$).

3.1.6 Boundary Conditions

The total pressure $p^{(j)}$ ($j = 1, \dots, N$) within each cell is determined by applying the boundary condition of no lateral force on the unconfined edges (parallel to $\hat{\mathbf{x}}$), which gives

$$p^{(j)} = \alpha_2^{(j)} \mathscr{W}_2^{(j)} + 2\eta^{(j)} \dot{\alpha}_2^{(j)}, \quad (j = 1, \dots, N). \quad (3.11)$$

The total force exerted by an individual cell on its neighbours then takes the form

$$\begin{aligned} \mathbf{F}_{\pm}^{(j)} &= F_{\pm}^{(j)} \hat{\mathbf{x}} = \int_{-\frac{1}{2}W^{(j\pm 1/2)}}^{\frac{1}{2}W^{(j\pm 1/2)}} \boldsymbol{\sigma}^{(j)} \cdot (\mp \hat{\mathbf{x}}) \, dy \\ &= \mp \hat{\mathbf{x}} W^{(j\pm 1/2)} \left(\alpha_1^{(j)} \mathscr{W}_1^{(j)} - \alpha_2^{(j)} \mathscr{W}_2^{(j)} + 2\eta^{(j)} \left(\dot{\alpha}_1^{(j)} - \dot{\alpha}_2^{(j)} \right) \right), \quad (j = 1, \dots, N); \end{aligned} \quad (3.12)$$

$W^{(j\pm 1/2)}$ again represents the length of the shared boundary between cells j and $j \pm 1$, which we approximate by the mean of the cell widths

$$W^{(j\pm 1/2)} = \frac{1}{2} \left(W^{(j\pm 1)} + W^{(j)} \right), \quad (3.13)$$

where $W^{(j)} = W_0 \alpha_2^{(j)} = W_0 g_2^{(j)} \alpha_2^{(j)}$. The resultant force across the cell boundary between cells j and $j + 1$ is denoted

$$F_b^{(j+1/2)} = F_+^{(j)} + F_-^{(j+1)}, \quad (j = 1, \dots, N - 1). \quad (3.14)$$

This net force will drive motion and deformation of the line of cells.

3.1.7 Cell growth rate

Since we are considering a toy problem, in this study we assume that the cell only grows in the x -direction ($g_2^{(j)} = 1$, $j = 1, \dots, N$). This is not realistic of the myocardium or typical of cancerous cells, however we use this assumption to test a simple system. We assume the rate of growth is dependent on the local stress, with the ODE

$$\frac{dg_1^{(j)}}{dt} = \frac{1}{2} G_m \left(1 + \tanh \left(\frac{\sigma_1^{(j)}}{\sigma_0^{(j)}} \right) \right), \quad (j = 1, \dots, N), \quad (3.15)$$

where G_m is the maximum growth rate of an individual cell, $\sigma_0^{(j)}$ (represents the typical compressive stress where growth is suppressed for cell j) and $\sigma_1^{(j)}$ is the principal stress in the

x -direction, defined by

$$\sigma_1^{(j)} = \left(\alpha_1^{(j)} \mathscr{W}_1^{(j)} - \alpha_2^{(j)} \mathscr{W}_2^{(j)} + 2\eta^{(j)} \left(\dot{\alpha}_1^{(j)} - \dot{\alpha}_2^{(j)} \right) \right), \quad (j = 1, \dots, N). \quad (3.16)$$

In our models the cells are never in extension, so $\sigma_1^{(j)} \geq 1$ and the maximal growth rate arises when the cells are unstressed ($\sigma_1^{(j)} = 0$) and the growth rate approaches zero as the compression level increases.

3.1.8 Cell Division

Cells can divide when they become sufficiently large: in this study we assume that once the volume of an individual cell reaches a target volume, it will divide into two identical daughter cells. We further assume that the cell divides its mass equally along a line parallel to the y -direction, with each daughter cell half the total length of the parent cell, while maintaining its width. At each division, an extra boundary at the midpoint of the divided cell is introduced, and the number of cells increases by one and the cells are re-indexed to ensure a sequential increase along the line. In particular, we assume a cell will divide when its current volume, $V^{(j)}$, becomes twice its initial (ungrown) value and the resting length of the two new daughter cells is chosen to be half the resting length of the parent at division. However, this length can differ from the resting length of the original cells.

3.1.9 Governing Equations

We consider the additional possibility that the cells are binding and unbinding to a substrate which is fixed in the plane of the page ($z = 0$): the resulting damping force is assumed proportional to the rate of change of the position of the centre of mass of the cell relative to the substrate, and the dimensionless function

$$\kappa = \left(\frac{A^{(j)}}{A_0^{(j)}} \right)^m \quad (3.17)$$

where $A^{(j)} = g_1^{(j)} g_2^{(j)} L_0 W_0$ is the area of cell j , with some constant of proportionality $K^{(j)}$, ($j = 1, \dots, N$). We will consider two particular cases: where $m = 0$ and $m = 1$. This damping is based on velocity relative to the substrate and can be attributed to friction in the cell movement as it moves past tissue or fibres in the ECM, hence is proportional to the area of the cell connected to the substrate. This can be interpreted as each cell having a viscous dashpot connected to some fixed point in the reference configuration. This setup is shown in Fig. 2.1. In this case, applying Newton's second law to each internal cell and neglecting inertial effects, we express the global

force balance as

$$\kappa K^{(j)} \frac{dx_c^{(j)}}{dt} = F_b^{(j-1/2)} + F_b^{(j+1/2)}, \quad (j = 1, \dots, N). \quad (3.18)$$

The cell's centre of mass location is

$$x_c^{(j)} = \frac{1}{2} \left(x_b^{(j-1/2)} + x_b^{(j+1/2)} \right), \quad (j = 1, \dots, N). \quad (3.19)$$

3.1.10 Global Boundary Conditions

To complete the system we define boundary conditions on the outer boundaries. For all systems outlined here, the boundary of cell $j = 1$ at $x = 0$ remains fixed, so $x_b^{(1/2)}(t) = 0$. At the other end of the domain we prescribe zero applied force, such that

$$F_-^{(N+1)} = 0, \quad (3.20)$$

which means that the force balance on boundary $N + 1/2$ can be expressed as

$$F_b^{(N+1/2)} = F_+^{(N)}. \quad (3.21)$$

3.1.11 Initial Conditions

Initially the cell boundaries are located at

$$x_b^{(1/2)} = 0, \quad x_b^{(j+1/2)} = \sum_{i=1}^j L_0^{(i)}, \quad (j = 1, \dots, N). \quad (3.22)$$

However, in simulations below we assume all cells are initially the same length $L_0^{(j)} = L_0$ ($j = 1, \dots, N$) and width $W_0^{(j)} = W_0$ ($j = 1, \dots, N$). This is not a necessary assumption but significantly simplifies the specification of the model and the upscaling to a continuum model for Sec 3.2. In this case, (3.22) reduces to

$$x_b^{(j-1/2)} = L_0(j-1), \quad (j = 1, \dots, N+1). \quad (3.23)$$

To further simplify the analysis, in this study we assume that the parameters governing viscous damping and those involved in the growth rate function are all uniform along the array, in the form

$$K^{(j)} = K, \quad \eta^{(j)} = \eta, \quad G_m^{(j)} = G_m, \quad \sigma_0^{(j)} = \sigma_0, \quad (j = 1, \dots, N). \quad (3.24)$$

3.1.12 Non-dimensional variables

It is useful to consider the system in terms of non-dimensional variables (denoted with an overbar). We scale time on the timescale of growth, G_m^{-1} , lengths on L_0 , forces per unit length on $\mu_0 L_0$, pressures and stresses on μ_0 so that

$$(L^{(j)}, W^{(j)}) = L_0(\bar{L}^{(j)}, \bar{W}^{(j)}), \quad \sigma_1^{(j)} = \mu_0 \bar{\sigma}_1^{(j)}, \quad (j = 1, \dots, N), \quad (3.25)$$

$$t = \bar{t} G_m^{-1}, \quad \mu = \mu_0. \quad (3.26)$$

This results in the following dimensionless groups

$$\bar{\gamma}_0 = \frac{W_0}{L_0}, \quad \bar{\eta} = \frac{2\eta G_m}{\mu_0}, \quad \bar{K} = \frac{K G_m}{2\mu_0}, \quad \bar{\sigma}_0 = \frac{\sigma_0}{\mu_0}, \quad (3.27)$$

representing the planar aspect ratio of the cells, and the dimensionless viscous and substrate damping coefficients and the typical compressive stress where growth is suppressed respectively. We include this factor of $\frac{1}{2}$ in \bar{K} for simplicity in defining the system in terms of cell boundaries below. We further define the dimensionless domain length, intracellular force, cell width and strain-energy function derivatives as

$$l(t) = L_0 \bar{l}(\bar{t}), \quad F_b(t) = \mu_0 L_0 \bar{F}_b(\bar{t}), \quad \bar{W}^{(j)}(t) = \frac{\bar{\gamma}_0 g_2^{(j)}(\bar{t})}{\alpha_1^{(j)}(\bar{t})}, \quad \mathcal{W}_{1,2}^{(j)} = \mu_0 \bar{\mathcal{W}}_{1,2}^{(j)} \quad (j = 1, \dots, N). \quad (3.28)$$

The final non-dimensional system takes the form

$$2\kappa \bar{K} \frac{d\bar{x}_c^{(j)}}{d\bar{t}} = \bar{W}^{(j+1/2)} \left(\bar{\sigma}_1^{(j+1)} - \bar{\sigma}_1^{(j)} \right) - \bar{W}^{(j-1/2)} \left(\bar{\sigma}_1^{(j)} - \bar{\sigma}_1^{(j-1)} \right), \quad (j = 1, \dots, N), \quad (3.29a)$$

where

$$\bar{W}^{(j+1/2)} = \gamma_0 \left(g_2^{(j+1)} \alpha_2^{(j+1)} + g_2^{(j)} \alpha_2^{(j)} \right), \quad (j = 1, \dots, N), \quad (3.29b)$$

$$\bar{\sigma}_1^{(j)} = \alpha_1^{(j)} \bar{\mathcal{W}}_1^{(j)} - \alpha_2^{(j)} \bar{\mathcal{W}}_2^{(j)} + \bar{\eta} \left(\dot{\alpha}_1^{(j)} - \dot{\alpha}_2^{(j)} \right), \quad (j = 1, \dots, N), \quad (3.29c)$$

$$\alpha_1^{(j)} = \frac{\bar{x}_b^{(j+1/2)} - \bar{x}_b^{(j-1/2)}}{g_1^{(j)}} \quad \text{and} \quad \alpha_2^{(j)} = \frac{1}{\alpha_1^{(j)}}, \quad (j = 1, \dots, N). \quad (3.29d)$$

The cell centre of mass in terms of cell boundary locations (3.19) in non-dimensional variables is

$$\bar{x}_c^{(j)} = \frac{1}{2} \left(\bar{x}_b^{(j-1/2)} + \bar{x}_b^{(j+1/2)} \right). \quad (3.29e)$$

The cell pressure from (3.11) is

$$\tilde{p}^{(j)} = \alpha_2^{(j)} \mathcal{W}_2^{(j)} + \bar{\eta} \dot{\alpha}_2^{(j)}. \quad (3.29f)$$

Substituting (3.29e) into (3.29a) and applying the fixed boundary condition at $x = 0$ we compute

$$\kappa \bar{K} \frac{d\bar{x}_b^{(j+1/2)}}{d\bar{t}} = \bar{W}^{(j+1/2)} \left(\bar{\sigma}_1^{(j+1)} - \bar{\sigma}_1^{(j)} \right), \quad (j = 1, \dots, N-1). \quad (3.29g)$$

This form of the governing equations is used in numerical solutions of the discrete model.

The stress dependent growth rate (3.15) has non-dimensional form

$$\frac{dg_1^{(j)}}{d\bar{t}} = \frac{1}{2} \left(1 + \tanh \left(\frac{\bar{\sigma}_1^{(j)}}{\bar{\sigma}_0} \right) \right), \quad (j = 1, \dots, N). \quad (3.29h)$$

The boundary conditions take the form

$$\bar{x}_b^{(1/2)} = 0 \quad \kappa \bar{K} \frac{d\bar{x}_b^{(N+1/2)}}{d\bar{t}} = -\bar{W}^{(N)} \bar{\sigma}_1^{(N)} \quad (3.29i)$$

where

$$\bar{W}^{(N)} = \gamma_0 g_2^{(N)} \alpha_2^{(N)}. \quad (3.29j)$$

The initial condition is

$$\bar{x}_b^{(j-1/2)}(0) = (j-1), \quad (j = 1, \dots, N+1). \quad (3.29k)$$

Henceforth, we drop over-bars for notational convenience and consider only non-dimensional variables in the simulations below.

3.1.13 Numerical method

As in chapter 2, the discrete system (3.29) is a closed system of ODEs which is solved numerically using MATLAB solver `ode15s`. The MATLAB code for this system is outlined in Appendix A.1 for a system in the absence of proliferation (without division). Due to the viscous stress component, the equation of motion (3.29a) includes the term $\dot{\alpha}_1^{(j)}$ ($j = 1, \dots, N$), which is defined by

$$\frac{d\alpha_1^{(j)}}{dt} = \frac{1}{g_1^{(j)}} \left(\frac{dx_b^{(j+1/2)}}{dt} - \frac{dx_b^{(j-1/2)}}{dt} \right) - \frac{dg_1^{(j)}}{dt} \left(x_b^{j+1/2} - x_b^{j-1/2} \right), \quad (j = 1, \dots, N). \quad (3.30)$$

However, the definition of $\dot{g}_1^{(j)}$ ($j = 1, \dots, N$) in (3.29h) along with (3.29c), also includes the term $\dot{\alpha}_1^{(j)}$ ($j = 1, \dots, N$) within $\sigma_1^{(j)}$ in the tanh function. Hence the system is not straight-forward to solve. In order to solve this system for x_b , due to the additional time-derivatives from both the viscous stress component and the growth rate, one must solve the system with $\dot{\alpha}_1^{(j)}$ as an intermediate variable. We form a vector of length $3N + 1$, defined by

$$\begin{bmatrix} \mathbf{x}_b \\ \mathbf{g}_1 \\ \dot{\boldsymbol{\alpha}}_1 \end{bmatrix} \quad (3.31)$$

where \mathbf{x}_b is the vector of boundary locations ($x_b^{(j+1/2)}$; $j = 0, \dots, N$), \mathbf{g}_1 is the vector of the growth function in the x -direction ($g_1^{(j)}$; $j = 1, \dots, N$) and $\dot{\boldsymbol{\alpha}}_1$ is the vector of the rate of change of elastic stretch in the x -direction ($\dot{\alpha}_1^{(j)}$; $j = 1, \dots, N$). MATLAB solver ode15s is used to solve for all three variables, with solutions for $\dot{\boldsymbol{\alpha}}$ constructed as an algebraic constraint in the solver, defined by

$$\begin{aligned} \frac{d\alpha_1^{(j)}}{dt} - \left(g_1^{(j)}\right)^{-1} \left(\frac{dx_b^{(j+1/2)}}{dt} + \frac{dx_b^{(j-1/2)}}{dt} \right) \\ + \left(g_1^{(j)}\right)^{-2} \frac{dg_1^{(j)}}{dt} \left(x_b^{j+1/2} - x_b^{j-1/2}\right) = 0, \quad (j = 1, \dots, N). \end{aligned} \quad (3.32)$$

Given $\dot{\alpha}_1^{(j)}$ ($j = 1, \dots, N$), the cell momentum equations are then expressed as a matrix problem for the rate of change of the cell boundary locations, $\dot{x}_b^{(j+1/2)}$ ($j = 1, \dots, N$). Once these are known, we can solve the ODEs for $x_b^{(j+1/2)}$ explicitly.

We input the initial conditions for \mathbf{x}_b as defined in (3.29k), $g_1^{(j)}(0) = 1$ ($j = 1, \dots, N$) and use `fsolve` to find an initial value for $\dot{\alpha}_1^{(j)}$ consistent with the governing equations subject to the initial conditions.

Numerical solutions of this IBM are discussed in Sec. 3.3 below. This discrete formulation does not require any regularity or smoothness of material properties, which can be sampled randomly. However, to construct a continuum (PDE) model of this arrangement of cells, we must assume that the material properties vary smoothly along the array over a prescribed lengthscale.

3.2 Upscaling to Continuum Model (Incompressible Cells)

We now describe the discrete model of Sec. 3.1 using a (PDE) continuum model to facilitate a macroscale description. In this approach we utilise discrete-to-continuum upscaling to map the discrete equations (3.29) to a PDE [82, 115], similar to chapter 2.

To facilitate this upscaling we assume the initial number of cells is large and introduce a small parameter $\varepsilon = N_0^{-1} \ll 1$. We assume that the lengthscale of a typical deformation is long

($\mathcal{O}(\varepsilon^{-1})$) compared to that of an individual cell ($\mathcal{O}(1)$), and so take a long wavelength rescaling of the independent variables in the form

$$X = \varepsilon x, \quad T = \varepsilon t, \quad (3.33a)$$

so that $0 \leq X \leq 1$. Note that this reduction maintains an $\mathcal{O}(1)$ cell velocity. In accordance with this rescaling we then express the cell boundary positions as

$$\tilde{x}_b^{(j+1/2)}(T) = \varepsilon x_b^{(j+1/2)}(t), \quad (j = 0, \dots, N), \quad (3.33b)$$

where tilded variables are discrete functions of rescaled time, T . Furthermore, we rescale the discrete time-dependent descriptors of an individual cell in the form,

$$\left(\tilde{g}_{1,2}^{(j)}, \tilde{W}^{(j)}, \tilde{L}^{(j)}, \tilde{\alpha}^{(j)}, \tilde{\mathcal{W}}_{1,2}^{(j)} \right) = \left(g_{1,2}^{(j)}, W^{(j)}, \varepsilon L^{(j)}, \alpha^{(j)}, \mathcal{W}_{1,2}^{(j)} \right), \quad (j = 1, \dots, N). \quad (3.33c)$$

Note that we do not scale W (y-direction) as we do L (x-direction) so as to create a long, thin material so that the ratio of length scales is the aspect ratio of the system. We further rescale the two dimensionless damping parameters as $K = \varepsilon \tilde{K}$ and $\eta = \varepsilon^{-1} \tilde{\eta}$ to ensure a dominant balance.

We discretise the continuous variable X into N equally sized intervals, so that $X_j = j/N$, ($j = 0, \dots, N$), so the rescaled initial positions of the cell centre of mass and cell boundaries can be expressed as $\tilde{x}_b^{(1/2)}(0) = 0$ with

$$\tilde{x}_b^{(j+1/2)}(0) = X_j, \quad \tilde{x}_c^{(j)}(T) = X_{j-1/2} = \frac{1}{2}(X_{j-1} + X_j), \quad (j = 1, \dots, N). \quad (3.34)$$

We then express the cell boundary and centre of mass positions as a single continuum function $\check{x}(X, T)$ such that $\tilde{x}_b^{(1/2)}(T) = 0$

$$\tilde{x}_b^{(j+1/2)} = \check{x}(X_j, T), \quad \tilde{x}_c^{(j)} = \check{x}(X_{j-1/2}, T), \quad (j = 1, \dots, N), \quad (3.35a)$$

as well as continuum representations of the other dependent variables in the model, in the form

$$\tilde{W}^{(j)}(t) = \check{W}(X_{j-1/2}, T), \quad \tilde{g}_{1,2}^{(j)}(T) = \check{g}_{1,2}(X_{j-1/2}, T), \quad (3.35b)$$

$$\tilde{\alpha}^{(j)}(t) = \check{\alpha}(X_{j-1/2}, T), \quad \tilde{\mathcal{W}}_{1,2}^{(j)}(T) = \check{\mathcal{W}}_{1,2}(X_{j-1/2}, T), \quad (j = 1, \dots, N). \quad (3.35c)$$

As before, differences in discrete variables are mapped to derivatives of these continuum func-

tions using Taylor expansions. The governing equation becomes

$$\begin{aligned}
 \varepsilon \check{K} \check{\kappa} \frac{\partial \check{x}(j\varepsilon, T)}{\partial T} &= -\check{W}(j\varepsilon, T) \left(\check{\alpha}_1((j + \frac{1}{2})\varepsilon, T) \check{\mathcal{W}}_1((j + \frac{1}{2})\varepsilon, T) - \check{\alpha}_2((j + \frac{1}{2})\varepsilon, T) \check{\mathcal{W}}_2((j + \frac{1}{2})\varepsilon, T) \right. \\
 &\quad + \eta \frac{\partial}{\partial T} \left(\check{\alpha}_1((j + \frac{1}{2})\varepsilon, T) - \check{\alpha}_2((j + \frac{1}{2})\varepsilon, T) \right) \\
 &\quad - \check{\alpha}_1((j + \frac{3}{2})\varepsilon, T) \check{\mathcal{W}}_1((j + \frac{3}{2})\varepsilon, T) + \check{\alpha}_2((j + \frac{3}{2})\varepsilon, T) \check{\mathcal{W}}_2((j + \frac{3}{2})\varepsilon, T) \\
 &\quad \left. - \eta \frac{\partial}{\partial T} \left(\check{\alpha}((j + \frac{3}{2})\varepsilon, T) - \check{\lambda}_2((j + \frac{3}{2})\varepsilon, T) \right) \right). \tag{3.36}
 \end{aligned}$$

where

$$\check{\alpha}_{1,2}((j + \frac{1}{2})\varepsilon, T) = \check{\alpha}_{1,2}(j\varepsilon, T) + \frac{\varepsilon}{2} \frac{\partial \check{\alpha}_{1,2}(j\varepsilon, T)}{\partial X} + \mathcal{O}(\varepsilon^2), \tag{3.37}$$

$$\check{\alpha}_{1,2}((j + \frac{3}{2})\varepsilon, T) = \check{\alpha}_{1,2}(j\varepsilon, T) + \frac{3\varepsilon}{2} \frac{\partial \check{\alpha}_{1,2}(j\varepsilon, T)}{\partial X} + \mathcal{O}(\varepsilon^2), \tag{3.38}$$

$$\check{\mathcal{W}}_{1,2}((j + \frac{1}{2})\varepsilon, T) = \check{\mathcal{W}}_{1,2}(j\varepsilon, T) + \frac{\varepsilon}{2} \frac{\partial \check{\mathcal{W}}_{1,2}(j\varepsilon, T)}{\partial X} + \mathcal{O}(\varepsilon^2), \tag{3.39}$$

$$\check{\mathcal{W}}_{1,2}((j + \frac{3}{2})\varepsilon, T) = \check{\mathcal{W}}_{1,2}(j\varepsilon, T) + \frac{3\varepsilon}{2} \frac{\partial \check{\mathcal{W}}_{1,2}(j\varepsilon, T)}{\partial X} + \mathcal{O}(\varepsilon^2). \tag{3.40}$$

Substituting these expansions into (3.36) and simplifying yields

$$\check{\kappa} \check{K} \frac{\partial \check{x}}{\partial T} = \gamma_0 \check{g}_2 \check{\alpha}_1^{-1} \frac{\partial}{\partial X} \left(\check{\alpha}_1 \check{\mathcal{W}}_1 - \check{\alpha}_2 \check{\mathcal{W}}_2 + \check{\eta} \frac{\partial}{\partial T} (\check{\alpha}_1 - \check{\alpha}_2) \right), \quad (0 < X < 1). \tag{3.41}$$

We define continuum boundary conditions as follows. For the fixed boundary at $x = 0$, we define $\check{x}(0, T) = 0$. At the free boundary, (3.29i) gives

$$\varepsilon \check{\kappa} \check{K} \frac{\partial}{\partial T} (\check{x} + \mathcal{O}(\varepsilon)) = -\gamma_0 \check{g}_2 \check{\alpha}_1^{-1} \left(\check{\alpha}_1 \check{\mathcal{W}}_1 - \check{\alpha}_2 \check{\mathcal{W}}_2 + \check{\eta} \frac{\partial}{\partial T} (\check{\alpha}_1 - \check{\alpha}_1^{-1}) \right), \quad (X = 1), \tag{3.42}$$

which, to leading order, yields

$$\check{\alpha}_1 \check{\mathcal{W}}_1 - \check{\alpha}_2 \check{\mathcal{W}}_2 + \check{\eta} \frac{\partial \check{\alpha}_1}{\partial T} (1 + \check{\alpha}_1^{-2}) = 0, \quad (X = 1). \tag{3.43}$$

Finally, we rescale the continuum independent variables (X, T) back to the original parametrisation of the domain using $x = \varepsilon^{-1}X$, $t = \varepsilon^{-1}T$, $K = \varepsilon \check{K}$ and $\eta = \varepsilon^{-1} \check{\eta}$, and map the dependent variables according to

$$\check{g}_{1,2}(X, T) = \hat{g}_{1,2}(x, t), \quad \check{\mathcal{W}}_{1,2}(X, T) = \hat{\mathcal{W}}(x, t) \quad \check{x}(X, T) = \varepsilon \hat{x}(x, t), \tag{3.44a}$$

$$\check{W}(X, T) = \hat{W}(x, t), \quad \check{\alpha}(X, T) = \hat{\alpha}(x, t), \quad \check{\lambda}_{1,2}(X, T) = \hat{\lambda}_{1,2}(x, t). \tag{3.44b}$$

In this formulation, the continuum description of the full and elastic principal stretches are

respectively, to leading order, given by

$$\hat{\lambda}_1(x,t) = \frac{\partial \hat{x}}{\partial x}, \quad \hat{\alpha}_1(x,t) = \frac{1}{\hat{g}_1} \frac{\partial \hat{x}}{\partial x}, \quad (0 \leq x \leq l_0), \quad (3.45)$$

with resulting continuum constraints

$$\hat{\lambda}_2(x,t) = \frac{\hat{g}_2}{\hat{\alpha}_1}, \quad \hat{\alpha}_2(x,t) = \frac{1}{\hat{\alpha}_1}, \quad \hat{W}(x,t) = \gamma_0 \hat{\lambda}_2, \quad (0 \leq x \leq l_0). \quad (3.46)$$

The total pressure takes the continuum form

$$\hat{p}(x,t) = \hat{\alpha}_2 \hat{\mathcal{W}}_2 + \eta \frac{\partial \hat{\alpha}_2}{\partial t}, \quad (0 \leq x \leq l_0). \quad (3.47)$$

The upscaled governing equations (3.41) for a general strain energy functional, $\hat{\mathcal{W}}$, take the form

$$\hat{\kappa} K \frac{\partial \hat{x}}{\partial t} = \gamma_0 \hat{g}_2 \hat{\alpha}_1^{-1} \frac{\partial}{\partial x} \left(\hat{\alpha}_1 \hat{\mathcal{W}}_1 - \hat{\alpha}_2 \hat{\mathcal{W}}_2 + \eta \frac{\partial}{\partial t} (\hat{\alpha}_1 - \hat{\alpha}_2) \right), \quad (0 < x < l_0), \quad (3.48a)$$

where $\hat{\mathcal{W}}_1$ and $\hat{\mathcal{W}}_2$, are the upscaled continuum functions of $\mathcal{W}_1^{(j)}$ and $\mathcal{W}_2^{(j)}$ respectively. The fixed boundary at $x = 0$ is defined by $\hat{x}(0,t) = 0$ and the free boundary, (3.43) is replaced by

$$\hat{\alpha}_1 \hat{\mathcal{W}}_1 - \hat{\alpha}_2 \hat{\mathcal{W}}_2 + \eta \frac{\partial}{\partial t} (\hat{\alpha}_1 - \hat{\alpha}_2) = 0, \quad (x = l_0). \quad (3.48b)$$

Lastly, the continuum representation of the growth function (3.15) reduces to the form

$$\frac{d\hat{g}_1}{dt} = \frac{1}{2} \left(1 + \tanh \left(\frac{\hat{\sigma}_1}{\sigma_0} \right) \right), \quad (0 \leq x \leq l_0), \quad (3.49)$$

where

$$\hat{\sigma}_1 = \hat{\alpha}_1 \hat{\mathcal{W}}_1 - \hat{\alpha}_2 \hat{\mathcal{W}}_2 + \hat{\eta} \frac{\partial}{\partial t} (\hat{\alpha}_1 - \hat{\alpha}_2), \quad (0 \leq x \leq l_0). \quad (3.50)$$

3.2.1 Neo-Hookean Material

For a Neo-Hookean material with cell-level strain-energy function (3.7), we obtain the continuum PDE

$$\hat{\kappa} \hat{K} \frac{\partial \hat{x}}{\partial t} = \gamma_0 \hat{g}_2 \left(\frac{\partial \hat{x}}{\partial x} \right)^{-1} \frac{\partial}{\partial x} \left(\hat{\mu} (\hat{\alpha}_1^2 - \hat{\alpha}_1^{-2}) + \eta \frac{\partial}{\partial t} (\hat{\alpha}_1 - \hat{\alpha}_1^{-1}) \right), \quad (0 < x < l_0), \quad (3.51a)$$

with boundary conditions

$$\hat{x} = 0, \quad (x = 0), \quad (3.51b)$$

$$(\hat{\alpha}_1^2 - \hat{\alpha}_1^{-2}) + \eta \frac{\partial}{\partial t} (\hat{\alpha}_1 - \hat{\alpha}_1^{-1}) = 0, \quad (x = l_0), \quad (3.51c)$$

where

$$\hat{\alpha}_1 = \hat{g}_1^{-1} \frac{\partial \hat{x}}{\partial x}. \quad (3.51d)$$

3.2.2 Numerical Solutions

The continuum PDE system for Neo-Hookean cells (3.48a) is solved numerically using a semi-discretisation scheme and the MATLAB solver `ode15s`. The spatial domain ($0 \leq x \leq l_0$) is divided into n equally sized spatial intervals, and the spatial discretisation stencils chosen have an error of $\mathcal{O}(n^{-2})$. This code is presented in Appendix A.1. This numerical scheme converges to a fixed solution as the spatial grid is refined (for larger n) and, in the results below, we show good agreement with the discrete system.

Due to the viscous stress component, the equation of motion (3.48a) includes the term $\frac{\partial \hat{\alpha}_1}{\partial t}$ which is defined by

$$\frac{\partial \hat{\alpha}_1}{\partial t} = \frac{1}{\hat{g}_1} \frac{\partial^2 \hat{x}}{\partial x \partial t} - \frac{1}{\hat{g}_1^2} \frac{d\hat{g}_1}{dt} \frac{\partial \hat{x}}{\partial x}, \quad (0 \leq x \leq l_0). \quad (3.52)$$

However, as in the discrete system, the definition of $\frac{\partial \hat{g}_1}{\partial t}$ in (3.49), also includes the term $\frac{\partial \hat{\alpha}_1}{\partial t}$ within the $\hat{\sigma}_1$ term (3.50) inside the tanh function. Hence the system is not straight-forward to solve. We deal with this issue in an analogous manner by first solving for $\partial \hat{\alpha} / \partial t$ and, by constructing a matrix problem, solving for the rate of change of \hat{x} . Only then can we solve for \hat{x} explicitly.

For spatial discretisation we utilise n discretisation points and a second order centered-finite-difference scheme for the mid-points,

$$\frac{\partial \hat{x}^{(i)}}{\partial x} = \frac{1}{2dX} \left(\hat{x}^{(i+1)} - \hat{x}^{(i-1)} \right) + \mathcal{O}(dX^2) \quad (i = 2, \dots, n-1), \quad (3.53a)$$

$$\frac{\partial^2 \hat{x}^{(i)}}{\partial x^2} = \frac{1}{(dX)^2} \left(\hat{x}^{(i-1)} - 2\hat{x}^{(i)} + \hat{x}^{(i+1)} \right) + \mathcal{O}(dX^2) \quad (i = 2, \dots, n-1), \quad (3.53b)$$

where $dX = l_0/n$ is the step size and $\hat{x}^{(i)}$ is a discretisation point in the domain ($i = 1, \dots, n$). For the boundary conditions, we use a second order forward and backward finite-difference scheme

to avoid using points outside the domain,

$$\frac{\partial \hat{x}^{(1)}}{\partial x} = \frac{1}{2dX} \left(-3\hat{x}^{(1)} + 4\hat{x}^{(2)} - \hat{x}^{(3)} \right) + \mathcal{O}(dX^2), \quad (3.53c)$$

$$\frac{\partial \hat{x}^{(n)}}{\partial x} = \frac{1}{2dX} \left(3\hat{x}^{(n)} - 4\hat{x}^{(n-1)} + \hat{x}^{(n-2)} \right) + \mathcal{O}(dX^2). \quad (3.53d)$$

There is no need for this number of intervals to be the same as the number of discrete cells in the IBM, so this continuum PDE approach can result in a significant computational saving compared to the IBM when the number of discrete cells is large.

In the results in Sec. 3.3 below we compute the continuum pressure (3.45) and stretch (3.47), which are compared to the discrete simulations.

3.3 Results: Cell growth (Incompressible Cells)

In this section we consider unconstrained growth of a line of cells for various K and η . Cell growth is defined by (3.15) and (3.49) in the discrete and continuum systems respectively. In simulations below we choose $\sigma_0 = 0.1$ and $\gamma_0 = 1$. We use an initial $N = 100$ cells in the discrete system unless otherwise stated.

We implement a cell division law in Sec. 3.3.2, such that, for every growing cell, when a cell's area is twice the initial value ($A^{(j)} = 2A_0^{(j)}$), it divides into two identical daughter cells of exactly half the current length of the parent cell such that the two daughter cells occupy the same space as the parent cell. Each daughter cell has an initial resting length of $\frac{1}{2}L_0^{(j)}g_1^{(j)}$ for j the cell that divided. The daughter cell starts growing due to their individual prescribed growth functions and the process is repeated.

3.3.1 Case 1: Stress dependent cell growth (no proliferation)

In this section we consider stress-driven growth of the line of cells (with growth rate defined by (3.15) and (3.49) in the discrete and continuum systems, respectively). In order to assess the dynamics of growth in the presence of dissipation, Figure 3.1 considers the change in length of the array and the accompanying stretch profiles for various K and η . In the absence of internal dissipation ($\eta = 0$) we observe a linear increase of the domain length in time for all K (Fig. 3.1a). The rate of elongation increases with decreasing K (c.f. the length of the array attained by $t = 100$ decreases as K increases, Fig. 3.1a inset), as cells at the fixed end undergo a larger compression with larger K , as the forces between cells are transmitted along the line more slowly (Fig. 3.1b). Cells at the fixed end ($x = 0$) are more compressed (and hence, stressed) than those at the free boundary, which are almost unstressed (Fig. 3.1b). Hence, the growth rate of cells towards the fixed end ($x = 0$) will decrease due to their increased stress, and grow at a slower rate than cells at the free boundary.

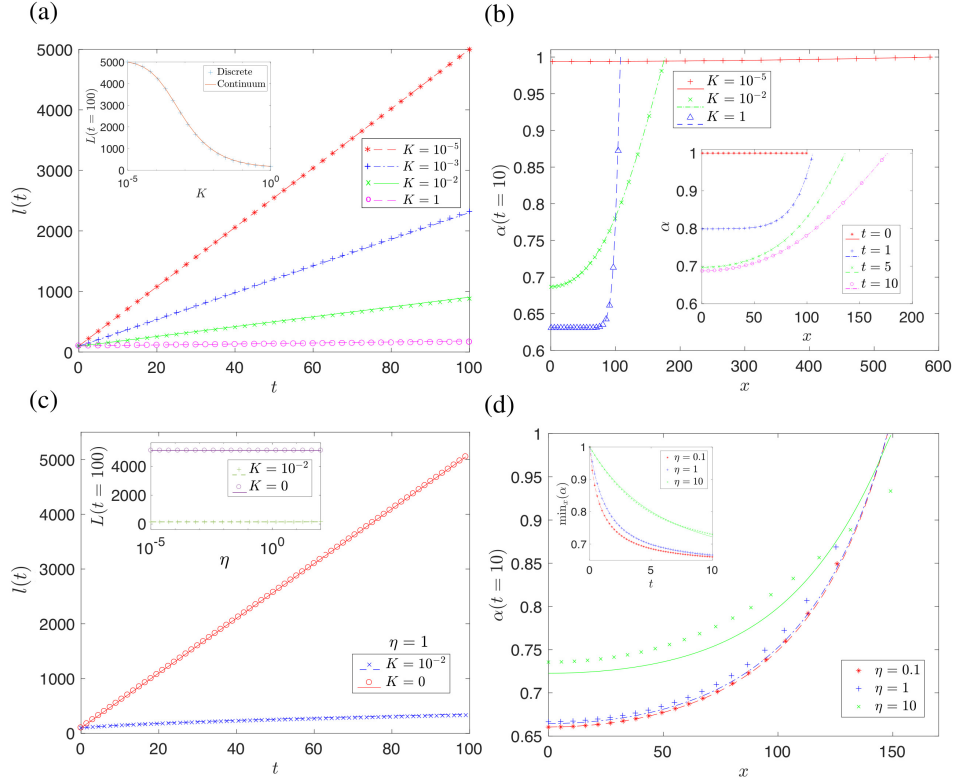


Figure 3.1: Solutions for a system of incompressible Neo-Hookean cells aligned in a single array subject to stress-driven growth. Solutions for $N = 100$ cells and uniform shear modulus $\mu = 1$, $\sigma_0 = 0.1$, with $\kappa = 1$. Discrete solutions (symbols) are displayed with corresponding upscaled continuum solutions (lines). (a) Length of the domain for $K = 10^{-5}, 10^{-3}, 10^{-2}, 10^{-1}, 1$, $\eta = 0$ for $t = 0$ to $t = 100$ (inset: length of the domain at $t = 100$ for $K = 10^{-5}$ to $K = 1$); (b) Stretch, α , at $t = 10$ for $K = 10^{-5}, 10^{-2}, 1$ and $\eta = 0$ (inset: elastic stretch across the domain at $t = 0, 1, 5, 10$ for $K = 10^{-2}$); (c) Length of array for $t = 0$ to $t = 100$ for $\eta = 1$ and $K = 0, 10^{-2}$ (inset: length of array at $t = 100$ for $\eta = 10^{-5}$ to $\eta = 1$ with $K = 0$ or $K = 10^{-2}$); (d) Stretch, α , at $t = 10$ for $\eta = 0.1, 1, 10$ and $K = 10^{-2}$ (inset: maximum compression in the array, $\min_x(\alpha)$, for $\eta = 0.1, 1, 10$ and $K = 10^{-2}$ for $t = 0$ to $t = 20$).

In the absence of substrate dissipation ($K = 0$) the length of the array again increases linearly with time, identically for values from $\eta = 10^{-5}$ to $\eta = 100$ (Fig. 3.1c). For K chosen small the total array length again increases linearly with time (identically for values of η from 10^{-5} to 100) but is shorter as the damping localises the motion to the free end of the array. For small K , the system experiences compression due to damping and reaches a steady profile of compression, with cells at $x = 0$ more compressed than those at the free end (Fig. 3.1d). The time taken to reach this steady compression profile increases with η (Fig. 3.1d inset).

In order to assess the role of substrate dissipation in localising the deformation, in Figure 3.2 we explore the two different choices of the function κ , namely $m = 0$ and $m = 1$. Linear dependency of κ on area ($m = 1$) results in slower (sublinear) growth compared to $m = 0$ (Fig. 3.2a) for both discrete and continuum models, and greater maximal compression for the same K (Fig. 3.2b). Since the dissipation is now proportional to cell area, as a cell grows it

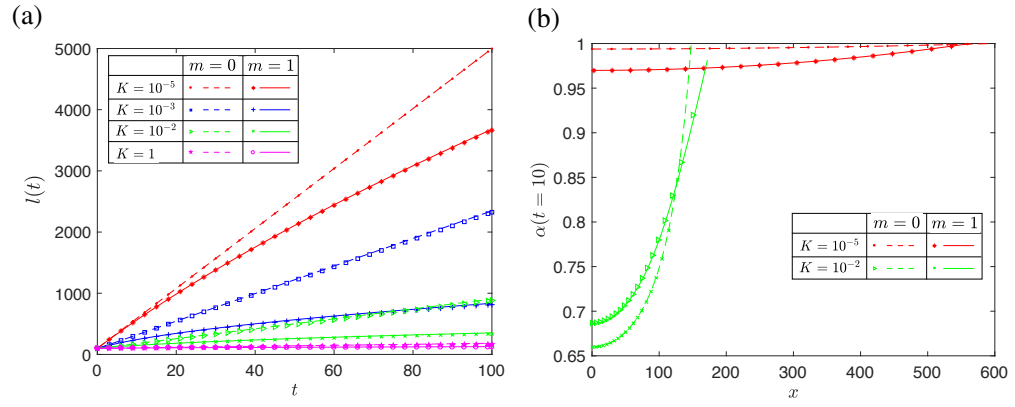


Figure 3.2: Solutions for a system of incompressible Neo-Hookean cells aligned in a single array subject to stress-driven growth. Solutions for $N = 100$ cells ($n = 101$ continuum nodes) and uniform shear modulus $\mu = 1$ with $\kappa = A(t)$. Discrete solutions (*, +, x, o) are displayed with corresponding upscaled continuum solutions (solid lines) and discrete (\cdot , \square , \triangleright , \star) and continuum (dash lines) solutions for comparison with $\kappa = 1$. System in the absence of viscous dissipation ($\eta = 0$): (a) Length of the domain for $K = 10^{-5}, 10^{-3}, 10^{-2}, 1$, $\eta = 0$ for $t = 0$ to $t = 100$; (b) Stretch at $t = 0$ for $K = 10^{-5}, 10^{-2}$ and $\eta = 0$.

is subject to an increase in dissipative forces, slowing the growth rate of the cell. Hence, this figure demonstrates that substrate dissipation proportional to cell area results in slower growth and greater maximal compression of the array.

3.3.2 Case 2: Stress dependent cell growth with proliferation

In order to assess how cell proliferation influences the rate of elongation of the array, Figure 3.3 considers the discrete model with a proliferation rule, where an individual cell is assumed to divide into two identical daughter cells when the volume of the parent cell has grown to twice the initial value ($A^{(j)} = 2A_0^{(j)}$). With proliferation, the length of the array (Fig. 3.3a,b) and the number of cells (Fig. 3.3a,b inset) grow linearly in time for long times for all K and for either choice of the dissipation function κ ($m = 0$ or $m = 1$). However, the rate of elongation is greater for smaller K (Fig. 3.3a,b) as the compressive stress is low enough to allow growth (c.f. Fig 3.1b). For $K = 10^{-5}$, the compressive stress is sufficiently low that the proliferation remains distributed across the entire array (Fig. 3.3c illustrates the relative location of division events) meaning that in this case only proliferation can result in faster growth of the array. We note the kinks in Fig. 3.3c in the temporal profiles of the division event locations demonstrate a wave of division events propagating down the array of cells such that all cells divide one after the other. By $t \approx 2.5$, all cells have undergone one division. The next set of division events starts at $t > 2.5$. However, from this point, all new sets of division events begin (that is, the cell at $x = l(t)$ divides) before the previous set has finished (that is, before the cell at $x = 0$ has divided the same amount of times as the other cells). When this new set of divisions starts, we observe a kink in the previous line of division events, at the moment they begin to overlap. For example,

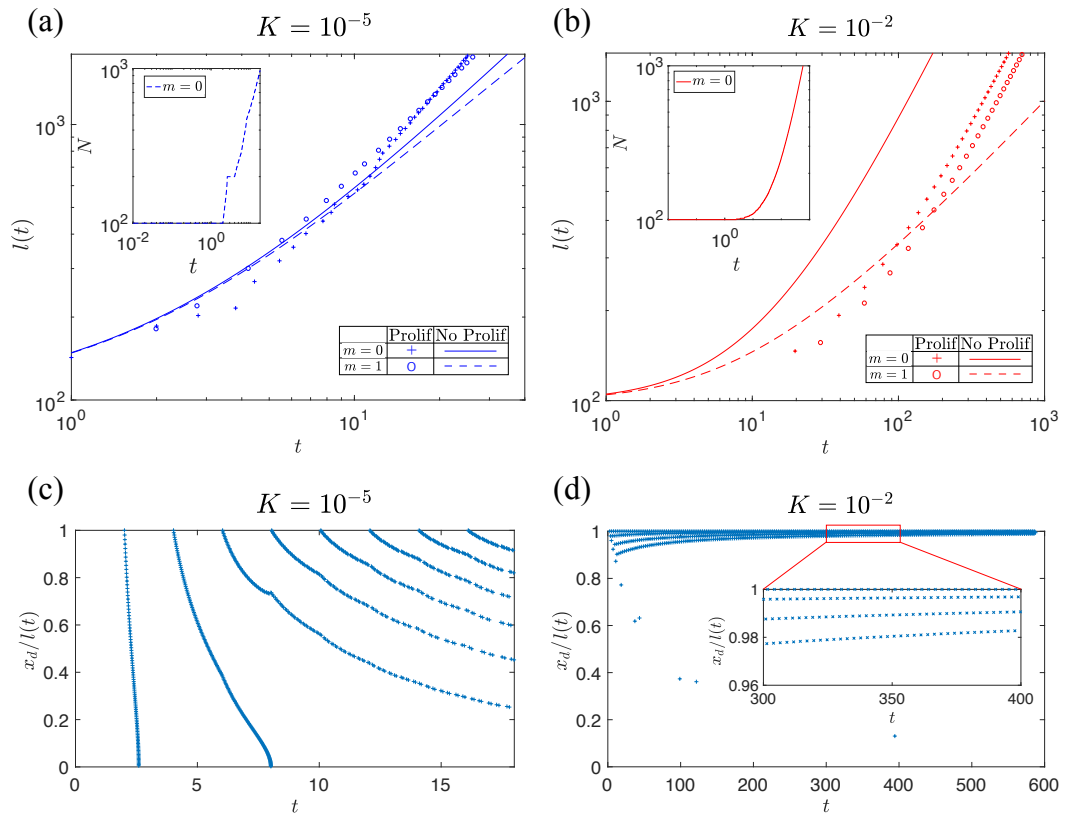


Figure 3.3: Solutions for a discrete system of incompressible Neo-Hookean cells aligned in a single array subject to stress-driven growth with substrate dissipation and cell division at $A^{(j)} = 2$. Solutions for $N_0 = 100$ cells and uniform shear modulus $\mu = 1$. (a) Domain length, $L(t)$, against t on a log-log scale for cases with and without proliferation, for $\kappa = 1$ and $\kappa = A(t)$ (inset: the number of cells, N , on a log-log scale for $\kappa = 1$) for $K = 10^{-5}$ for $t = 0$ to $t = 18$; (b) Domain length, $L(t)$, against t on a log-log scale for cases with and without proliferation, for $\kappa = 1$ and $\kappa = A(t)$ (inset: the number of cells, N , on a log-log scale for $\kappa = 1$) for $K = 10^{-2}$ for $t = 0$ to $t = 1000$; (c) Division event location, x_d , relative to current domain length, $L(t)$ for $m = 0$ and $K = 10^{-5}$ for $t = 0$ to $t = 18$; (d) Division event location, x_d , relative to current domain length, $L(t)$ for $m = 0$ and $K = 10^{-2}$ for $t = 0$ to $t = 1000$.

we observe a kink the third set of division events ($t \approx 8$) when the fourth set of division events begins and, more subtly, at $t \approx 10.1$ when the fifth set of division events begin. The start of a new set (line) of division events across the domain has a small halting effect on any current set of division events. It would make an interesting investigation in future work to consider the magnitude of this effect, and why it arises. However, for $K \geq 10^{-4}$ (shown here for $K = 10^{-2}$), the rate of elongation is substantially faster for $m = 0$ compared to $m = 1$ (Fig. 3.3b). In these cases, the behaviour with $\kappa = 1$ and no proliferation elongates most quickly as the system is not paying extra dissipation penalty for enlarging cells, and proliferation becomes localised to the free end of the domain (Fig. 3.3d). Note that Fig. 3.3d identifies divisions occurring away from the free end of the domain, which demonstrate that cells that were initially growing end up closer to the fixed end of the array, however were able to grow enough initially to eventually meet the division requirement, even with a slower growth due to compression at later times. In

summary, this figure demonstrates that cell proliferation generally leads to slower growth of the array (except in cases with very small substrate dissipation).

3.4 Summary

In this chapter we have utilised the theory of morphoelasticity [101, 107] to construct an IBM for a line of cells incorporating cell growth, and derived a corresponding continuum PDE model using discrete-to-continuum asymptotics. We investigated the role of dissipation on the system by considering two different dissipation functions, one constant and one dependent on the area of the cell in contact with the substrate. We conclude that substrate dissipation proportional to cell area results in slower growth and greater maximal compression of the array in most cases, due to the extra dissipative penalty paid by enlarging cells. For substrate dissipation (in the absence of internal dissipation) the array length increases linearly with time. Similarly, for internal dissipation in the absence of substrate dissipation, the array length also increases linearly with time, identically for all values of viscous dissipation constant η . Incorporating proliferation into the system, for all cases except extremely small values of substrate damping, proliferation becomes localised to the free end of the domain, mimicking the behaviour of a proliferating rim. A proliferating rim is of interest due to the behaviour of cancerous cells. Previous research on spherical clusters of cells (e.g. a tumor) show a characteristic structure of a proliferating rim and a necrotic core, where cells grow (and divide) outwards and at the centre can die [103]. We have therefore been able to reproduce a proliferating rim behaviour purely from a mechanical formulation of the system, in contrast to previous works in which this behaviour arises due to nutrient and cell-density profiles (e.g. [103]) or by constructing a model with discrete areas of proliferating, quiescent and necrotic cells (e.g. [126]).

Chapter 4

Two- and Three-Dimensional Discrete-to-Continuum Models

We now extend the geometry from Chapter 2 to three spatial dimensions to consider a three-dimensional sheet of incompressible nonlinearly elastic cells of constant density, arranged in an initially rectangular array atop a rigid substrate, as shown in Fig. 4.1. The array is constructed in an initial configuration of M identical rows of N cuboidal cells (i.e. M rows of the single array from Chapter 2).

We first formulate a discrete individual-based model (Sec. 4.1) and outline challenges in the general formulation. We then specify the cell deformation to first consider a uniaxial deformation (Sec. 4.2) for each cell, where one outer edge of the array is fixed and the outer edge parallel to it is subject to a prescribed deformation. This deformation is applied in one direction (uniaxial deformation) however the cells respond by deforming in all three dimensions. We consider two possibilities for the final two boundaries. Firstly, we impose symmetry of deformation along one of the edges perpendicular to the fixed edge and impose zero external stress in the other. Second, we assume that the two outer edges perpendicular to the fixed edge are periodic. We then move on to consider cells undergoing a simple shear deformation (Sec. 4.3) and investigate the response of the system when one outer edge is fixed and the other edge parallel to this is moved at a constant speed. This formulation reduces this particular model to two-dimensions, similar to Chapters 2 and 3..

4.1 The model

We consider a quasi-three dimensional sheet of discrete cells atop a substrate, as shown in Fig. 4.1a. In the plane of the substrate, one edge of the array is parametrised by the coordinate x , while the direction normal to this is parametrised by the coordinate y , with the z -direction normal to the substrate. On $z = 0$ we assume no motion in the z direction, while on the remaining surface normal to z we assume a boundary condition of zero stress. Cells are in contact along

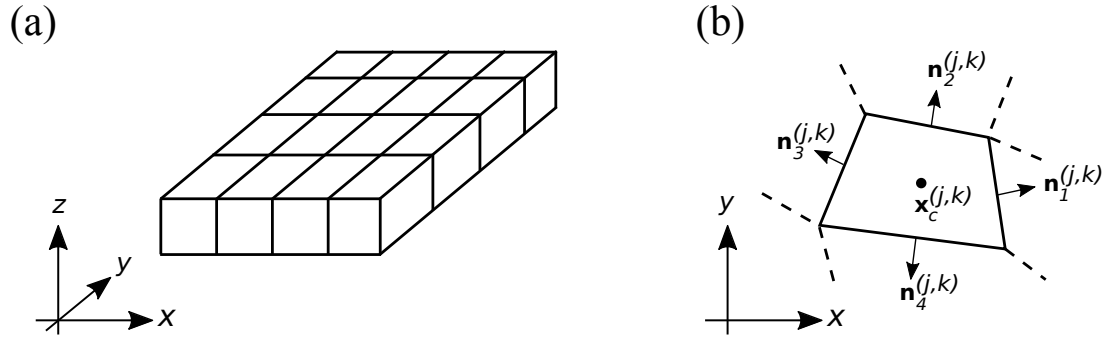


Figure 4.1: Geometrical set up of a quasi-three dimensional sheet of discrete cells. (a) three-dimensional rectangular cells; (b) vertex-model set up for four-sided cells in the (x, y) plane.

their shared edges, where stresses are transmitted (Fig. 4.1b). All cells are assumed to be incompressible, which imposes a local constraint on each cell deformation. We assume cell edges normal to $z = 0$ can slip past each other with no friction, hence the problem can be represented as a planar system in the (x, y) plane, as deformation in the third dimension can be implicitly solved for with the constraint of incompressibility. This reduces the system to a quasi-three dimensional model.

We consider an initially rectangular array of M rows of N discrete cells. These cells are indexed by the coordinate j ($j = 1, \dots, N$) in the x -direction and k ($k = 1, \dots, M$) in the y -direction. The properties of cell j, k are labelled with a superscript (j, k) . In general these individual cells can have complicated shapes and are embedded within an extracellular matrix. For simplicity we assume that each constituent cell can be modelled as a quadrilateral prism which deforms in a manner which allows it to remain in contact with its nearest neighbours (i.e. ignore bending of all edges in this formation). In the general formulation, a cell may not always have the same neighbour. A significant challenge would be to keep track of which cells are in contact. Here, we assume only small deformations and that that cells neighbours remain constant. In the (x, y) plane these cells are four-sided shapes. We denote the outer unit normal of edge i as $\mathbf{n}_i^{(j,k)}$ ($i = 1, 2, 3, 4$), as outlined in Fig. 4.1b.

We assume the cells have uniform density ρ , and characterise cells by the position of their centre of mass (which coincides with their geometric centre since the density is uniform) denoted $\mathbf{x}_c^{(j,k)} = (x_c^{(j,k)}(t), y_c^{(j,k)}(t), \frac{1}{2}H^{(j,k)}(t))$, for $j = 1, \dots, N$ and $k = 1, \dots, M$, where $H^{(j,k)}$ is the height (in the z -direction) of cell (j, k) .

The (local) reference coordinate system for cells is denoted $\mathbf{X}^{(j,k)} = (X^{(j,k)}, Y^{(j,k)}, Z^{(j,k)})$ where $X^{(j,k)} = x - x_c^{(j,k)}$, $Y^{(j,k)} = y - y_c^{(j,k)}$ and $Z^{(j,k)} = z - \frac{1}{2}H^{(j,k)}$, so that $-\frac{1}{2}L_0^{(j,k)} \leq X^{(j,k)} \leq \frac{1}{2}L_0^{(j,k)}$, $-\frac{1}{2}W_0^{(j,k)} \leq Y^{(j,k)} \leq \frac{1}{2}W_0^{(j,k)}$ and $-\frac{1}{2}H_0^{(j,k)} \leq Z^{(j,k)} \leq \frac{1}{2}H_0^{(j,k)}$, where $L_0^{(j,k)}$, $W_0^{(j,k)}$ and $H_0^{(j,k)}$ are the cells initial length (x -direction), width (y -direction) and height (z -direction), respectively. In the current configuration, the coordinate system for cells is defined by $\mathbf{x}^{(j,k)} = \boldsymbol{\chi}^{(j,k)}(\mathbf{X}^{(j,k)}, t)$ and the corresponding deformation gradient tensor is defined by $\mathbb{F}^{(j,k)} = \text{Grad}(\mathbf{x}^{(j,k)})$, where the gradient operator is measured with respect to the reference coordinate system $\mathbf{X}^{(j,k)}$

and the mapping $\boldsymbol{\chi}^{(j,k)}$ defines the deformation from the reference to the current configuration.

4.1.1 Elastic Deformation

We assume each cell undergoes a nonlinear elastic deformation, with deformation gradient $\mathbb{F}^{(j,k)}$. The constraint of incompressibility implies $\det(\mathbb{F}^{(j,k)}) = 1$. We wish to maintain generality and so do not yet define the form of the deformation gradient.

4.1.2 Elastic Stress

The elastic deformation of cell (j, k) follows from an incompressible strain energy functional

$$\mathcal{W}^{(j,k)} = \mathcal{W}^{(j,k)}(\lambda_1^{(j,k)}, \lambda_2^{(j,k)}, \lambda_3^{(j,k)}), \quad (j = 1, \dots, N; k = 1, \dots, M). \quad (4.1)$$

We characterise the elasticity of individual cells by their shear modulus, denoted $\mu^{(j,k)}$, ($j = 1, \dots, N; k = 1, \dots, M$), and denote μ_0 as a typical shear modulus (for example, the mean value for a healthy cell and in this chapter we use $\mu_0 = 1$) for cells in the array.

The corresponding Cauchy stress tensor for cell (j, k) is then given by

$$\boldsymbol{\sigma}^{(j,k)} = \mathbb{F}^{(j,k)} \frac{\partial \mathcal{W}^{(j,k)}}{\partial \mathbb{F}^{(j,k)}} - p^{(j,k)} \mathbb{I}, \quad (j = 1, \dots, N; k = 1, \dots, M) \quad (4.2)$$

where $p^{(j,k)}$ is a Lagrange multiplier interpreted as the internal pressure of cell (j, k) .

4.1.3 Boundary Conditions

The pressure within each cell, $p^{(j,k)}$ ($j = 1, \dots, N; k = 1, \dots, M$), is determined by applying the boundary condition of no lateral force on the upper surface (perpendicular to $\hat{\mathbf{z}}$) which gives

$$\mathbf{0} = \int_{z=H^{(j,k)}} \boldsymbol{\sigma}^{(j,k)} \cdot \hat{\mathbf{z}} \, dA^{(j,k)}, \quad (4.3)$$

where $A^{(j,k)}$ is the cross-sectional area in the (x, y) plane of cell (j, k) .

The force exerted from cell (j, k) on the edge i is given by

$$\mathbf{F}_i^{(j,k)} = \int \boldsymbol{\sigma}^{(j+1,k)} \cdot \mathbf{n}_i^{(j,k)} \, dS_i^{(j,k)}, \quad (i = 1, \dots, 4), \quad (4.4)$$

where $S_i^{(j,k)}$ represents the area of the edge with outer unit normal $\mathbf{n}_i^{(j,k)}$ ($i = 1, \dots, 4$).

We denote the external force on edge i from the neighbouring cell as $\mathbf{F}_i^{\prime(j,k)}$, which is given

by

$$\mathbf{F}_{i'}^{(j,k)} = \int \boldsymbol{\sigma}^{(p,q)} \cdot \mathbf{n}_{i'}^{(p,q)} dS_{i'}, \quad (4.5)$$

where (p, q) are the indices of the cell whose edge i' is the same as edge i of cell (j, k) and $\mathbf{n}_{i'}^{(p,q)} = -\mathbf{n}_i^{(j,k)}$. Hence the resultant force across the cell edge i is denoted

$$\mathbf{F}_{e_i}^{(j,k)} = \mathbf{F}_i^{(j,k)} + \mathbf{F}_{i'}^{(p,q)}. \quad (4.6)$$

These net forces drive the motion and deformation of the array of cells.

4.1.4 Governing Equations

We assume that the cells are binding and unbinding to a substrate which is fixed in the plane of the page: the resulting damping force is assumed proportional to the dimensionless function of the cell cross-sectional area in contact with the substrate

$$\kappa^{(j,k)} = \left(\frac{A^{(j,k)}}{A_0^{(j,k)}} \right)^m, \quad (j = 1, \dots, N; k = 1, \dots, M), \quad (4.7)$$

and the rate of change of the position of the centre of mass of the cell relative to the substrate, with constant of proportionality $K^{(j,k)}$ ($j = 1, \dots, N; k = 1, \dots, M$). Applying Newton's second law and neglecting inertial effects, we express the global force balance at the cell centre-of-mass,

$$\kappa^{(j,k)} K^{(j,k)} \frac{d\mathbf{x}_c^{(j,k)}}{dt} = \sum_{i=1}^4 \mathbf{F}_{e_i}^{(j,k)}, \quad (j = 1, \dots, N; k = 1, \dots, M), \quad (4.8)$$

where $\mathbf{F}_{e_i}^{(j,k)}$ is the force balance across the shared edge i , defined by (4.6).

However, it is difficult to compute a generalised $\boldsymbol{\sigma}^{(j,k)}$ for this system. A significant challenge is to keep track of cell vertices as the cell deforms as the force balance is at the centre of mass. The system requires additional constraints at each vertex to ensure cells meet perfectly and there are no gaps. It could be better to formulate this as a vertex model in terms of vertex locations (possible in one-dimension), however this would make it difficult to formulate dissipation and would require resolution of the stress singularities at the corners.

Instead, we make approximations to construct a consistent model in the form of simple assumptions about how the cell centre and the cell's vertices are related. Hence, we will consider two simple deformations of each cell to define this relation and allow cells to remain in contact with their nearest neighbours. First we assume cells undergo a simple uniaxial deformation in Sec. 4.2, and second we consider cells undergoing a simple shear deformation in Sec. 4.3.

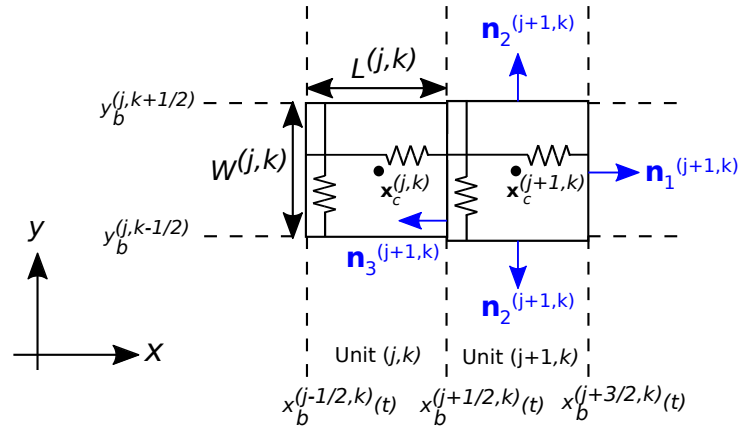


Figure 4.2: Geometrical set up of M rows of N elastic cells aligned end to end.

4.2 Uniaxial deformation

In order to define the deformation and Cauchy stress (and hence, governing equations) for each cell, we assume that each constituent cell from Sec. 4.1 can be modelled as a cuboid with a rectangular cross-section in the (x, y) plane, which deforms uniaxially. In a similar manner to Chapters 2 and 3 we use the index $(j + 1/2, k)$ to denote the boundary between cells (j, k) and $(j + 1, k)$ and the index $(j, k + 1/2)$ to denote the boundary between cells (j, k) and $(j, k + 1)$.

The length of a cell in the x -direction (along unit vector $\hat{\mathbf{x}}$) is given by

$$L^{(j,k)} = x_b^{(j+1/2,k)} - x_b^{(j-1/2,k)}, \quad (j = 1, \dots, N; k = 1, \dots, M), \quad (4.9)$$

(with initial value $L_0^{(j,k)}$), where $x_b^{(j+1/2,k)}$ ($j = 0, \dots, N; k = 1, \dots, M$) defines the x -coordinate of the boundary between cell (j, k) and $(j + 1, k)$. The width of a cell in the y -direction (along unit vector $\hat{\mathbf{y}}$) is given by

$$W^{(j,k)} = y_b^{(j,k+1/2)} - y_b^{(j,k-1/2)}, \quad (j = 1, \dots, N; k = 1, \dots, M), \quad (4.10)$$

(with initial value $W_0^{(j,k)}$), where $y_b^{(j,k+1/2)}$ ($j = 1, \dots, N; k = 0, \dots, M$) defines the y -coordinate of the boundary between cell (j, k) and $(j, k + 1/2)$. The height of a cell in the z -direction (along unit vector \mathbf{z}) is denoted $H^{(j,k)}$ (with initial value $H_0^{(j,k)}$), for $j = 1, \dots, N$ and $k = 1, \dots, M$.

In this configuration, each cell has four outward unit normals in the form

$$\begin{aligned} \mathbf{n}_1^{(j,k)} &= -\mathbf{n}_3^{(j,k)} = \hat{\mathbf{x}}, & (j = 1, \dots, N; k = 1, \dots, M) \\ \mathbf{n}_2^{(j,k)} &= -\mathbf{n}_4^{(j,k)} = \hat{\mathbf{y}}, & (j = 1, \dots, N; k = 1, \dots, M), \end{aligned} \quad (4.11)$$

as shown in Fig. 4.2.

4.2.1 Elastic Deformation

We assume each cell undergoes a nonlinear elastic deformation, with deformation gradient $\mathbb{F}^{(j,k)}$ of the form

$$\mathbb{F}^{(j,k)} = \begin{bmatrix} \lambda_1^{(j,k)} & 0 & 0 \\ 0 & \lambda_2^{(j,k)} & 0 \\ 0 & 0 & \lambda_3^{(j,k)} \end{bmatrix}, \quad (j = 1, \dots, N; k = 1, \dots, M), \quad (4.12)$$

where $\lambda_1^{(j,k)}$, $\lambda_2^{(j,k)}$ and $\lambda_3^{(j,k)}$ are the principal stretches of cell (j, k) ($j = 1, \dots, N; k = 1, \dots, M$), and

$$\lambda_1^{(j,k)} = \frac{x_b^{(j+1/2,k)} - x_b^{(j-1/2,k)}}{L_0^{(j,k)}}, \quad \lambda_2^{(j,k)} = \frac{y_b^{(j,k+1/2)} - y_b^{(j,k-1/2)}}{W_0^{(j,k)}}, \quad (j = 1, \dots, N; k = 1, \dots, M). \quad (4.13)$$

4.2.2 Incompressibility

The constraint of incompressibility implies $\det(\mathbb{F}^{(j,k)}) = 1$. Hence

$$\lambda_3^{(j,k)} = \frac{1}{\lambda_1^{(j,k)} \lambda_2^{(j,k)}}, \quad (j = 1, \dots, N; k = 1, \dots, M), \quad (4.14)$$

and so we use this constraint to eliminate $\lambda_3^{(j,k)}$ from the final equations in favour of the other stretches.

4.2.3 Elastic Stress

When specifying the model, we consider the incompressible Neo-Hookean strain energy functional for each cell

$$\mathcal{W}^{(j,k)} = \frac{1}{2} \mu^{(j,k)} \left(\left(\lambda_1^{(j,k)} \right)^2 + \left(\lambda_2^{(j,k)} \right)^2 + \left(\lambda_3^{(j,k)} \right)^2 - 3 \right), \quad (j = 1, \dots, N; k = 1, \dots, M). \quad (4.15)$$

The Cauchy stress (4.2) takes the simple form

$$\begin{aligned} \boldsymbol{\sigma}^{(j,k)} &= \mathbb{F}^{(j,k)} \left(\mathbb{F}^{(j,k)} \right)^T - p^{(j,k)} \mathbb{I}, \quad (j = 1, \dots, N; k = 1, \dots, M) \quad (4.16) \\ &= \begin{bmatrix} \mu^{(j,k)} \left(\lambda_1^{(j,k)} \right)^2 - p^{(j,k)} & 0 & 0 \\ 0 & \mu^{(j,k)} \left(\lambda_2^{(j,k)} \right)^2 - p^{(j,k)} & 0 \\ 0 & 0 & \mu^{(j,k)} \left(\lambda_3^{(j,k)} \right)^2 - p^{(j,k)} \end{bmatrix}. \quad (4.17) \end{aligned}$$

4.2.4 Boundary Conditions

Applying the condition (4.3) of zero external stress on $z = H^{(j,k)}$ yields

$$p^{(j,k)} = \mu^{(j,k)} \left(\lambda_3^{(j,k)} \right)^2 = \mu^{(j,k)} \left(\lambda_1^{(j,k)} \lambda_2^{(j,k)} \right)^{-2}, \quad (j = 1, \dots, N; k = 1, \dots, M), \quad (4.18)$$

and hence the only non-zero components of $\boldsymbol{\sigma}$ are

$$\sigma_{11}^{(j,k)} = \mu^{(j,k)} \left(\left(\lambda_1^{(j,k)} \right)^2 - \left(\lambda_1^{(j,k)} \lambda_2^{(j,k)} \right)^{-2} \right), \quad (j = 1, \dots, N; k = 1, \dots, M), \quad (4.19a)$$

$$\sigma_{22}^{(j,k)} = \mu^{(j,k)} \left(\left(\lambda_2^{(j,k)} \right)^2 - \left(\lambda_1^{(j,k)} \lambda_2^{(j,k)} \right)^{-2} \right), \quad (j = 1, \dots, N; k = 1, \dots, M). \quad (4.19b)$$

The force from cell (j, k) on cell $(j \pm 1, k)$ is given by

$$\mathbf{F}_{x\pm}^{(j,k)} = \int_0^{H^{(j\pm 1/2,k)}} \int_{-\frac{1}{2}W^{(j\pm 1/2,k)}}^{\frac{1}{2}W^{(j\pm 1/2,k)}} \boldsymbol{\sigma}^{(j,k)} \cdot (\mp \hat{\mathbf{x}}) \, dy \, dz, \quad (4.20)$$

$$= \mp H^{(j\pm 1/2,k)} W^{(j\pm 1/2,k)} \sigma_{11}^{(j,k)} \hat{\mathbf{x}}, \quad (4.21)$$

where $W^{(j\pm 1/2,k)}$ represents the length in the y -direction of the shared boundary between cells (j, k) and $(j \pm 1, k)$, which we approximate by the mean of the cell widths

$$W^{(j\pm 1/2,k)} = \frac{1}{2} \left(W^{(j,k)} + W^{(j\pm 1,k)} \right), \quad (j = 1, \dots, N; k = 1, \dots, M) \quad (4.22)$$

where $W^{(j,k)} = W_0 \lambda_2^{(j,k)}$, and $H^{(j\pm 1/2,k)}$ represents the length in the z -direction of the shared boundary between cells (j, k) and $(j \pm 1, k)$, which we approximate by the mean of the cell heights

$$H^{(j\pm 1/2,k)} = \frac{1}{2} \left(H^{(j,k)} + H^{(j\pm 1,k)} \right), \quad (j = 1, \dots, N; k = 1, \dots, M) \quad (4.23)$$

where $H^{(j,k)} = H_0^{(j,k)} \left(\lambda_1^{(j,k)} \lambda_2^{(j,k)} \right)^{-1}$ is the current cell height.

The force from cell (j, k) on cell $(j, k \pm 1)$ is given by

$$\mathbf{F}_{y\pm}^{(j,k)} = \int_0^{H^{(j,k\pm 1/2)}} \int_{-\frac{1}{2}L^{(j,k\pm 1/2)}}^{\frac{1}{2}L^{(j,k\pm 1/2)}} \boldsymbol{\sigma}^{(j,k)} \cdot (\mp \hat{\mathbf{y}}) \, dx \, dz \quad (4.24)$$

$$= \mp H^{(j,k\pm 1/2)} L^{(j,k\pm 1/2)} \sigma_{22}^{(j,k)} \hat{\mathbf{y}} \quad (4.25)$$

where $L^{(j,k\pm 1/2)}$ represents the length of the shared boundary between cells (j, k) and $(j, k \pm 1)$, which we approximate by the mean of the cell lengths

$$L^{(j,k\pm 1/2)} = \frac{1}{2} \left(L^{(j,k)} + L^{(j,k\pm 1)} \right), \quad (j = 1, \dots, N; k = 1, \dots, M) \quad (4.26)$$

where $L^{(j,k)} = L_0 \lambda_1^{(j,k)}$.

The resultant force across the cell boundary between cells (j, k) and $(j+1, k)$ is denoted

$$\mathbf{F}_{b_x}^{(j+1/2,k)} = \mathbf{F}_{x^+}^{(j,k)} + \mathbf{F}_{x^-}^{(j+1,k)}, \quad (j = 1, \dots, N-1; k = 1, \dots, M) \quad (4.27)$$

while the resultant force across the cell boundary between cells (j, k) and $(j, k+1)$ is denoted

$$\mathbf{F}_{b_y}^{(j,k+1/2)} = \mathbf{F}_{y^+}^{(j,k)} + \mathbf{F}_{y^-}^{(j,k+1)}, \quad (j = 1, \dots, N; k = 1, \dots, M-1) \quad (4.28)$$

These net forces drive the motion and deformation of the array of cells.

4.2.5 Discrete governing equations

The governing equation (4.8) along with the forces (4.27) and (4.28) yield the equations

$$\begin{aligned} \kappa^{(j,k)} K \frac{dx_c^{(j,k)}}{dt} &= H^{(j+1/2,k)} W^{(j+1/2,k)} \left(\sigma_{11}^{(j+1,k)} - \sigma_{11}^{(j,k)} \right) \\ &\quad + H^{(j-1/2,k)} W^{(j-1/2,k)} \left(\sigma_{11}^{(j,k)} - \sigma_{11}^{(j-1,k)} \right), \end{aligned} \quad (4.29)$$

$$\begin{aligned} \kappa^{(j,k)} K \frac{dy_c^{(j,k)}}{dt} &= H^{(j,k+1/2)} L^{(j,k+1/2)} \left(\sigma_{22}^{(j,k+1)} - \sigma_{22}^{(j,k)} \right) \\ &\quad + H^{(j,k-1/2)} L^{(j,k-1/2,k)} \left(\sigma_{22}^{(j,k)} - \sigma_{22}^{(j,k-1)} \right), \end{aligned} \quad (4.30)$$

(for $j = 1, \dots, N; k = 1, \dots, M$), where $\sigma_{11}^{(j,k)}$, $\sigma_{22}^{(j,k)}$ are defined in (4.19a) and (4.19b) respectively, $\lambda_1^{(j,k)}$ and $\lambda_2^{(j,k)}$ are defined in (4.13) and $H^{(j\pm 1/2, k\pm 1/2)}$, $W^{(j\pm 1/2)}$, $L^{(j, k\pm 1/2)}$ are as defined in (4.44a), (4.44b) and (4.44c) respectively. Note that these equations are analogous to those presented in Chs. 2 and 3.

4.2.6 Initial Conditions

Initially, the cells are arranged in a rectangular array, where all cells are the same size and shape (cuboidal, with a rectangular cross section in the (x, y) plane). The geometry of the cell is initially defined by

$$x_b^{(j-1/2,k)}(0) = \sum_{i=1}^j L_0^{(j,k)}, \quad (j = 1, \dots, N+1; k = 1, \dots, M), \quad (4.31a)$$

$$y_b^{(j,k-1/2)}(0) = \sum_{i=1}^k W_0^{(j,k)}, \quad (j = 1, \dots, N; k = 1, \dots, M+1), \quad (4.31b)$$

$$H^{(j,k)}(0) = H_0^{(j,k)}, \quad (j = 1, \dots, N; k = 1, \dots, M+1). \quad (4.31c)$$

with $x_b^{(1/2)} = 0$ and $y_b^{(1/2)} = 0$. In the simulations below we assume all cells are initially the same length $L_0^{(j,k)} = L_0$, width $W_0^{(j,k)} = W_0$ and height, $H_0^{(j,k)} = H_0$ ($j = 1, \dots, N$; $k = 1, \dots, M$). This is not a necessary assumption but significantly simplifies the specification of the model and the upscaling to a continuum model for Sec 4.2.9. In this case, (4.31a) reduces to

$$x_b^{(j-1/2,k)}(0) = L_0(j-1), \quad (j = 1, \dots, N+1; k = 1, \dots, M), \quad (4.32a)$$

$$y_b^{(j,k-1/2)}(0) = W_0(k-1), \quad (j = 1, \dots, N; k = 1, \dots, M+1), \quad (4.32b)$$

$$H^{(j,k)}(0) = H_0, \quad (j = 1, \dots, N; k = 1, \dots, M+1). \quad (4.32c)$$

4.2.7 Discrete global boundary conditions

To fully specify the problem we must specify boundary conditions on all four outer edges ($x = 0$, $x = l_0$, $y = 0$, $y = w_0$). For all systems, we constrain the edge of the array along $x = 0$ to enforce no displacement in the x -direction, and prescribe a displacement at the edge of the array at $x = l_0$, such that

$$x_b^{(1/2,k)} = 0, \quad x_b^{(N+1/2,k)} = l(t), \quad (k = 1, \dots, M). \quad (4.33)$$

Similar to Chapter 2, we consider a prescribed deformation over a timescale t_p . We consider two different choices for the remainder of the global boundary conditions. Firstly in Sec. 4.2.12, we consider a test problem with simple boundary conditions, and assume

$$y_b^{(j,1/2)} = 0, \quad (4.34)$$

with a boundary condition of no external stress, such that

$$F_{y^-}^{(j,M+1)} = 0, \quad (j = 1, \dots, N), \quad (4.35)$$

meaning the force balance on boundaries ($j, M + 1/2$) can be expressed as

$$\mathbf{F}_{b_y}^{(j,M+1/2)} = \mathbf{F}_{y^+}^{(j,M)}, \quad (j = 1, \dots, N). \quad (4.36)$$

and hence

$$\begin{aligned} \kappa^{(j,M)} K \frac{dy_c^{(j,M)}}{dt} &= -H^{(j,M)} L^{(j,M)} \sigma_{22}^{(j,M)} \\ &+ H^{(j,M-1/2)} L^{(j,M-1/2)} \left(\sigma_{22}^{(j,M)} - \sigma_{22}^{(j,M-1)} \right), \quad (j = 1, \dots, N). \end{aligned} \quad (4.37)$$

Secondly in Sec. 4.2.13, we assume the domain is periodic in the interval $0 \leq y \leq y_0$, so

$$y_b^{(j,M+1/2)}(t) - y_b^{(j,M+1/2)}(0) = y_b^{(j,1/2)}(t), \quad (j = 1, \dots, N). \quad (4.38)$$

4.2.8 Non-dimensional variables

It is useful to consider the system in terms of non-dimensional variables (denoted with an overbar). We scale time on the timescale of prescribed deformation t_p (similar to Chapter 2), lengths on L_0 , forces per unit area on $\mu_0 L_0^2$ and pressures and other stress-like parameters on μ_0 , such that

$$\begin{aligned} (x_c^{(j,k)}, y_c^{(j,k)}, L^{(j,k)}, W^{(j,k)}, H^{(j,k)}) &= L_0(\bar{x}^{(j,k)}, \bar{y}^{(j,k)}, \bar{L}^{(j,k)}, \bar{W}^{(j,k)}, \bar{H}^{(j,k)}), \\ \mu^{(j,k)} &= \mu_0 \bar{\mu}^{(j,k)}, \quad \mathcal{W}^{(j,k)} = \mu_0 \bar{\mathcal{W}}^{(j,k)}, \quad (j = 1, \dots, N; k = 1, \dots, M), \end{aligned} \quad (4.39)$$

and

$$\begin{aligned} x_b^{(j-1/2,k)} &= L_0 \bar{x}_b^{(j-1/2,k)} \quad (j = 1, \dots, N+1; k = 1, \dots, M), \\ x_b^{(j,k-1/2)} &= L_0 \bar{y}_b^{(j,k-1/2)} \quad (j = 1, \dots, N; k = 1, \dots, M+1). \end{aligned} \quad (4.40)$$

This results in the following dimensionless groups

$$\bar{\gamma}_0 = \frac{W_0}{L_0}, \quad \bar{\beta}_0 = \frac{H_0}{L_0}, \quad \bar{K}^{(j,k)} = \frac{K^{(j,k)}}{t_0 \mu_0 L_0}, \quad (j = 1, \dots, N; k = 1, \dots, M), \quad (4.41)$$

representing the planar aspect ratio of the cells and the dimensionless substrate damping coefficient. We further define

$$\begin{aligned} l(t) &= L_0 \bar{l}(\bar{t}), & F_b(t) &= \mu_0 L_0^2 \bar{F}_b(\bar{t}), & \boldsymbol{\sigma} &= \mu_0 \bar{\boldsymbol{\sigma}}, \\ \bar{L}^{(j,k)}(t) &= \lambda_1^{(j,k)}(\bar{t}), & \bar{W}^{(j,k)}(t) &= \bar{\gamma}_0 \lambda_2^{(j,k)}(\bar{t}), \\ \bar{H}^{(j,k)}(t) &= \frac{\bar{\beta}_0}{\lambda_1^{(j,k)}(\bar{t}) \lambda_2^{(j,k)}(\bar{t})}, & \bar{A}^{(j,k)}(t) &= \bar{\gamma}_0 \lambda_1^{(j,k)} \lambda_2^{(j,k)}, \quad (j = 1, \dots, N; k = 1, \dots, M). \end{aligned} \quad (4.42)$$

The final non-dimensional system takes the form of the ODEs

$$\begin{aligned} \kappa^{(j,k)} \bar{K}^{(j,k)} \frac{d\bar{x}_c^{(j,k)}}{d\bar{t}} &= \bar{H}^{(j+1/2,k)} \bar{W}^{(j+1/2,k)} \left(\bar{\sigma}_{11}^{(j+1,k)} - \bar{\sigma}_{11}^{(j,k)} \right) \\ &\quad + \bar{H}^{(j-1/2,k)} \bar{W}^{(j-1/2,k)} \left(\bar{\sigma}_{11}^{(j,k)} - \bar{\sigma}_{11}^{(j-1,k)} \right), \quad (j = 1, \dots, N; k = 1, \dots, M), \end{aligned} \quad (4.43a)$$

$$\begin{aligned} \kappa^{(j,k)} \bar{K}^{(j,k)} \frac{d\bar{y}_c^{(j,k)}}{d\bar{t}} &= \bar{H}^{(j,k+1/2)} \bar{L}^{(j,k+1/2)} \left(\bar{\sigma}_{22}^{(j,k+1)} - \bar{\sigma}_{22}^{(j,k)} \right) \\ &\quad + \bar{H}^{(j,k-1/2)} \bar{L}^{(j,k-1/2)} \left(\bar{\sigma}_{22}^{(j,k)} - \bar{\sigma}_{22}^{(j,k-1)} \right), \quad (j = 1, \dots, N; k = 1, \dots, M), \end{aligned} \quad (4.43b)$$

where

$$\bar{H}^{(j\pm 1/2,k)} = \frac{\bar{\beta}_0}{2} \left(\frac{1}{\lambda_1^{(j,k)} \lambda_2^{(j,k)}} + \frac{1}{\lambda_1^{(j\pm 1,k)} \lambda_2^{(j\pm 1,k)}} \right), \quad (j = 1, \dots, N; k = 1, \dots, M), \quad (4.44a)$$

$$\bar{W}^{(j\pm 1/2,k)} = \frac{\bar{\gamma}_0}{2} \left(\lambda_2^{(j,k)} + \lambda_2^{(j\pm 1,k)} \right), \quad (j = 1, \dots, N; k = 1, \dots, M), \quad (4.44b)$$

$$\bar{L}^{(j,k\pm 1/2)} = \frac{1}{2} \left(\lambda_1^{(j,k)} + \lambda_1^{(j,k)} \right), \quad (j = 1, \dots, N; k = 1, \dots, M). \quad (4.44c)$$

The prescribed deformation boundary conditions (4.33) take non-dimensional form

$$\bar{x}_b^{(1/2,k)} = 0, \quad \bar{x}_b^{(N+1/2,k)} = \bar{l}(t), \quad (k = 1, \dots, M). \quad (4.45)$$

with either a zero-external stress boundary condition at $y = w_0$ (4.37),

$$\begin{aligned} \bar{\kappa}^{(j,M)} \bar{K} \frac{d\bar{y}_c^{(j,M)}}{d\bar{t}} &= -\bar{H}^{(j,M)} \bar{L}^{(j,M)} \bar{\sigma}_{22}^{(j,M)} \\ &\quad + \bar{H}^{(j,M-1/2)} \bar{L}^{(j,M-1/2)} \left(\bar{\sigma}_{22}^{(j,M)} - \bar{\sigma}_{22}^{(j,M-1)} \right), \quad (j = 1, \dots, N), \end{aligned} \quad (4.46)$$

or periodicity across $0 \leq y \leq l_0$ (4.38),

$$\bar{y}_b^{(j,M+1/2)}(t) - \bar{y}_b^{(j,M+1/2)}(0) = \bar{y}_b^{(j,1/2)}(t), \quad (j = 1, \dots, N). \quad (4.47)$$

The initial condition is given by

$$\bar{x}_b^{(j-1/2,k)}(0) = (j-1), \quad (j = 1, \dots, N+1; k = 1, \dots, M), \quad (4.48)$$

$$\bar{y}_b^{(j,k-1/2)}(0) = (k-1), \quad (j = 1, \dots, N; k = 1, \dots, M+1), \quad (4.49)$$

$$\bar{H}^{(j,k)}(0) = \bar{\beta}_0, \quad (j = 1, \dots, N; k = 1, \dots, M+1). \quad (4.50)$$

Henceforth, we drop over-bars for notational convenience and consider only non-dimensional variables.

4.2.9 Upscaling to continuum

We now describe the discrete model of Sec. 4.2.8 using a (PDE) continuum model to facilitate a macroscale description. In this approach we utilise discrete-to-continuum upscaling to map the discrete equations (4.43) to a PDE [82, 115].

We assume the initial number of cells in the x - and y -directions are of the same order, i.e. $\mathcal{O}(v_0) = 1$ (where $v_0 = M/N$) and that this number is large, and introduce a small parameter $\varepsilon = N^{-1} \ll 1$. We assume that the lengthscale of a typical deformation is long ($\mathcal{O}(\varepsilon^{-1})$) compared to that of an individual cell ($\mathcal{O}(1)$). This approach uses Taylor expansions local to each cell to transform discrete differences to derivatives, which requires that the properties of the individual cells (e.g. $\mu^{(j,k)}$, $K^{(j,k)}$) vary smoothly across the sheet, hence we assume that the lengthscale of variations in material properties are also $\mathcal{O}(\varepsilon^{-1})$. For simplicity we also assume $K^{(j,k)} = K$ and $\mu^{(j,k)} = \mu$ are uniform across the sheet. We take a long wavelength rescaling of the independent variables in the form

$$X = \varepsilon x, \quad Y = \varepsilon y, \quad T = \varepsilon t, \quad (4.51)$$

so that $0 \leq X \leq 1$ and $0 \leq Y \leq 1$. Note that this reduction maintains an $\mathcal{O}(1)$ cell velocity. We then rescale the cell boundary positions according to

$$x_c^{(j,k)}(t) = \varepsilon^{-1} \tilde{x}^{(j,k)}(T), \quad (j = 1, \dots, N; k = 1, \dots, M), \quad (4.52a)$$

$$y_c^{(j,k)}(t) = \varepsilon^{-1} \tilde{y}^{(j,k)}(T), \quad (j = 1, \dots, N; k = 1, \dots, M), \quad (4.52b)$$

where tilded variables are functions of rescaled time, T . Furthermore, we rescale the discrete properties for an individual cell,

$$(W, W_0, L, L_0, H_0, H)^{(j,k)} = (\varepsilon^{-1} \tilde{W}, \varepsilon^{-1} \tilde{W}_0, \varepsilon^{-1} \tilde{L}, \varepsilon^{-1} \tilde{L}_0, \tilde{H}_0, H)^{(j,k)}, \quad (j = 1, \dots, N; k = 1, \dots, M). \quad (4.52c)$$

with $l_0 = \varepsilon^{-1} \tilde{l}_0 = \tilde{L}_0$, and $w_0 = \varepsilon^{-1} \tilde{w}_0 = v_0 \tilde{W}_0$. Note that we do not scale H (z -direction) as we do L and W (x - and y -direction respectively) so as to create a long and wide, thin material so that the ratio of length scales is the aspect ratio of the system. This is similar to Chapters 2 and 3, however now the thickness is used for the aspect ratio rather than width. We rescale the dimensionless damping parameter K as $K = \varepsilon \tilde{K}$ to ensure a dominant balance.

We discretise the continuous variable X into N equally sized intervals, so that $X_j = j/N$, ($j = 0, \dots, N$), and discretise the continuous variable Y into M equally sized intervals, so that $Y_k = k/M$, ($k = 0, \dots, M$), so the rescaled initial positions of the cell centre of mass and cell

boundaries can be expressed as $\tilde{x}_b^{(1/2,k)}(0) = 0$ ($k = 1, \dots, M$) with

$$\tilde{x}_b^{(j+1/2,k)}(0) = X_j, \quad \tilde{x}_c^{(j,k)}(0) = X_{j-1/2} = \frac{1}{2}(X_{j-1} + X_j), \quad (j = 1, \dots, N; k = 1, \dots, M), \quad (4.53)$$

$$\tilde{y}_b^{(j,k+1/2)}(0) = Y_j, \quad \tilde{x}_c^{(j,k)}(0) = Y_{k-1/2} = \frac{1}{2}(Y_{k-1} + Y_k), \quad (j = 1, \dots, N; k = 1, \dots, M), \quad (4.54)$$

We then express the cell boundary and centre of mass positions as a single continuum function $\check{x}(X, T)$ such that $\tilde{x}_b^{(1/2,k)}(T) = 0$ ($k = 1, \dots, M$)

$$\tilde{x}_b^{(j+1/2,k)} = \check{x}(X_j, Y_k, T), \quad \tilde{x}_c^{(j,k)} = \check{x}(X_{j-1/2}, Y_k, T), \quad (j = 1, \dots, N; k = 1, \dots, M), \quad (4.55)$$

$$\tilde{y}_b^{(j,k+1/2)} = \check{y}(X_j, Y_k, T), \quad \tilde{y}_c^{(j)} = \check{x}(X_j, Y_{k-1/2}, T), \quad (j = 1, \dots, N; k = 1, \dots, M), \quad (4.56)$$

as well as continuum representations of the other dependent variables in the model, in the form

$$\begin{aligned} \mathcal{W}^{(j,k)}(T) &= \check{\mathcal{W}}(X_j, Y_k, T), \quad \tilde{x}_b^{(j+1/2,k)} = \check{x}(X_{j+1/2}, Y_k, T), \quad \tilde{W}^{(j,k)}(t) = \check{W}(X_j, Y_k, T), \\ \tilde{H}^{(j,k)} &= \check{H}(X_j, Y_k, T), \quad \kappa^{(j,k)} = \check{\kappa}(X_j, Y_k, T), \quad (j = 1, \dots, N; k = 1, \dots, M). \end{aligned} \quad (4.57)$$

In this case differences in discrete variables can be mapped to derivatives of these continuum functions using Taylor expansions. Hence, expanding about $(j\varepsilon, k\varepsilon)$, (4.43b) and (4.43b) become

$$\begin{aligned} \check{\kappa}\varepsilon\check{K} \frac{\partial \check{x}}{\partial T} &= \left(\check{H} + \varepsilon \frac{\partial \check{H}}{\partial X} + \mathcal{O}(\varepsilon^2) \right) \left(\check{W} + \varepsilon \frac{\partial \check{W}}{\partial X} + \mathcal{O}(\varepsilon^2) \right) \left(\left(\check{\sigma}_{11} + \varepsilon \frac{\partial \check{\sigma}_{11}}{\partial X} + \mathcal{O}(\varepsilon^2) \right) - \check{\sigma}_{11} \right) \\ &\quad + \left(\check{H} - \varepsilon \frac{\partial \check{H}}{\partial X} + \mathcal{O}(\varepsilon^2) \right) \left(\check{W} - \varepsilon \frac{\partial \check{W}}{\partial X} + \mathcal{O}(\varepsilon^2) \right) \left(\check{\sigma}_{11} - \left(\check{\sigma}_{11} - \varepsilon \frac{\partial \check{\sigma}_{11}}{\partial X} + \mathcal{O}(\varepsilon^2) \right) \right), \end{aligned} \quad (4.58a)$$

$$\begin{aligned} \check{\kappa}\varepsilon\check{K} \frac{\partial \check{y}}{\partial T} &= \left(\check{H} + \varepsilon \frac{\partial \check{H}}{\partial Y} + \mathcal{O}(\varepsilon^2) \right) \left(\check{L} + \varepsilon \frac{\partial \check{L}}{\partial Y} + \mathcal{O}(\varepsilon^2) \right) \left(\left(\check{\sigma}_{22} + \varepsilon \frac{\partial \check{\sigma}_{22}}{\partial Y} + \mathcal{O}(\varepsilon^2) \right) - \check{\sigma}_{22} \right) \\ &\quad + \left(\check{H} - \varepsilon \frac{\partial \check{H}}{\partial Y} + \mathcal{O}(\varepsilon^2) \right) \left(\check{L} - \varepsilon \frac{\partial \check{L}}{\partial Y} + \mathcal{O}(\varepsilon^2) \right) \left(\check{\sigma}_{22} - \left(\check{\sigma}_{22} - \varepsilon \frac{\partial \check{\sigma}_{22}}{\partial Y} + \mathcal{O}(\varepsilon^2) \right) \right). \end{aligned} \quad (4.58b)$$

Note that

$$\check{\sigma}_{11} = \mu \left(\check{\lambda}_1^2 - \left(\check{\lambda}_1 \check{\lambda}_2 \right)^{-2} \right), \quad (4.58c)$$

$$\check{\sigma}_{22} = \mu \left(\check{\lambda}_2^2 - \left(\check{\lambda}_1 \check{\lambda}_2 \right)^{-2} \right), \quad (4.58d)$$

and hence the governing equations simplify to

$$\check{\kappa} \check{K} \frac{\partial \check{x}}{\partial T} = \check{H} \check{W} \mu \frac{\partial}{\partial X} \left(\check{\lambda}_1^2 - \left(\check{\lambda}_1 \check{\lambda}_2 \right)^{-2} \right), \quad (4.58e)$$

$$\check{\kappa} \check{K} \frac{\partial \check{y}}{\partial T} = \check{H} \check{L} \mu \frac{\partial}{\partial Y} \left(\check{\lambda}_2^2 - \left(\check{\lambda}_1 \check{\lambda}_2 \right)^{-2} \right), \quad (4.58f)$$

where $\check{H} = \beta_0 \left(\check{\lambda}_1 \check{\lambda}_2 \right)^{-1}$, $\check{W} = \gamma \check{\lambda}_2$ and $\check{L} = \check{\lambda}_1$. The continuum stretches, to leading order, are given by

$$\check{\lambda}_1(X, Y, T) = \frac{\partial \check{x}}{\partial X}, \quad \check{\lambda}_2(X, Y, T) = \frac{\partial \check{y}}{\partial Y}. \quad (4.59)$$

Furthermore, we can rescale the continuum independent variables (X, Y, T) back to the original parametrisation of the domain using $x = \varepsilon^{-1}X$, $y = \varepsilon^{-1}Y$ and $t = \varepsilon^{-1}T$, with

$$\begin{aligned} \check{\lambda}_{1,2,3}(X, Y, T) &= \hat{\lambda}_{1,2,3}(x, y, t), \quad \check{\mathcal{W}}(X, Y, T) = \hat{\mathcal{W}}(x, y, t), \\ \check{\kappa}(X, Y, T) &= \hat{\kappa}(x, y, t) \quad \check{x}(X, Y, T) = \hat{x}(x, y, t), \quad \check{y}(X, Y, T) = \hat{y}(x, y, t), \\ \check{W}(X, Y, T) &= \hat{W}(x, y, t), \quad \check{H}(X, Y, T) = \hat{H}(x, y, t), \quad (0 \leq x \leq l_0; 0 \leq y \leq w_0). \end{aligned} \quad (4.60)$$

In the continuum formulation, the description of the full and elastic principal stretches are respectively, to leading order, given by

$$\hat{\lambda}_1(x, y, t) = \frac{\partial \hat{x}}{\partial x}, \quad \hat{\lambda}_2(x, y, t) = \frac{\partial \hat{y}}{\partial y}, \quad (0 \leq x \leq l_0; 0 \leq y \leq w_0), \quad (4.61)$$

and the constraint of incompressibility takes the continuum form

$$\hat{\lambda}_3(x, y, t) = \frac{1}{\hat{\lambda}_1 \hat{\lambda}_2}, \quad (0 \leq x \leq l_0; 0 \leq y \leq w_0). \quad (4.62)$$

while the pressure takes the continuum form

$$\hat{p}(x, t) = \mu \left(\frac{1}{\hat{\lambda}_1 \hat{\lambda}_2} \right)^2, \quad (0 \leq x \leq l_0; 0 \leq y \leq w_0). \quad (4.63)$$

The upscaled continuum governing equations equivalent to the discrete system (4.29) for a

uniaxial deformation in a neo-Hookean material take the form

$$\hat{\kappa}K \frac{\partial \hat{x}}{\partial t} = 2\beta_0\gamma_0\mu \left(\frac{\partial \hat{x}}{\partial x} \right)^{-1} \frac{\partial}{\partial x} \left(\left(\frac{\partial \hat{x}}{\partial x} \right)^2 - \left(\frac{\partial \hat{x}}{\partial x} \right)^{-2} \left(\frac{\partial \hat{y}}{\partial y} \right)^{-2} \right), \quad (0 \leq x \leq l_0; 0 \leq y \leq w_0), \quad (4.64a)$$

$$\hat{\kappa}K \frac{\partial \hat{y}}{\partial t} = 2\beta_0\mu \left(\frac{\partial \hat{y}}{\partial y} \right)^{-1} \frac{\partial}{\partial y} \left(\left(\frac{\partial \hat{y}}{\partial y} \right)^2 - \left(\frac{\partial \hat{x}}{\partial x} \right)^{-2} \left(\frac{\partial \hat{y}}{\partial y} \right)^{-2} \right), \quad (0 \leq x \leq l_0; 0 \leq y \leq w_0). \quad (4.64b)$$

The continuum approximations of (4.33) and (4.34) are given by

$$\begin{aligned} \hat{x}(0, y, t) = 0, \quad \hat{x}(l_0, y, t) = l(t), \quad (0 \leq y \leq w_0), \\ \hat{y}(x, 0, t) = 0, \quad (0 \leq x \leq l_0), \end{aligned} \quad (4.65)$$

with the continuum approximation of (4.37), a free boundary at $y = w_0$;

$$\left(\frac{\partial \hat{y}}{\partial y} \right)^2 - \left(\frac{\partial \hat{x}}{\partial x} \right)^{-2} \left(\frac{\partial \hat{y}}{\partial y} \right)^{-2} = 0, \quad (0 \leq x \leq l_0; y = w_0) \quad (4.66)$$

or the continuum approximation of (4.38), a periodic boundary at $y = w_0$ in the form

$$\hat{y}(x, 0, t) = \hat{y}(x, w_0, t) - \hat{y}(x, w_0, 0), \quad (0 \leq x \leq l_0). \quad (4.67)$$

4.2.10 Small displacements in a neo-Hookean material

We linearise the solutions (assuming $\hat{\kappa} = 1$ and $\beta_0 = \gamma_0 = 1$) by taking $\hat{x} = x + k_1 \hat{a}(x, y, t)$ and $\hat{y} = y + k_1 \hat{b}(x, y, t)$ where $k_1 \ll 1$, and \hat{a} and \hat{b} are the displacements of \hat{x} and \hat{y} respectively. To leading order, the governing equations (4.64) become

$$K \frac{\partial \hat{a}}{\partial t} = 4 \left(2 \frac{\partial^2 \hat{a}}{\partial x^2} + \frac{\partial^2 \hat{b}}{\partial x \partial y} \right), \quad (0 \leq x \leq l_0; 0 \leq y \leq w_0) \quad (4.68a)$$

$$K \frac{\partial \hat{b}}{\partial t} = 4 \left(2 \frac{\partial^2 \hat{b}}{\partial y^2} + \frac{\partial^2 \hat{a}}{\partial x \partial y} \right), \quad (0 \leq x \leq l_0; 0 \leq y \leq w_0). \quad (4.68b)$$

Note that if we make \hat{a} and \hat{b} independent of y , (4.68a) takes the form of (2.39) with $\eta = 0$. The boundary conditions (4.65) and (4.66), take the form

$$\hat{a}(0, y) = 0, \quad \hat{a}(l_0, y) = \frac{l(t) - l_0}{k_1}, \quad (4.69)$$

$$\hat{b}(x, 0) = 0, \quad 2 \frac{\partial \hat{b}}{\partial y} + \frac{\partial \hat{a}}{\partial x} = 0, \quad (0 \leq x \leq l_0; y = w_0). \quad (4.70)$$

Assuming steady-state solutions ($\partial/\partial t = 0$) we differentiate (4.68a) by y and (4.68b) by x and manipulate to obtain

$$0 = \frac{\partial^3 \hat{a}}{\partial x^2 \partial y}, \quad (0 \leq x \leq l_0; 0 \leq y \leq w_0), \quad (4.71)$$

$$0 = \frac{\partial^3 \hat{b}}{\partial y^2 \partial x}, \quad (0 \leq x \leq l_0; 0 \leq y \leq w_0). \quad (4.72)$$

Integrating, and implementing the initial and boundary conditions, we obtain $\hat{a} = -x$ and $\hat{b} = \frac{y}{2}$, and so

$$\hat{x} = x(1 - k_1), \quad \hat{y} = y \left(1 + \frac{k_1}{2} \right). \quad (4.73)$$

4.2.11 Numerical method

The discrete system (4.29) is a closed system of ODEs which is solved numerically using MATLAB solver `ode15s`. Numerical solutions of this IBM are discussed in Sec. 4.2.12 for one free boundary and Sec. 4.2.13 for a periodic boundary.

The continuum PDE system for Neo-Hookean cells (4.64) is solved numerically using a semi-discretisation scheme where finite-difference formulae for spatial derivatives are substituted into the PDEs which are solved numerically using MATLAB solver `ode15s`. The spatial domain ($0 \leq x \leq l_0$, $0 \leq y \leq w_0$) is divided into n and m equally sized spatial intervals in the x and y direction respectively. We discretise spatial derivatives using second order centred finite differences, for any variable \hat{u}

$$\frac{\partial \hat{u}^{(p,q)}}{\partial x} = \frac{1}{2dX} \left(\hat{u}^{(p-1,q)} - \hat{u}^{(p+1,q)} \right) + \mathcal{O}(dX^2) \quad (p = 2, \dots, n-1; q = 1, \dots, m), \quad (4.74a)$$

$$\frac{\partial \hat{u}^{(p,q)}}{\partial y} = \frac{1}{2dY} \left(\hat{u}^{(p,q-1)} - \hat{u}^{(p,q+1)} \right) + \mathcal{O}(dY^2) \quad (p = 1, \dots, n; q = 2, \dots, m-1), \quad (4.74b)$$

$$\begin{aligned} \frac{\partial^2 \hat{u}^{(p,q)}}{\partial x \partial y} = & \frac{1}{4dXdY} \left(\hat{u}^{(p-1,q-1)} - \hat{u}^{(p-1,q+1)} - \hat{u}^{(p+1,q-1)} \right. \\ & \left. + \hat{u}^{(p+1,q+1)} \right) + \mathcal{O}(dX^2 dY^2) \quad (p = 2, \dots, n-1; q = 2, \dots, m-1), \end{aligned} \quad (4.74c)$$

where $dX = l_0/n$ is the step size in the x -direction and $dY = w_0/m$ is the step size in the y -direction and the superscript (p, q) represents the p -th discretisation point in the x direction and the q -th discretisation point in the y direction. For the boundary conditions, we use a second order forward and backward finite-difference stencils (to ensure only points within the domain

are used) in the form,

$$\frac{\partial \hat{u}^{(1,q)}}{\partial x} = \frac{1}{2dX} \left(-3\hat{u}^{(1,q)} + 4\hat{u}^{(2,q)} - \hat{u}^{(3,q)} \right) + \mathcal{O}(dX^2), \quad (q = 1, \dots, m), \quad (4.74d)$$

$$\frac{\partial \hat{u}^{(n,q)}}{\partial x} = \frac{1}{2dX} \left(3\hat{u}^{(n,q)} - 4\hat{u}^{(n-1,q)} + \hat{u}^{(n-2,q)} \right) + \mathcal{O}(dX^2), \quad (q = 1, \dots, m), \quad (4.74e)$$

$$\frac{\partial \hat{u}^{(p,1)}}{\partial y} = \frac{1}{2dY} \left(-3\hat{u}^{(p,1)} + 4\hat{u}^{(p,2)} - \hat{u}^{(p,3)} \right) + \mathcal{O}(dY^2), \quad (p = 1, \dots, n), \quad (4.74f)$$

$$\frac{\partial \hat{u}^{(p,n)}}{\partial x} = \frac{1}{2dX} \left(3\hat{u}^{(p,n)} - 4\hat{u}^{(p,n-1)} + \hat{u}^{(p,n-2)} \right) + \mathcal{O}(dY^2), \quad (p = 1, \dots, n), \quad (4.74g)$$

The discretisation scheme used in this system was a second-order centred finite-difference scheme. In simulations we used $n = 50$ and $m = 50$ discretisation points, however there is no need for this number of intervals to be the same as the number of discrete cells in the IBM. This continuum PDE approach can result in a significant computational saving compared to the IBM when the number of discrete cells is large.

In the results below we compute the continuum pressure and stretches, which are compared to the discrete simulations.

4.2.12 Results Case 1: Free boundary condition along $y = w_0$

We solve the discrete and continuum systems with $\gamma_0 = \beta_0 = 1$ and $\mu = 1$. We use $M = 10$ by $N = 10$ (hence $v_0 = 1$) cells to investigate the model in a small toy problem. We consider two different forms of the dissipation function: $\kappa^{(j,k)} = 1$ and $\kappa^{(j,k)} = A^{(j,k)}$ for $j = 1, \dots, N$; $k = 1, \dots, M$. We consider a system with a prescribed displacement of the form

$$l(t) = l_0(1 - k_1) + k_1 \exp(-t), \quad (4.75)$$

where k_1 (constant) represents the fractional decrease in length of the array in the x -direction. In simulations we consider a range of values for k_1 .

The typical response of the system is shown in Fig.4.3. The system responds to the deformation in the x -direction in both other dimensions (Fig. 4.3a). This indicates that cells are able to change their height (in the z -direction) and hence the cross-sectional area in the (x, y) plane in contact with the substrate does not remain constant (however the volume of each cell remains constant due to the incompressibility constraint). Hence we observe a slight difference between the dissipative choices $m = 0$ and $m = 1$. We note that the choice $m = 1$ is a more realistic choice, since dissipation due to a substrate would be proportional to the area of the cell in contact to the substrate, rather than a fixed value. In response to this deformation, the cell area in contact with the substrate decreases, i.e. $A^{(j)} \leq 1$, and hence the resistance to motion due to the substrate decreases for $m = 1$ compared to $m = 0$ (i.e. dissipative effects are greater for $m = 0$). This is outlined in the maximum pressure across the sheet ($\max_{x,y}(p)$), as this saturates to equilibrium

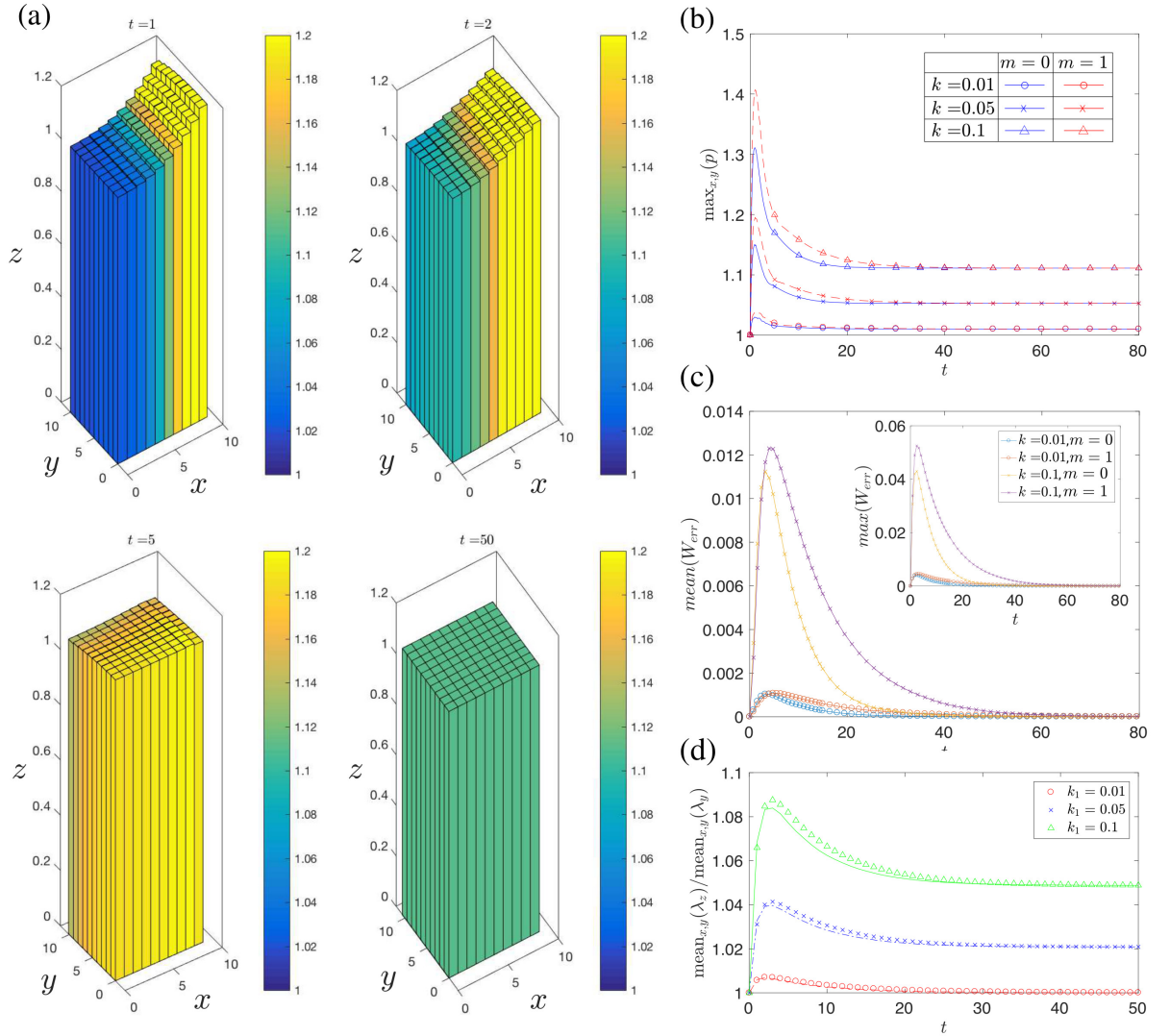


Figure 4.3: Solutions for a discrete system of incompressible Neo-Hookean cells aligned in a two-dimensional array subject to a prescribed displacement at $x = l_0$. Solutions for $N = 10$, $M = 10$, cells and uniform shear modulus $\mu = 1$. (a) The array, with fill-colour representing the internal cell pressure, is displayed for $t = 1, 2, 5, 100$ for $k_1 = 0.1$, $K = 1$ and $\kappa = A$; (b) The maximum pressure in the array, $\max_{x,y}(p)$ for $K = 1$ and $k_1 = 0.01, 0.05, 0.1$ for both dissipative systems, $\kappa = 1, A^{(j)}$; (c) The mean (inset: maximum) error between assumed shared boundary width, $W^{(j+1/2,k)}$, and real shared boundary width, for $K = 1$ and displacement $k_1 = 0.01, 0.05, 0.1, 0.2$; (d) The ratio of the average stretch in the z -direction and the average stretch in the y -direction ($\text{mean}(\lambda_z)/\text{mean}(\lambda_y)$) for $K = 1$ and displacement $k_1 = 0.01, 0.05, 0.1$.

faster for $m = 1$ (Fig. 4.3(b)).

We define the error in calculated and actual shared boundaries between neighbouring cells, $W^{(j+1/2,k)}$,

$$W_{\text{err}} = \left| W^{(j+1/2,k)} - W_s^{(j+1/2,k)} \right|, \quad (4.76)$$

where $W_s^{(j+1/2,k)}$ is the numerically calculated length of the shared boundary between cells (j, k)

and $(j+1, k)$ ($j = 1, \dots, N-1$; $k = 1, \dots, M$), defined by

$$W_s^{(j+1/2)} = \min(y_b^{(j,k+1/2)}, y_b^{(j+1,k+1/2)}) - \min(y_b^{(j,k-1/2)}, y_b^{(j+1,k-1/2)}). \quad (4.77)$$

As depicted in Fig. 4.3(a) at $t = 5$, we clearly see cells towards the upper layer and the prescribed displacement end, are disjoint from neighbouring cells. We calculate the shared boundary as the average widths of the cells either side of the boundary. The error in this assumption relative to the actual shared boundary in the simulations is outlined in Fig. 4.3(c). This error remains small for most values of k_1 , but the maximum error (which occurs in cell (N, M)) increases for larger deformations ($k_1 = 0.2, 0.1$).

Fig. 4.3(d) shows the ratio between the principal stretches in the y and z direction, averaged over all cells in the sheet ($\text{mean}_{x,y}(\lambda_2)$ and $\text{mean}_{x,y}(\lambda_3)$ respectively). For these parameter values, the system accounts for the prescribed deformation (compression) in the x direction by shortening the cells in the y and z directions. In this case we observe that the deformation occurs mainly in the z direction (presumably due to the dissipative penalty associated with deformation in y), with the stretch in the z direction larger than that in the y direction (Fig. 4.3d).

4.2.13 Results Case 2: Periodic boundary condition

We now consider the same system as Sec. 4.2.12, defined by (4.38) in the discrete model and (4.67) in the continuum system, but instead impose that the domain $0 \leq y \leq w_0$ is periodic. This configuration mimics a three-dimensional cylinder. However, similar to Sec. 2.4.1, this approximation neglects curvature effects and would only be valid when the resting width of cells (in the y -direction) is much smaller than the circumference (length of the array in the y -direction), i.e. for large M . In simulations we consider a range of values for k_1 .

In this case, the response to the prescribed deformation in the x -direction is accounted for completely in the z -direction, with cells changing their thickness (Fig. 4.4a) but not their widths. That is, the system exhibits no motion of deformation in the y -direction (the width of the array), driven by the enforcement of periodicity. Cells close to the prescribed deformation undergo a larger compression than those closer to $x = 0$, which remain in equilibrium until forces are eventually transmitted across cell boundaries (Fig. 4.4a). As in Chapter 2, this delay is driven by substrate dissipation. As expected, the mean thickness across the sheet increases as k_1 increases (Fig. 4.4b). This is also reflected in the mean pressure across the cells in the sheet (Fig. 4.4c).

4.3 Simple shear deformation

We now make the assumption that each constituent cell from Sec. 4.1 can be modelled as a cuboid such that the initially rectangular cross-section in the (x, y) plane undergoes a simple shear deformation parallel to the x -direction. Each cell is characterised by their angle of shear,

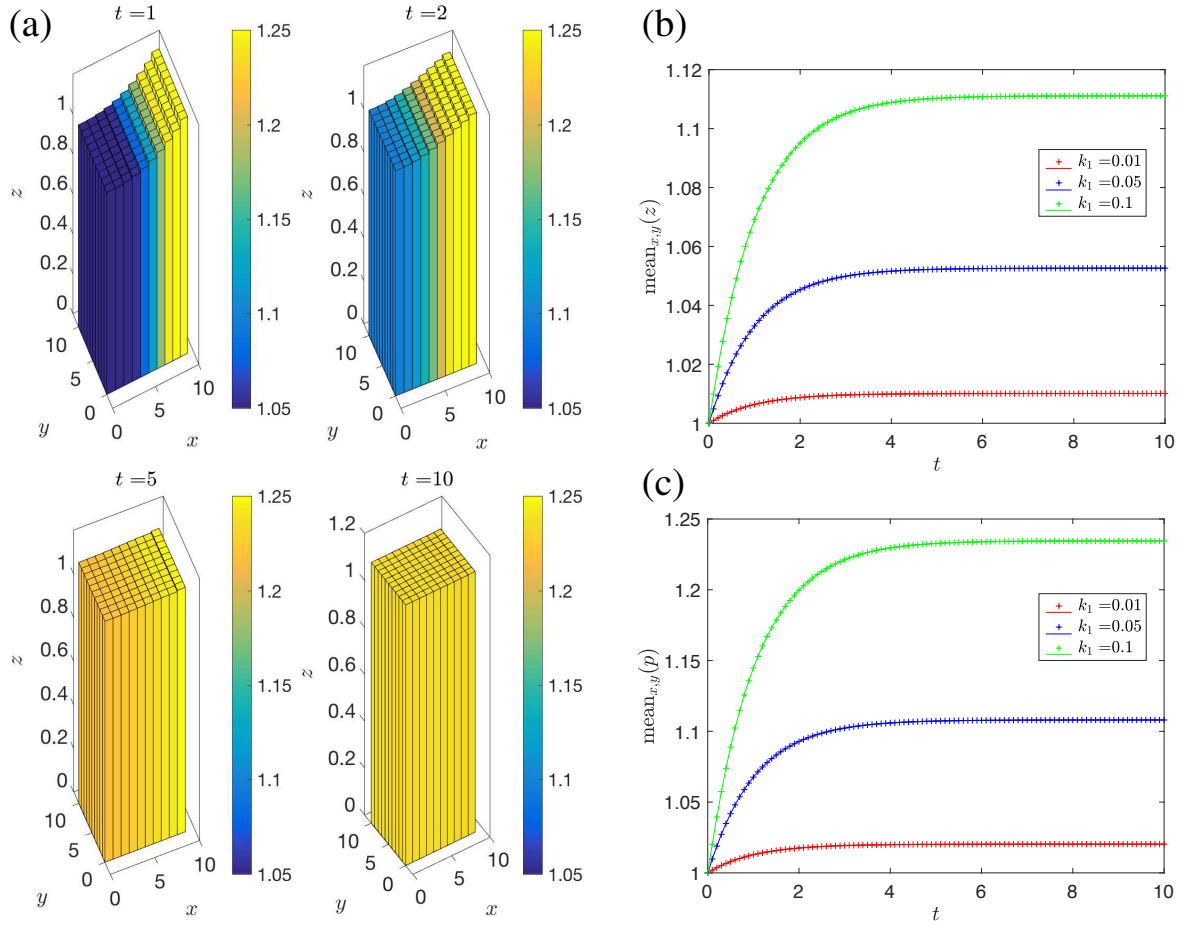


Figure 4.4: Solutions for a discrete system of incompressible neo-Hookean cells aligned in a two-dimensional array subject to a prescribed displacement at $x = l_0$, with a periodic boundary condition at $y = w_0$ ($y = 0$). Solutions for $N = 10$, $M = 10$, cells, $K = 1$ and uniform shear modulus $\mu = 1$. (a) The array, with colour representing cell pressure, for $t = 1, 2, 5, 10$ and $k_1 = 0.5$; (b) The mean height of all cells in the array, $\text{mean}_{x,y}(z)$, for $t = 0$ to $t = 10$ for $k_1 = 0.01, 0.05, 0.1$; (c) The average pressure of all cells in the array, $\text{mean}_{x,y}(p)$, for $t = 0$ to $t = 10$ for $k_1 = 0.01, 0.05, 0.1$.

denoted $\theta^{(j,k)}$ (with initial value 0) measured relative to edge perpendicular to the shear deformation. Each cell has initial length $L_0^{(j,k)}$ (along unit vector $\hat{\mathbf{x}}$), width $W_0^{(j,k)}$ (along unit vector $\hat{\mathbf{y}}$) and height $H_0^{(j,k)}$ (along unit vector $\hat{\mathbf{z}}$) for $j = 1, \dots, N$ and $k = 1, \dots, M$. We assume cells cannot slide over each other and remain in contact with their original neighbours, however this is not necessarily how cells would behave in real life.

We apply the constraint of no motion of the cell centre of mass in the $\hat{\mathbf{y}}$ direction and assume the domain $0 \leq x \leq l_0$ is periodic. Hence, we may consider only one column of cells without loss of generality, i.e. $j = 1$ and we may drop the index j , reducing the problem to a two-dimensional model, similar to Chapters 2 and 3. Note that this is only true if the cell properties are invariant in the x direction. This results in each row having uniform shear modulus, $\mu^{(j,k)} = \mu^{(k)}$, angle of shear, $\theta^{(j,k)} = \theta^{(k)}$, and pressure, $p^{(j,k)} = p^{(k)}$. Since the deformation is purely simple shear, the

length, width and height of each cell remains constant, with $L^{(k)} = L_0^{(k)}$, $W^{(k)} = W_0^{(k)}$, $H^{(j,k)} = H_0^{(k)}$. This system is outlined in Fig. 4.5.

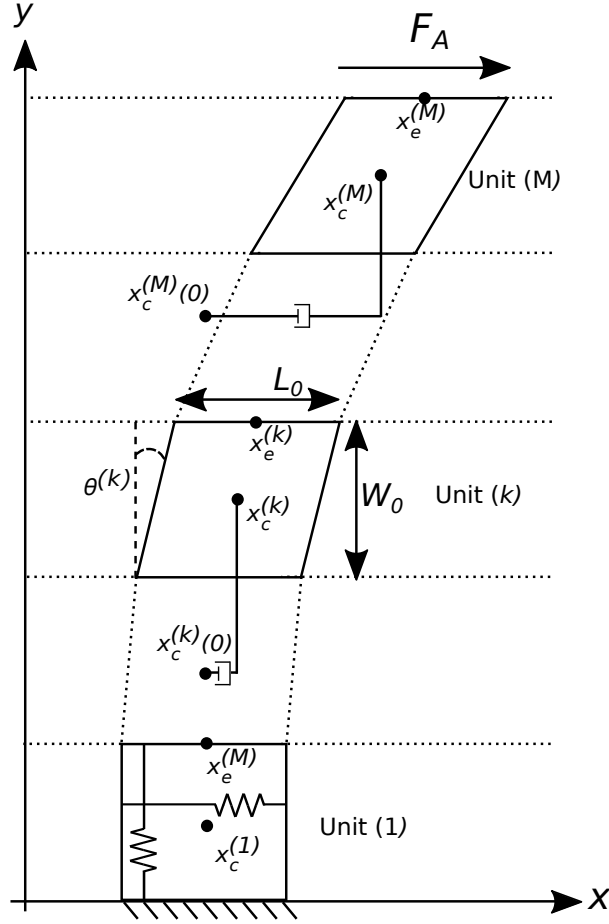


Figure 4.5: Set up of M elastic cells aligned end to end subject to a shearing force on the outer boundary of cell M . Cell k has shearing angle $\theta^{(j,k)}$, centre of mass position $x_c^{(j,k)}$ and experiences no motion in the y -direction. All cells have uniform, constant length, L_0 , and width, W_0 . The system is subject to substrate dissipation (damping relative to initial position), represented by a dashpot connected to the initial position of the cell centre of mass.

4.3.1 Elastic deformation

We assume each cell undergoes an incompressible nonlinear elastic deformation due to a prescribed shearing force with deformation gradient tensor (as defined in [27]) of the form

$$\mathbb{F}^{(k)} = \begin{bmatrix} 1 & \tan \theta^{(k)} & 0 \\ 0 & 1 & 0 \\ 0 & 0 & 1 \end{bmatrix}, \quad (k = 1, \dots, M), \quad (4.78)$$

The incompressibility constraint, $\det(\mathbb{F}^{(k)}) = 1$ is immediately satisfied.

4.3.2 Elastic Stress

When specifying the model, we consider the incompressible neo-Hookean strain energy functional, as in (4.15). The corresponding Cauchy stress tensor takes the form

$$\boldsymbol{\sigma}^{(k)} = \begin{bmatrix} \mu^{(k)} (1 + \tan^2 \theta^{(k)}) - p^{(k)} & \mu^{(k)} \tan \theta^{(k)} & 0 \\ \mu^{(k)} \tan \theta^{(k)} & \mu^{(k)} - p^{(k)} & 0 \\ 0 & 0 & \mu^{(k)} - p^{(k)} \end{bmatrix}. \quad (4.79)$$

4.3.3 Boundary Conditions

Enforcing no motion in the y -direction by balancing forces yields

$$\begin{aligned} 0 &= \left(\int_0^{H_0} \int_{-\frac{1}{2}L_0}^{\frac{1}{2}L_0} \boldsymbol{\sigma}^{(k)} \cdot \hat{\mathbf{y}} dx dz \right) \cdot \mathbf{y}, \\ &= \mu^{(k)} - p^{(k)}, \quad (k = 1, \dots, M). \end{aligned} \quad (4.80)$$

This also satisfies the condition (4.3) of zero external stress on surfaces perpendicular to $\hat{\mathbf{z}}$ ($z \neq 0$) and so we find

$$p^{(k)} = \mu^{(k)}, \quad (k = 1, \dots, M). \quad (4.81)$$

Hence, the only non-zero components of the Cauchy stress are

$$\sigma_{11}^{(k)} = \mu^{(k)} \tan^2 \theta^{(k)}, \quad (k = 1, \dots, M), \quad (4.82a)$$

$$\sigma_{12}^{(k)} = \sigma_{21}^{(k)} = \mu^{(k)} \tan \theta^{(k)}, \quad (k = 1, \dots, M). \quad (4.82b)$$

The force from cell (k) on cell $(k \pm 1)$ is given by

$$\mathbf{F}_{y^\pm}^{(k)} = \int_0^{H_0} \int_{-\frac{1}{2}L_0}^{\frac{1}{2}L_0} \boldsymbol{\sigma}^{(k)} \cdot (\mp \hat{\mathbf{y}}) dx dz = \mp H_0 L_0 \mu^{(k)} \tan \theta^{(k)} \hat{\mathbf{x}}, \quad (k = 1, \dots, M). \quad (4.83)$$

The force at the boundary $(k + 1/2)$ is given by

$$\mathbf{F}_b^{(k+1/2)} = \mathbf{F}_{y^+}^{(k)} + \mathbf{F}_{y^-}^{(k+1)}, \quad (k = 1, \dots, M-1), \quad (4.84)$$

where $\mathbf{F}_b^{(M+1/2)}$ is defined below by the global boundary condition at $y = w_0$.

4.3.4 Discrete governing equations

In this system we take the dissipative function with $m = 0$ since the area in contact with the substrate will always be constant and consider only the dissipative constant of proportionality $K^{(k)}$ ($k = 1, \dots, M$). The discrete governing equation (4.8) along with the forces (4.83) for a

simple shear deformation take the form

$$K^{(k)} \frac{dx_c^{(k)}}{dt} = H_0 L_0 \left(\mu^{(k+1)} \tan \theta^{(k+1)} - \mu^{(k-1)} \tan \theta^{(k-1)} \right), \quad (k = 2, \dots, M-1). \quad (4.85)$$

4.3.5 Initial Conditions

Initially, the cells are arranged in a single rectangular array (column) where all cells are the same size and shape (cuboidal, with a rectangular cross section in the (x, y) plane), and we define the origin ($x = 0$) at initial midpoint of the column of cells, such that

$$x_c^{(k)}(0) = 0, \quad (k = 1, \dots, M), \quad (4.86)$$

$$y_c^{(k)}(0) = -\frac{1}{2} W_0^{(k)} + \sum_{i=1}^k W_0^{(i)}, \quad (k = 1, \dots, M), \quad (4.87)$$

$$H^{(k)}(0) = H_0^{(k)}, \quad (k = 1, \dots, M). \quad (4.88)$$

In simulations below we assume all cells are initially the same length $L_0^{(k)} = L_0$, width $W_0^{(k)} = W_0$ and height $H_0^{(k)} = H_0$ ($k = 1, \dots, M$). this is not necessary but significantly simplifies the specification of the model and upscaling in Sec. 4.3.9. In this case, (4.86) reduces to

$$x_c^{(k)} = 0, \quad (k = 1, \dots, M), \quad (4.89)$$

$$y_c^{(k)} = W_0 \left(k - \frac{1}{2} \right), \quad (k = 1, \dots, M), \quad (4.90)$$

$$H^{(k)} = H_0, \quad (k = 1, \dots, M). \quad (4.91)$$

4.3.6 Discrete global boundary conditions

We impose a shearing force along the upper boundary of cell M at $y = w_0$, $\mathbf{F}_A = F_A \hat{\mathbf{x}}$, such that

$$\mathbf{F}_b^{(M+1/2)} = \mathbf{F}_{y+}^{(M)} + \mathbf{F}_A, \quad (4.92a)$$

which results in

$$K^{(k)} \frac{dx_c^{(M)}}{dt} = F_A - H_0 L_0 \mu^{(M-1)} \tan \theta^{(M-1)}. \quad (4.92b)$$

We fix the boundary at $y = 0$ such that $y_b^{(1/2)}(t) = 0$ and at $x = 0$ such that

$$K \frac{dx_c^{(1)}}{dt} = H_0 L_0 \left(\mu^{(2)} \tan \theta^{(2)} - \mu^{(1)} \tan \theta^{(1)} \right). \quad (4.92c)$$

4.3.7 Angle of shear

We introduce the variable $x_e^{(k)}$ to describe the midpoint of the upper boundary of cell k in the x -direction, defined by

$$x_e^{(k)} = 2x_c^{(k)} - x_e^{(k-1)}, \quad (k = 2, \dots, M) \quad (4.93)$$

with $x_e^{(1)} = 2x_c^{(1)}$. We may define

$$x_e^{(k)} = 2 \sum_{i=1}^k (-1)^{k-i} x_c^{(i)}. \quad (4.94)$$

Using trigonometric identities for a right angled triangle, we deduce

$$\tan \theta^{(k)} = \frac{2}{W_0} \left(x_e^{(k)}(t) - x_c^{(k)}(t) \right) = \frac{1}{W_0} \left(x_e^{(k)}(t) - x_e^{(k-1)}(t) \right), \quad (k = 1, \dots, M). \quad (4.95)$$

4.3.8 Non-dimensional variables

We again wish to consider the system in terms of non-dimensional variables (denoted with an overbar). For simplicity, we assume $K^{(k)} = K$ ($k = 1, \dots, M$). We scale time on a pertinent timescale t_0 (defined below), lengths on L_0 , forces on $\mu_0 L_0^2$ and pressures on μ_0 such that

$$t = t_0 \bar{t}, \quad x_c^{(k)} = L_0 \bar{x}_c^{(k)}, \quad \mu^{(k)} = \mu_0 \bar{\mu}^{(k)}, \quad F_A = \mu_0 L_0^2 \bar{F}_A, \quad (k = 1, \dots, M), \quad (4.96)$$

and we have the following dimensionless groups

$$\bar{\gamma}_0 = \frac{W_0}{L_0}, \quad \bar{\beta}_0 = \frac{H_0}{L_0}, \quad \bar{K} = \frac{K}{t_0 \mu_0 L_0}, \quad (k = 1, \dots, M). \quad (4.97)$$

Since there is no obvious inherent timescale in this system, we are able to choose $t_0 = K/\mu_0$, such that the non-dimensional discrete governing equation (4.85) reduces to

$$\frac{d\bar{x}_c^{(k)}}{d\bar{t}} = \bar{\beta}_0 \left(\bar{\mu}^{(k+1)} \tan \theta^{(k+1)} - \bar{\mu}^{(k-1)} \tan \theta^{(k-1)} \right), \quad (k = 2, \dots, M-1). \quad (4.98a)$$

The boundary condition (4.92b) takes the form

$$\frac{d\bar{x}_c^{(M)}}{d\bar{t}} = \bar{F}_A - \bar{\beta}_0 \bar{\mu}^{(M-1)} \tan \theta^{(M-1)}. \quad (4.98b)$$

and the boundary condition (4.92c) becomes

$$\frac{d\bar{x}_c^{(1)}}{d\bar{t}} = \bar{\beta}_0 \left(\bar{\mu}^{(2)} \tan \theta^{(2)} - \bar{\mu}^{(1)} \tan \theta^{(1)} \right). \quad (4.98c)$$

Furthermore, the constraint (4.93) becomes

$$\bar{x}_e^{(k)} = 2\bar{x}_c^{(k)} - \bar{x}_e^{(k-1)}, \quad (k = 2, \dots, M) \quad (4.98d)$$

and so the tangent to the shear angle takes the non-dimensional form

$$\tan \theta^{(k)} = \frac{2}{\gamma_0} \left(\bar{x}_e^{(k)}(t) - \bar{x}_c^{(k)}(t) \right) = \frac{1}{\gamma_0} \left(\bar{x}_e^{(k)}(t) - \bar{x}_e^{(k-1)}(t) \right), \quad (k = 1, \dots, M). \quad (4.98e)$$

The initial condition (4.89) takes non-dimensional form

$$\bar{x}_c^{(k)}(0) = \frac{1}{2}, \quad (k = 1, \dots, M), \quad (4.98f)$$

$$\bar{y}_c^{(k)}(0) = \bar{\gamma}_0 \left(k - \frac{1}{2} \right), \quad (k = 1, \dots, M), \quad (4.98g)$$

$$\bar{H}^{(k)}(0) = \bar{\beta}_0, \quad (k = 1, \dots, M). \quad (4.98h)$$

Henceforth, we drop over-bars for notational convenience and consider only non-dimensional variables in the simulations.

4.3.9 Upscaling

As in previous chapters, we now upscale the discrete model (4.98) to a continuum PDE description using discrete-to-continuum asymptotics.

We assume the initial number of cells in the y -direction is large and introduce a small parameter $\varepsilon = M^{-1} \ll 1$. We assume that the lengthscale of a typical deformation is long ($\mathcal{O}(\varepsilon^{-1})$) compared to that of an individual cell ($\mathcal{O}(1)$). This approach uses Taylor expansions local to each cell to transform discrete differences to derivatives, which requires that the properties of the individual cells (e.g. $\mu^{(k)}$, $K^{(k)}$) vary smoothly across the entire array (i.e. derivatives with respect to Y are $\mathcal{O}(1)$). For simplicity we also assume and $\mu^{(k)} = 1$ across the array. To maintain an $\mathcal{O}(1)$ cell velocity we also rescale $t = \varepsilon^{-1}T$. We then rescale the cell centre-of-mass positions according to

$$x_c^{(k)}(t) = \tilde{x}^{(k+1/2)}(T), \quad x_e^{(k)} = \tilde{x}^{(k)}, \quad y_c^{(k)}(t) = \varepsilon^{-1}\tilde{y}^{(k)}(T), \quad (k = 1, \dots, M), \quad (4.99)$$

where tilded variables are functions of rescaled time, T .

We introduce a continuous variable, $Y \in [0, \gamma_0]$, which parametrises the (unstressed) initial configuration of the system, such that $Y_k = \gamma_0(k - 1/2)\varepsilon$ ($k = 1, \dots, M$). We express discrete variables and parameters in the IBM as continuum functions of Y and T such that

$$\begin{aligned} \tilde{x}_c^{(k)}(t) &= \check{x}(Y_k, T), & \tilde{x}_e^{(k)} &= \check{x}(Y_{k+1/2}, T), \\ \tilde{y}_c^{(k)}(t) &= \check{y}_c(Y_k, T), & \theta^{(k)}(t) &= \check{\theta}(Y_k, T), \end{aligned} \quad (k = 1, \dots, M). \quad (4.100)$$

Expanding Taylor series and taking the leading order, the governing equation (4.98a) with (4.98e) becomes

$$\frac{\partial \check{x}}{\partial T} = 2\beta_0\mu \frac{\partial}{\partial y} (\tan \check{\theta}) + \mathcal{O}(\varepsilon), \quad (0 < y < w_0). \quad (4.101)$$

The boundary condition (4.98b) takes the form

$$\varepsilon \frac{\partial \check{x}}{\partial T} = F_A - \beta_0\mu \tan \check{\theta} + \mathcal{O}(\varepsilon), \quad (y = w_0), \quad (4.102)$$

which to leading order gives

$$0 = F_A - \beta_0\mu \tan \check{\theta}, \quad (y = w_0), \quad (4.103)$$

The angle of shear, (4.98e), to leading order, becomes

$$\tan \check{\theta} = \frac{1}{\gamma_0} \frac{\partial \check{x}}{\partial y}, \quad (0 \leq y \leq w_0). \quad (4.104)$$

Furthermore, we can rescale the continuum independent variables (Y, T) back to the original parametrisation of the domain using $y = \varepsilon^{-1}Y$ and $t = \varepsilon^{-1}T$, with

$$\check{x}(Y, T) = \hat{x}(y, t), \quad \check{y}(Y, T) = \hat{y}(y, t), \quad (0 \leq y \leq w_0). \quad (4.105)$$

In the continuum formulation, the non-dimensional pressure is

$$\hat{p}(y) = 1, \quad (0 \leq y \leq w_0). \quad (4.106)$$

and the governing equation (4.98a) takes the form

$$\frac{\partial \hat{x}}{\partial t} = 2 \frac{\beta_0}{\gamma_0} \frac{\partial^2 \hat{x}}{\partial y^2}, \quad (0 < y < w_0). \quad (4.107a)$$

with boundary conditions

$$\hat{x}(0, t) = 0, \quad (4.107b)$$

with the prescribed shear condition (4.98b) taking the form

$$F_A - \frac{\beta_0}{\gamma_0} \frac{\partial \hat{x}}{\partial y} = 0, \quad (y = w_0). \quad (4.107c)$$

4.3.10 Analytical Solutions

We set $\hat{x} = F_A y + g(y, t)$, where $g(y, t)$ is some unknown function. We rescale $y = \check{y}\beta_0/\gamma_0$ and $t = \check{t}\beta_0/\gamma_0$. Substituting this in to (4.107) yields

$$\frac{\partial g}{\partial \check{t}} = \frac{\partial^2 g}{\partial \check{y}^2}, \quad (0 < \check{y} < \frac{w_0 \gamma_0}{\beta_0}) \quad (4.108)$$

with boundary conditions (4.107b) and (4.107c) given by

$$g = 0, \quad (\check{y} = 0), \quad (4.109)$$

$$\frac{\partial g}{\partial \check{y}} = 0, \quad (\check{y} = \frac{w_0 \gamma_0}{\beta_0}). \quad (4.110)$$

We use separation of variables, with $g = T(\check{t})Y(\check{y})$ where $T(\check{t})$ is some function of \check{t} and $Y(\check{y})$ is some function of \check{y} to be determined. Substituting this in to (4.108) and manipulating yields

$$\frac{T'}{T} = \frac{Y''}{Y} = -k^2, \quad (4.111)$$

where k is a constant and $'$ and $''$ denotes the first and second derivatives of a function with respect to its argument, respectively. Hence we obtain two equations to solve. First, we consider the ODE for T . We have

$$\frac{T'}{T} = -k^2, \quad (\check{t} \geq 0), \quad (4.112)$$

which has solution

$$T = T_0 \exp(-k^2 \check{t}), \quad (\check{t} \geq 0), \quad (4.113)$$

where T_0 is the initial value of T . Second, we consider the corresponding ODE for Y ,

$$\frac{Y''}{Y} = -k^2, \quad (4.114)$$

with $Y(0) = 0$ and $Y'(\frac{w_0 \gamma_0}{\beta_0}) = 0$. Substituting the ansatz $Y = A \sin(k\check{y}) + B \cos(k\check{y})$ and applying the boundary conditions yields $B = 0$ and either

$$k = \frac{\beta_0(2j+1)\pi}{2w_0\gamma_0} \quad (j \in \mathbb{Z}) \quad \text{or} \quad k = 0. \quad (4.115)$$

Hence,

$$g(\check{y}, \check{t}) = \sum_{j=-\infty}^{j=\infty} a_j \exp(-k_j^2 \check{t}) \sin(k_j \check{y}), \quad (0 \leq \check{y} \leq 1), \quad (4.116)$$

and the full analytical solution is given by

$$\hat{x} = F_A y + \sum_{j=-\infty}^{j=\infty} a_j \exp\left(-\frac{k_j^2 \beta_0}{\gamma_0} t\right) \sin\left(\frac{k_j}{w_0} \check{y}\right), \quad (0 \leq y \leq w_0), \quad (4.117)$$

where a_j are set by initial conditions.

4.3.11 Results: Simple Shear

We solve the discrete and continuum systems with $\gamma_0 = \beta_0 = 1$ and $\mu = 1$. We investigate the response of the system to an applied shearing force $F_A = 0.01, 0.1, 1, 10$ for $M = 10$ cells (we investigate a small number of cells to investigate the model for small times using a small toy-problem - we also demonstrate some results for $M = 50$ cells and show the slower response of the system for larger number of cells).

Cells close to $y = w_0$, where the shearing force is applied, respond to the applied forcing first. As in previous examples, there is a delay in this force being transmitted down the array due to the substrate dissipation and so the column of cells curves in the y -direction. For long enough times, all cells align with the same angle of shear as the system saturates towards equilibrium (Fig. 4.6a,b,c). The delay in force transmission results in a transient difference in shear angles along the array (Fig. 4.6b), where cells close to the applied force are initially more sheared than those close to the fixed boundary ($y = 0$). This difference increases as the applied force, F_A , increases. The angle of shear in the steady solution of the system increases with increasing applied force (Fig. 4.6b inset). While the discrete and continuum systems saturate towards the same equilibrium solution, Figure 4.6c highlights a slight difference in the dynamics of the two systems in the transient behaviour of the shear angle, where the difference between the maximum and minimum shear amounts in the column is larger for early times in the discrete system than in the continuum system. For early times, the displacement across the domain is a non-linear function of y . The displacement becomes linear in y for long times, as expected (Fig. 4.6d). For a larger number of cells, this non-linear behaviour takes longer to saturate to a steady solution as forces must be transmitted along a larger number of cells (Fig. 4.6d inset). This behaviour is reflected in the spatial profile of the shear angle in Figure 4.6e). For all simulations, the discrete and continuum agree well, with agreement better for a smaller F_A or for larger times.

4.4 Summary

In this chapter we have constructed a quasi-three dimensional IBM for a sheet of hyperelastic cells subject to prescribed deformation along one edge. We have outlined the challenges in defining a self-consistent model for a general deformation and strain-energy functional. To simplify the analysis we introduced (simple) specific deformations for each cell: uniaxial deformation or simple shear. We derived the corresponding continuum PDE models using discrete-to-continuum asymptotics for each system and investigated the passive response subject to a prescribed deformation. The agreement between discrete and continuum systems for uniaxial deformation was good, and the system exhibited a three-dimensional deformation in response to a prescribed compression in one direction: for our parameter choices, the surface area of the cell in contact with the substrate is not constant, and so the choice of dissipative function is important. In the simple shear formulation, the dissipative forces result in a transient difference in shear angles along the array, and so the column of cells is curved in the y -direction for early times. The agreement between discrete and continuum systems was good, however we observe a slight difference in the dynamics of the two systems in the transient behaviour of the shear angle.

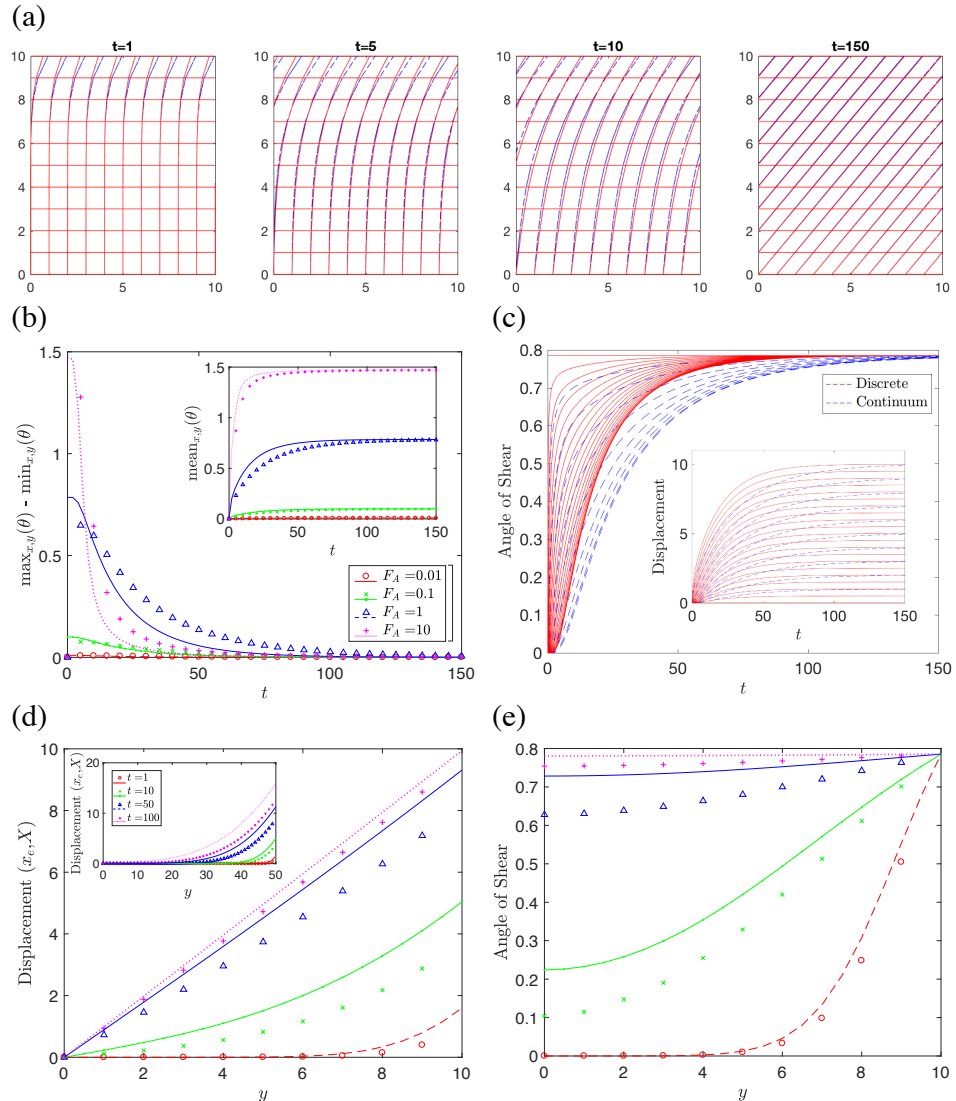


Figure 4.6: Solutions for $M = 10$ cells subject to simple shear. (a) Profiles for $F_A = 1$ at $t = 150$; (b) Maximum difference in shear angle in the array for $F_A = 0.01, 0.1, 1, 10$ (inset: mean shear angle in array); (c) Shear angle of all cells (discrete, dashes) and at discretisation points (continuum, lines) for $t = 0$ to $t = 150$ (inset: displacement); (d) Spatial profile of displacement $t = 1, 10, 50, 100$ for $F = 1$ (discrete, symbols; continuum, lines) (inset: $M = 50$); (e) Spatial profile of shear angle at $t = 1, 10, 50, 100$ for $F = 1$ (discrete, symbols; continuum, lines).

Chapter 5

Discussion

This work has proposed an alternative formulation of discrete IBMs compared to the current framework of cell IBMs (discussed in Chapter. 1, e.g. [26,67,68]). This approach has previously been used to model epithelial tissues, and we now apply this to other soft tissues. We have formulated a new discrete IBM derived in the framework of rational continuum mechanics rather than incorporating forces exerted by cells simplistically with linear springs (e.g. [67]) or with generic force laws (e.g. [68]).

These mechanical formulations focus on an individual cell at the microscale, and consider force balances across cell boundaries, rather than equations of motion derived based on energy minimisation as considered in vertex models, outlining a new approach for creating soft tissue cell IBMs. The general framework presented in Chapter. 2 means that both discrete and continuum systems can easily be implemented for any isotropic strain-energy functional, making it applicable to a wide array of materials, or more realistic strain-energy functions for myocardium or other soft tissue.

In this work we utilised discrete-to-continuum asymptotics [96] to derive new continuum macroscale PDE models. This method was utilised as it has the advantage of not requiring a homogeneous or periodic problem at the cell level, allowing us to consider heterogeneous cell properties and capturing this detail in the upscaled equations, which is an advantage over the usual homogenisation techniques. The agreement between discrete and continuum systems across all models is excellent. These agreements demonstrate how the new PDE models formulated can accurately replicate the results of the IBMs considered, indicating the robustness of this upscaling approach.

The models presented in this thesis are simplified approximations of soft tissue, neglecting, for example, transmural pressure differences, or the fibrous nature of soft tissues. To develop these models further, one should extend the framework to include more complex characteristics (e.g. fibres, curvature effects) and ECM to more accurately represent the make-up of biological soft tissues. This would enable progression towards a full three-dimensional model, encapsulating more properties and characteristics of biological soft tissue.

We conclude this thesis with a summary of the results. First we considered a quasi-two-dimensional array of incompressible viscoelastic cells, maintaining generality in the strain-energy-functional in both discrete and continuum formulations in Chapter 2. We implemented this system for the specific case of a neo-Hookean strain energy function, to investigate the system's passive response subject to a prescribed deformation on the array in Sec. 2.3.1. The static version of the upscaled PDE with a neo-Hookean strain energy function can equally be derived from a continuum model with a long, thin beam approximation. The analytical solutions of this continuum model agree well with numerical solutions of the upscaled PDE (Fig. 2.6). However, we are able to capture the non-linear time-dependent behaviour by deriving the time-dependent upscaled PDE. For higher values of the dissipation constant, the response to the prescribed deformation was more non-uniform, as forces were transmitted slower between cells (Fig. 2.5). For a system with viscoelasticity in the absence of dissipation, the response of the systems are spatially uniform and the effect of the viscous parameter can be seen in the internal cell pressure before the deformation saturates (Fig. 2.7c). We considered a case with non-uniform shear modulus across the array, representing a rigid cluster of cells towards the centre of the domain to mimic a section of dead cells in a tissue, for example, post myocardial infarction in the myocardium. In this case, the deformation is carried by the softer cells in the array which undergo a larger deformation to account for the lack of deformation in the stiffer cells. This shows cells in the surrounding area of a cluster of stiffer (or dead) cells bear a greater load in deformations (Fig. 2.9). This model was then further extended in Sec. 2.4 to investigate active contraction in a periodic domain, which resulted in travelling waves of contracted (shorter, wider) cells through the domain, with the remaining cells stretching to account for the contracted cells (Fig. 2.10). For all cases considered in this chapter, the discrete and continuum systems demonstrated excellent agreement.

To investigate the role of growth and proliferation, in Chapter 3 we used the theory of morphoelasticity to incorporate growth into the quasi-two-dimensional array of cells [107, 116]. In this system, we considered two formulations of dissipation function: a constant of proportionality and one dependent on the current cell area. We consider a stress-dependent growth function, where maximum growth occurs when a cell is unstressed (as we do not consider cells in extension in this model). In Sec. 3.3.1, we investigated the system with growth and no proliferation. In the absence of internal viscoelasticity, a linear increase of the domain length was observed for all choices of dissipative functions and values (Fig. 3.1a). This rate of elongation is slower for dissipation proportional to cell area. In this case, cells exhibit slower growth as they are paying an extra dissipation penalty for changing their area (Fig. 3.2). In the absence of substrate dissipation, the array length also increases linearly with time, at an identical rate for all values of the viscous parameter. However, for a small amount of substrate dissipation, the time taken for the system to reach a steady level of compression increases with the viscoelastic coefficient (Fig. 3.1d). In all systems, the discrete and continuum models agree well. In Sec. 3.3.2,

we formulate a novel proliferation model by implementing a division event in the discrete cell growth model, whereby a growing cell divides into two daughter cells when it reaches double the initial area. We conclude from comparisons with a system without proliferation that cell proliferation generally leads to slower growth of the array, except in cases with very small substrate dissipation (Fig. 3.3a,b). Furthermore, for a system with sufficient substrate dissipation, we observe a proliferating rim, with division occurring only towards the free end (Fig. 3.3d). This proliferating rim behaviour is arising purely from the mechanical formulation of this model, in contrast with previous works investigating proliferating rims due to nutrient and cell-density profiles (e.g. [103]) or by constructing a model with discrete areas of proliferating, quiescent and necrotic cells (e.g. [126]).

In chapter 4 we then formulated a three-dimensional sheet of nonlinearly elastic cells of constant density atop a rigid substrate. First we considered the case where each cell undergoes a uniaxial deformation (Sec. 4.2) and investigated the response to a prescribed displacement. We observed a deformation in all three dimensions and that the cross sectional area in contact with the substrate decreased, hence the dissipative effects were reduced for dissipation proportional to cross sectional area in contact with the substrate (Fig. 4.3). We then implemented this system in a periodic domain (Sec. 4.2.13) and observed deformation in only one dimension (other than the prescribed deformation) (Fig. 4.4). For both of these systems, the agreement between discrete and continuum models was very good. Lastly, we considered the three-dimensional sheet with the assumption that each cell was subject to a simple shear deformation. We observed that for a larger shear force, there was a larger non-uniformity in shear angle across the domain (Fig. 4.6b). The discrete and continuum saturate towards the same equilibrium solution, however we observe a slight difference in the dynamics of the two systems in the transient behaviour of the shear angle (Fig. 4.6c). For early times, the spatial profile of displacement is non-linear, but becomes linear (spatially) for longer times, as expected.

A number of assumptions have been made to simplify the models presented in this thesis. Some natural extensions to this work would be to address these in order to relax any assumptions and approximations made, to build a more realistic model. The main assumptions and extensions will now be discussed.

- We assume that the external pressure on the cells is zero. This is implemented in Chapters 2 and 3 by setting the external pressure above and below (in the y -direction) the array equal to zero, while in Chapter 4 this is implemented by setting the external pressure on the upper surface normal to the $z = 0$ plane to be zero. We rationalise this assumption by considering pressure differences between parallel lines of cells is small and therefore neglected. However, this is not entirely realistic. For example, in the heart the pressure inside the chamber (due to the blood flow) is higher than the pressure outside the heart wall. A simple extension to this model would be to consider a non-zero external pressure on cells, to better mimic the conditions in myocardium.

- We assume simple deformations (uniaxial and simple shear) of a cuboidal cell in all models. One should be able to consider more complex deformations (e.g. a combination of shearing and stretching). In Chapter 4, this would also include the added challenge of keeping track of cell vertices and keeping track of cell neighbours (which could change). If one were to consider a different shape of cell (e.g. sphere) then the model would need to redefine the rules on what surfaces the cells interact with one another. In this work, we approximated this contact surface as the average of the cell widths, however the minimum widths of the cells interacting is a more accurate value. For other shapes, a new approximation would be needed to define the shared surface over which cells are interacting.
- We model cell viscoelasticity using a linear Kelvin-Voigt model. This model describes creep compliance (an increase in plastic strain under constant stress) but fails to describe stress relaxation (a decrease in stress under constant strain) [127]. The linear Kelvin-Voigt (and Maxwell) model is unable to capture multiple relaxation times [127], a disadvantage when modelling materials which are inherently multiscale (e.g. soft tissues). Soft tissues exhibit highly complex viscoelastic behaviour, and this simplistic model cannot accurately describe real soft tissue responses [128]. In future work, one should investigate alternative ways to model cell viscoelasticity (e.g. a combination of Maxwell and Kelvin-Voigt or non-linear models) and compare the system with one using a Maxwell model for viscoelasticity.
- In Chapter 3 we assume growth only in one-dimension to test the model as a toy problem. This formulation can be easily extended to growth in two-dimensions, since we have maintained generality in the derivation of the governing equations.
- In Chapter 3, we consider only one form of growth rate and one division law. One could consider a growth rate developed from experimental data, or consider an alternative division law. For example, cells tend to divide when they reach a size where their surface area is no longer able to take in enough nutrients for the cell's volume [6] - i.e. when the surface area to volume ratio is small. Implementing this law could lead to a more realistic proliferation model.

Another extension to this work would be to develop a continuum description of the proliferation model in Sec. 3.3.2. In previous works (e.g. [67]) proliferation has been modelled as a source term in the continuum equations, however in the current formulation one could construct a semi-continuum model by implementing a division event into the continuum growth model to replicate the proliferating system. Furthermore, it would be interesting to formulate a model incorporating both the mechanical response from the systems outlined in this thesis, and the nutrient- or cell-density -dependent proliferation models readily available, to investigate how the competition between these factors influences both the proliferating rim, and each other.

In conclusion, the work in this thesis has developed a new IBM for an array of cells based on the framework of rational continuum mechanics. Using discrete-to-continuum upscaling techniques we have formulated new continuum PDE models which have been applied to investigate active contraction, cell growth and proliferation. This work provides a framework on which to build more complex models of soft tissues.

Appendix A

Listing of Matlab Codes

A.1 Growth

The following code solves the system outlined in Sections 3.1 and 3.2 for the results in Section 3.3.1 for the discrete and continuum systems of a quasi-two dimensional array of a single line of incompressible neo-Hookean cells, with stress-driven growth and substrate dissipation.

```
1  %% Growth (With K)
2  % Roxanna Barry
3  % University of Glasgow
4  %
5  % Numerical Solution for single line of Neo-Hookean
6  % incompressible cells, with stress-dependent growth and
7  % substrate dissipation.
8  %
9  % Either Free boundary condition, or constrained boundary
10 % can be chosen in the ODE and PDE functions at the end of
11 % the code (make sure to change in both the ode solvers and
12 % the initial condition solvers for a0)
13 %
14 % kappa = A is defined, for kappa=1 follow instructions in
15 % solver comments at the end of the code
16
17 function GrowthWithK
18
19 tic
20
21 %% System Parameters
22
23 %
```

```
24 % % Discrete System
25 %
26
27 % Number of cells
28 N = 100;
29 % Shear modulus
30 mu = 1;
31 % Resting/initial width of cells
32 W0=1;
33 % Resting/initial length of array
34 l0 = N;
35 % Non-dimensional length-width ratio
36 gam0 = W0;
37 % % Number of points in parameter space plots
38 param = 15;
39 % Non-dimensional Stokes Damping Coefficient
40 Ks = 1e-2*ones(1,param);
41 % Non-dimensional Kelvin Dissipation Coefficient
42 % % linspace
43 etas = logspace(-5,2,param);
44
45 % Time Span
46 dt = 0.01;
47 tspan = 0:dt:10;
48
49 % Initialise matrix storage for data
50 maxp = zeros(length(tspan),param);
51 minp = zeros(length(tspan),param);
52 minalpha = zeros(length(tspan),param);
53 maxsig = zeros(length(tspan),param);
54 minsig = zeros(length(tspan),param);
55 maxg1 = zeros(length(tspan),param);
56 ming1 = zeros(length(tspan),param);
57 L = zeros(length(tspan),param);
58
59 %
60 % % Continuum System
61 %
62 % Discretisation Points
63 nc = 101;
64 % Discretisation Step Size
```

```

65 dX = 10/(nc-1);
66 % Continuum Time Span
67 Tspan = tspan;
68
69 % % Initialise matrix storage for data
70 maxphat = zeros(length(Tspan),param);
71 minphat = zeros(length(Tspan),param);
72 minalphahat = zeros(length(tspan),param);
73 maxsigihat = zeros(length(tspan),param);
74 minsigihat = zeros(length(tspan),param);
75 maxglhat = zeros(length(tspan),param);
76 minglhat = zeros(length(tspan),param);
77 Lhat = zeros(length(Tspan),param);
78
79 %% Initial Conditions
80
81 %
82 % % Discrete System
83 %
84
85 % Cell boundary locations
86 x0=0:1:10;
87 % Initial Condition growth
88 g0 = ones(1,N);
89 % Define homeostatic stress value
90 sig0 = 1;
91 % Initial guess for a=dalpha/dt
92 a0 = -0.5*ones(1,N);
93
94 %
95 % % Continuum System
96 %
97
98 % Discretisation point locations
99 X0 = 0:dX:10;
100 % Initial Condition growth
101 G0 = ones(1,nc);
102 % Initial guess for ahat=dalphahat/dt
103 A0 = -0.5*ones(1,nc);
104
105

```

```

106 %% Loop over K/eta values
107
108 for loop = 1:param
109
110     % Non-dimensional Stokes Damping Coefficient
111     K = Ks(loop);
112     % Non-dimensional Kelvin Dissipation Coefficient
113     eta = etas(loop);
114
115     % % Initial Condition
116     % Discrete
117     % Solve for initial guess consistent with system
118     a = fsolve(@ICdisc,a0);
119     % Full Initial condition of x and g
120     ic = [x0,g0,a];
121     % Continuum
122     % Solve for initial guess consistent with system
123     A = fsolve(@ICcont,A0);
124     % Full Initial condition of X and G
125     IC = [X0,G0,A];
126
127 %% Solve the ODE/PDE System
128
129 %
130 % % Discrete System
131 %
132
133 % Alter mass matrix to account for algebraic constraint
134 % for d(alpha)/dt
135 m = eye(3*N+1,3*N+1);
136 for mit = 2*N+2:3*N+1
137     m(mit,mit) = 0;
138 end
139 % If eta = 10 use values: a=1e-8, r=1e-4;
140 % else use: a=1e-4, r=1e-3.
141 a = 1e-6;
142 r = 1e-4;
143 options = odeset('Mass',m,'AbsTol',a,'RelTol',r);
144 [t,x] = ode23t(@NHBdry_ODE_SG_AW, tspan, ic,options);
145
146 %

```

```

147 % % Continuum System
148 %
149
150 % Alter mass matrix to account for algebraic constraint
151 % for  $d(\alpha)/dt$ 
152 M = eye(3*nc,3*nc);
153 for Mit = 2*nc+1:3*nc
154     M(Mit,Mit) = 0;
155 end
156 % If eta = 10 use values: a=1e-8, r=1e-4;
157 % else use: a=1e-4, r=1e-3.
158 A = 1e-6;
159 R = 1e-4;
160 Options = odeset('Mass',M,'AbsTol',A,'RelTol',R);
161 [T,X] = ode15s(@NHBdry_contODE_SG_AW, Tspan, IC,Options);
162
163
164 %% Growth
165
166 % % Discrete
167 g1 = x(:,N+2:2*N+1);
168 maxg1(:,loop) = max(g1,[],2);
169 ming1(:,loop) = min(g1,[],2);
170
171 % % % Continuum
172 glhat = X(:,nc+1:2*nc);
173 maxglhat(:,loop) = max(glhat,[],2);
174 minglhat(:,loop) = min(glhat,[],2);
175
176 %% Formulating Data to Save
177
178 %
179 % % Discrete System
180 %
181
182 xcpos=zeros(length(t),N);
183 for it4=1:N
184     xcpos(:,it4) = (x(:,it4+1) + x(:,it4))/2;
185 end
186
187 % Array Length

```

```

188 L(:,loop) = x(:,N+1);
189
190
191 % % Continuum System : Average Widths
192 Xpos = X;
193 for it6=1:nc
194     Xpos(:,it6) = X(:,it6) - X(:,1);
195 end
196 X=Xpos;
197
198 % Array Length
199 Lhat(:,loop) = X(:,nc);
200
201 %
202 % % Pressure and Stress and Elastic Stretch
203 %
204
205 sig = zeros(length(Tspan),N);
206 p = zeros(length(Tspan),N);
207 alpha = zeros(length(Tspan),N);
208 sighat = zeros(length(Tspan),nc);
209 phat = zeros(length(Tspan),nc);
210 alpht = zeros(length(Tspan),nc);
211
212 for i = 1:length(t)
213
214     [s, pe, aa, dg] = NHBdry_ODE_SG_AW_psig(t(i),x(i,:));
215
216     [sh,ph,ah,dgh] = NHBdry_contODE_SG_AW_psighat(T(i),X(i,:));
217
218     sig(i,:) = s;
219     p(i,:) = pe;
220     alpha(i,:) = aa;
221     dgldt(i,:) = dg;
222
223     sighat(i,:) = sh;
224     phat(i,:) = ph;
225     alpht(i,:) = ah;
226     dg1hatdt(i,:) = dgh;
227
228 end

```

```

229
230 % Discrete
231 minalpha(:,loop) = min(alpha,[],2);
232 maxp(:,loop) = max(p,[],2);
233 minp(:,loop) = min(p,[],2);
234 maxsig(:,loop) = max(sig,[],2);
235 minsig(:,loop) = min(sig,[],2);
236
237 % Continuum
238 minalphahat(:,loop) = min(alphat,[],2);
239 maxphat(:,loop) = max(phat,[],2);
240 minphat(:,loop) = min(phat,[],2);
241 maxsighat(:,loop) = max(sighat,[],2);
242 minsighat(:,loop) = min(sighat,[],2);
243
244 %
245 % % Save data for each simulation
246 %
247 save(['K' num2str(K) 'eta' num2str(eta) '_SGD_D_x.dat'],'x')
248 save(['K' num2str(K) 'eta' num2str(eta) '_SGC_C_x.dat'],'X')
249 save(['K' num2str(K) 'eta' num2str(eta) '_SGD_D_alph.dat'],'alpha')
250 save(['K' num2str(K) 'eta' num2str(eta) '_SGC_C_alph.dat'],'alphat')
251 save(['K' num2str(K) 'eta' num2str(eta) '_SGD_D_sig.dat'],'sig')
252 save(['K' num2str(K) 'eta' num2str(eta) '_SGC_C_sig.dat'],'sighat')
253 save(['K' num2str(K) 'eta' num2str(eta) '_SGD_D_p.dat'],'p')
254 save(['K' num2str(K) 'eta' num2str(eta) '_SGC_C_p.dat'],'phat')
255 save(['K' num2str(K) 'eta' num2str(eta) '_SGD_D_t.dat'],'t')
256 save(['K' num2str(K) 'eta' num2str(eta) '_SGC_C_T.dat'],'T')
257
258 % keep track of how many simulations have been completed & saved
259 disp(['Sim ' num2str(loop) ' of ' num2str(param) ' completed'])
260
261 end
262
263 %
264 % % Save Parameter Data
265 %
266 save('D_SG_Ks.dat','Ks')
267 save('D_SG_etas.dat','etas')
268 save('D_SG_MaxP.dat','maxp')
269 save('C_SG_MaxP.dat','maxphat')

```

```

270 save('D_SG_MinP.dat','minp')
271 save('C_SG_MinP.dat','minphat')
272 save('D_SG_MinAlpha.dat','minalpha')
273 save('C_SG_MinAlpha.dat','minalphahat')
274 save('D_SG_MaxSig.dat','maxsig')
275 save('C_SG_MaxSig.dat','maxsighat')
276 save('D_SG_MinSig.dat','minsig')
277 save('C_SG_MinSig.dat','minsighat')
278 save('D_SG_Maxg1.dat','maxg1')
279 save('C_SG_Maxg1.dat','maxg1hat')
280 save('D_SG_Ming1.dat','ming1')
281 save('C_SG_Ming1.dat','ming1hat')
282 save('D_SG_L.dat','L')
283 save('C_SG_Lhat.dat','Lhat')
284
285 toc
286
287 %% IN SCRIPT FUNCTIONS
288
289 %% Discrete ODE
290
291 function dudt = NHBdry_ODE_SG_AW(~,u)
292
293 % Define growth
294 growth1 = u(N+2:2*N+1);
295 % Define boundary locs
296 xb = u(1:N+1);
297
298 % % Cell stretches
299 stretch = (xb(2:N+1)-xb(1:N));
300 alph = (stretch./growth1);
301 % Cell width (incompressibility constraint)
302 growth2 = 1;
303 Width = growth2*gam0./alph;
304
305 % % Define dgdt
306 fg1 = 1/2*(...
307     1 + tanh(sig0*(...
308     mu*(alph.^2 - alph.^(-2)) ...
309     + eta*(1 + alph.^(-2)).*u(2*N+2:3*N+1) ...
310     ))...

```

```

311     );
312
313     % % define dxdt
314     % Shared boundary width
315     Wforce=1/2*(Width(1:N-1)+Width(2:N));
316     % Initialise Force Vector for dxbdt
317     fxb = zeros(length(xb),1);
318     % Force balance at boundaries
319     fxb(2:N) = -Wforce.*(mu*(alph(1:N-1).^2 - alph(1:N-1).^(-2))...
320               - mu*(alph(2:N).^2 - alph(2:N).^(-2))...
321               + eta*(...
322               + u(2*N+2:3*N).*( 1 + alph(1:N-1).^(-2) ) ...
323               - u(2*N+3:3*N+1).*( 1 + alph(2:N).^(-2) ) ...
324               )...
325     );
326
327     % Free boundary (for fixed boundary, comment out)
328     fxb(N+1) = -Width(N)*(...
329               mu*(alph((N))^2 - alph((N))^(-2))...
330               + eta*( 1+alph(N).^(-2) ) * u(3*N+1) ...
331               );
332
333     % New force for COM formulation
334     fs = zeros(N+1,1);
335     fs(2:N+1) = fxb(1:N)+fxb(2:N+1);
336
337     % Mass matrix
338     % for kappa=K ::Mxb(q,q)=Mxb(q,q-1) = K
339     % for kappa=K*A ::Mxb(q,q)=Mxb(q,q-1)=K*growth1(q-1)*growth2
340     Mxb = eye(N+1,N+1);
341     for q = 2:N+1
342         Mxb(q,q) = K*growth1(q-1)*growth2;
343         Mxb(q,q-1) = K*growth1(q-1)*growth2;
344     end
345
346     % define dxdt
347     dxdt = Mxb\fs;
348
349     % % Define relation for d(alpha)/dt, g1, x
350     falpht = u(2*N+2:3*N+1) ...
351             - growth1.^(-1).*((fxb(2:N+1)-fxb(1:N))) ...

```

```

352     + alph./growth1.*fg1;
353
354 % Define full dudt
355 dudt = zeros(length(u),1);
356 dudt(1:N+1) = dxdt;
357 dudt(N+2:2*N+1) = fg1;
358 dudt(2*N+2:3*N+1) = falpht;
359
360 end
361
362
363 %% Continuum PDE
364
365 function dUdT = NHBdry_contODE_SG_AW(~,U)
366
367 % Define growth
368 gro1h = U(nc+1:2*nc);
369 gro2h= 1;
370 % Define boundary locs
371 xbhat = U(1:nc);
372
373 % Spatial derivative stencils
374 % x
375 dxbhatdx = zeros(nc,1);
376 dxbhatdx(2:nc-1) = (xbhat(3:nc) - xbhat(1:nc-2))/2/dX;
377 dxbhatdx(1) = (-3*xbhat(1) + 4*xbhat(2) - xbhat(3))/2/dX;
378 dxbhatdx(nc) = (3*xbhat(nc) - 4*xbhat(nc-1) + xbhat(nc-2))/2/dX;
379
380 % alpha
381 alphht = dxbhatdx./gro1h;
382
383 dalphhtdx = zeros(nc,1);
384 dalphhtdx(2:nc-1) = (alphht(3:nc) - alphht(1:nc-2))/2/dX;
385 dalphhtdx(1) = (-3*alphht(1) + 4*alphht(2) - alphht(3))/2/dX;
386 dalphhtdx(nc) = (3*alphht(nc) - 4*alphht(nc-1) + alphht(nc-2))/2/dX;
387
388 dalphhtdtdx = zeros(nc,1);
389 dalphhtdtdx(2:nc-1) = (U(2*nc+3:3*nc) - U(2*nc+1:3*nc-2))/2/dX;
390 dalphhtdtdx(1) = (-3*U(2*nc+1) + 4*U(2*nc+2) - U(2*nc+3))/2/dX;
391 dalphhtdtdx(nc) = (3*U(3*nc) - 4*U(3*nc-1) + U(3*nc-2))/2/dX;
392

```

```

393 % % Initialise Force Vector for dgldt
394 fglhat = 1/2*(...
395     1 + tanh(sig0*(...
396     mu*(alphht.^2 - alphht.^(-2)) ...
397     + eta*(1 + alphht.^(-2)).*U(2*nc+1:3*nc) ...
398     ))...
399 );
400
401 % % Initialise Force Vector for dxbdt
402 fxbhat = zeros(length(xbhat),1);
403 % Force balance at boundaries
404 fxbhat(2:nc-1) = gro2h*gam0./alphht(2:nc-1).*...
405     ( 2*mu*( alphht(3:nc) - alphht(1:nc-2))/dX ) ...
406     .*( alphht(2:nc-1) + alphht(2:nc-1).^(-3) ) ...
407     + eta*((1 + alphht(2:nc-1).^(-2)).*...
408     dalphhtdtdx(2:nc-1) - 2*alphht(2:nc-1).^(-3)...
409     .*dalphhtdx(2:nc-1).*U(2*nc+2:3*nc-1) ) );
410 % Free boundary (for fixed boundary, comment out)
411 fxbhat(nc) = -gam0*gro2h/alphht(nc)*...
412     (mu*(alphht(nc)^2 - alphht(nc).^(-2))...
413     + eta*( (1+alphht(nc).^(-2))*U(3*nc) ) )/K;
414 % for kappa=K :: fxbhat = fxbhat/K;
415 % for kappa=K*A :: fxbhat = fxbhat/K./gro1h(2:nc-1)/gro2h;
416 fxbhat = fxbhat/K./gro1h/gro2h;
417
418 % Alg constraint for d(alpha)/dt
419 fahat = zeros(nc,1);
420 fahat(2:nc-1) = U(2*nc+2:3*nc-1) - 1/2/dX*( fxbhat(3:nc) ...
421     - fxbhat(1:nc-2) ) ./gro1h(2:nc-1) ...
422     + gro1h(2:nc-1).^(-1).*fglhat(2:nc-1).*alphht(2:nc-1);
423 fahat(1) = U(2*nc+1) ...
424     - 1/2/dX*( -3*fxbhat(1)+4*fxbhat(2)-fxbhat(3) ) / ...
425     gro1h(1)+ gro1h(1).^(-1).*fglhat(1).*alphht(1);
426 fahat(nc) = U(3*nc) ...
427     - 1/2/dX*( 3*fxbhat(nc)-4*fxbhat(nc-1)+fxbhat(nc-2) ) / ...
428     gro1h(nc)+ gro1h(nc).^(-1).*fglhat(nc).*alphht(nc);
429
430 % % Next define full dudt
431 dUdT = zeros(length(U),1);
432 dUdT(1:nc) = fxbhat;
433 dUdT(nc+1:2*nc) = fglhat;

```

```

434 dUdT(2*nc+1:3*nc) = fahat;
435
436 end
437
438
439 %% Discrete Pressure, Stress, Stretch and Growth Rate
440
441 function [st, pr, al, fg1] = NHBdry_ODE_SG_AW_psig(~,u)
442
443 % Define growth
444 growth1 = u(N+2:2*N+1);
445 % Define boundary locs
446 xb = u(1:N+1);
447
448 %% Cell stretches
449 stretch = (xb(2:N+1)-xb(1:N));
450 al = (stretch./growth1);
451
452
453 st = mu*(al.^2 - al.^(-2)) ...
454     + eta*(1 + al.^(-2)).*u(2*N+2:3*N+1);
455
456 pr = mu*al.^(-2) + eta*al.^(-2).*u(2*N+2:3*N+1);
457
458 fg1 = 1/2*(...
459     1 + tanh(sig0*(...
460     mu*(al.^2 - al.^(-2)) ...
461     + eta*(1 + al.^(-2)).*u(2*N+2:3*N+1) ...
462     ))...
463     );
464
465
466 end
467
468
469 %% Continuum Pressure, Stress, Stretch and Growth Rate
470
471 function [sth, prh, alh, fg1h] = NHBdry_contODE_SG_AW_psighat(~,U)
472
473 % Define growth
474 growth1hat = U(nc+1:2*nc);

```

```

475 % Define boundary locs
476 xbhat = U(1:nc);
477
478 % First Derivative
479 % x
480 dxbhatdx = zeros(nc,1);
481 dxbhatdx(2:nc-1) = (xbhat(3:nc) - xbhat(1:nc-2))/2/dX;
482 dxbhatdx(1) = (-3*xbhat(1) + 4*xbhat(2) - xbhat(3))/2/dX;
483 dxbhatdx(nc) = (3*xbhat(nc) - 4*xbhat(nc-1) + xbhat(nc-2))/2/dX;
484
485 % alpha
486 alh = dxbhatdx./growth1hat;
487
488 sth = mu*(alh.^2 - alh.^(-2)) ...
489       + eta*(1 + alh.^(-2)).*U(2*nc+1:3*nc);
490
491 prh = mu*(alh.^(-2)) + eta*alh.^(-2).*U(2*nc+1:3*nc);
492
493 fg1h = 1/2*(...
494         1 + ...
495         tanh(sig0*(...
496         mu*(alh.^2 - alh.^(-2)) ...
497         + eta*(1 + alh.^(-2)).*U(2*nc+1:3*nc) ...
498         ))...
499       );
500
501
502 end
503
504 %% Discrete Initial Condition for Alpha
505
506 function dudt = ICdisc(u)
507
508 % Define growth
509 growth1 = g0;
510 % Define boundary locs
511 xb =x0;
512
513 % % Cell stretches
514 stretch = (xb(2:N+1)-xb(1:N));
515 alph = (stretch./growth1);

```

```

516 % Cell width (incompressibility constraint)
517 growth2 = 1;
518 Width = growth2*gam0./alph;
519
520 % % Define dgdt
521 fg1 = 1/2*(...
522     1 + tanh(sig0*(...
523     mu*(alph.^2 - alph.^(-2)) ...
524     + eta*(1 + alph.^(-2)).*u ...
525     ))...
526 );
527
528 % % define dxdt
529 % Shared boundary width
530 Wforce=1/2*(Width(1:N-1)+Width(2:N));
531 % Initialise Force Vector for dxbdt
532 fxb = zeros(length(xb),1);
533 % Force balance at boundaries
534 fxb(2:N) = -Wforce.*(mu*(alph(1:N-1).^2 - alph(1:N-1).^(-2))...
535     - mu*(alph(2:N).^2 - alph(2:N).^(-2))...
536     + eta*(...
537     + u(1:N-1).*( 1 + alph(1:N-1).^(-2) ) ...
538     - u(2:N).*( 1 + alph(2:N).^(-2) ) ...
539     )...
540 );
541
542 % Free boundary (for fixed boundary, comment out)
543 fxb(N+1) = -Width(N)*(...
544     mu*(alph((N))^2 - alph((N))^(-2))...
545     + eta*( 1+alph(N)^(-2) ) *u(N);
546
547 % can use kappa = K for initial condition
548 fxb=fxb'/K;
549
550 % % Define relation for d(alpha)/dt, g1, x
551 falpht = u ...
552     - growth1.^(-1).*((fxb(2:N+1)-fxb(1:N)) ...
553     + alph./growth1.*fg1;
554
555 % Next define dudt
556 dudt = falpht;

```

```

557
558 end
559
560
561 %% Continuum Initial Condition for Alpha
562
563 function dUdT = ICcont(U)
564
565 % Define growth
566 gro1h = G0;
567 gro2h = 1;
568 % Define boundary locs
569 xbhat = X0;
570
571 % First Derivative
572 % x
573 dxbhtdx = zeros(nc,1)';
574 dxbhtdx(2:nc-1) = (xbhat(3:nc)-xbhat(1:nc-2))/2/dX;
575 dxbhtdx(1) = (-3*xbhat(1)+4*xbhat(2)-xbhat(3))/2/dX;
576 dxbhtdx(nc) = (3*xbhat(nc)-4*xbhat(nc-1)+xbhat(nc-2))/2/dX;
577
578 % alpha
579 alphht = dxbhtdx./gro1h;
580 dalphhtdx = zeros(nc,1)';
581 dalphhtdx(2:nc-1) = (alphht(3:nc)-alphht(1:nc-2))/2/dX;
582 dalphhtdx(1) = (-3*alphht(1)+4*alphht(2)-alphht(3))/2/dX;
583 dalphhtdx(nc) = (3*alphht(nc)-4*alphht(nc-1)+alphht(nc-2))/2/dX;
584
585 % dalpha/dt
586 dalphhtdtdx = zeros(nc,1)';
587 dalphhtdtdx(2:nc-1) = (U(3:nc) - U(1:nc-2))/2/dX;
588 dalphhtdtdx(1) = (-3*U(1) + 4*U(2) - U(3))/2/dX;
589 dalphhtdtdx(nc) = (3*U(nc) - 4*U(nc-1) + U(nc-2))/2/dX;
590
591 %% Initialise Force Vector for dglDt
592 fg1hat = 1/2*(...
593     1 + tanh(sig0*(...
594     mu*(alphht.^2 - alphht.^(-2)) ...
595     + eta*(1 + alphht.^(-2)).*U ...
596     ))...
597 );

```

```

598
599 % % Initialise Force Vector for dxbdT
600 fxbhat = zeros(length(xbhat),1);
601 % Force balance at boundaries
602 fxbhat(2:nc-1) = gro2h*gam0./alphht(2:nc-1).*...
603     ( 2*mu*( alphht(3:nc) - alphht(1:nc-2))/2/dX ) ...
604     .*( alphht(2:nc-1) + alphht(2:nc-1).^(-3) ) ...
605     + eta*(...
606     (1 + alphht(2:nc-1).^(-2)).* dalphhtdt dx(2:nc-1) ...
607     - 2*alphht(2:nc-1).^(-3).*dalphht dx(2:nc-1).*U(2:nc-1) ...
608     ) );
609 % Free boundary (for fixed boundary, comment out)
610 fxbhat(nc) = -gam0*gro2h/alphht(nc)*...
611     (mu*(alphht(nc)^2 - alphht(nc)^(-2))...
612     + eta*( (1+alphht(nc)^(-2))*U(nc) ) )/K;
613
614 % can use kappa=K for initial condition;
615 fxbhat = fxbhat'/K;
616
617 % Alg constraint for d(alpha)/dt
618 fahat = zeros(nc,1)';
619 fahat(2:nc-1) = U(2:nc-1) - 1/2/dX*(fxbhat(3:nc) ...
620     - fxbhat(1:nc-2))./gro1h(2:nc-1)...
621     + gro1h(2:nc-1).^(-2).*fg1hat(2:nc-1).*dxbdT dx(2:nc-1);
622 fahat(1) = U(1) ...
623     - 1/2/dX*( -3*fxbhat(1)+4*fxbhat(2)-fxbhat(3) )/...
624     gro1h(1)+ gro1h(1)^(-2)*fg1hat(1)*dxbdT dx(1);
625 fahat(nc) = U(nc) ...
626     - 1/2/dX*( 3*fxbhat(nc)-4*fxbhat(nc-1)+fxbhat(nc-2) )/...
627     gro1h(nc)+ gro1h(nc)^(-2)*fg1hat(nc)*dxbdT dx(nc);
628
629 % Next define dudt
630 dUdT = fahat;
631
632 end
633
634 end

```

Bibliography

- [1] M. Banaji et al. A physiological model of cerebral blood flow control. *Mathematical Biosciences*, 194(2):125–73, 2005.
- [2] W. Elliott et al. In vitro model of physiological and pathological blood flow with application to investigations of vascular cell remodeling. *Journal of Visualized Experiments*, 3:e53224, 2015.
- [3] M. U. Qureshi et al. Numerical simulation of blood flow and pressure drop in the pulmonary arterial and venous circulation. *Biomechanics and Modeling in Mechanobiology*, 13(5):1137–1154, 2014.
- [4] A. M. Zöllner et al. Stretching skeletal muscle: Chronic muscle lengthening through sarcomerogenesis. *PLoS ONE*, 7(10):e45661, 2012.
- [5] David Boal. *Mechanics of the Cell*. Cambridge University Press, 2002.
- [6] B. Alberts et al. *Essential Cell Biology (Second Edition)*. Garland Science, 2004.
- [7] D. Latchman. *Basic Molecular and Cell Biology*. B.M.J. Publishing Group, 1997.
- [8] J. Maxwell. *A treatise on electricity and magnetism*. MacMillan and Co., Oxford at the Clarendon Press, London, 1873.
- [9] A. Einstein. Eine neue bestimmung der moleküldimensionen. *Annals of Physics*, 324(2):289–306, 1906.
- [10] B. D. Wood and S. Whitaker. Multi-species diffusion and reaction in biofilms and cellular media. *Chemical Engineering Science*, 55:3397–3418, 2000.
- [11] Y. Davit et al. Hydrodynamic dispersion within porous biofilms. *Physical Review E*, 87:012718, 2013.
- [12] S. Lorthois and F. Cassot. Fractal analysis of vascular networks: Insights from morphogenesis. *Journal of Theoretical Biology*, 262(4):614–633, 2010.

- [13] J. Weickenmeier and M. Jabareen. Elastic-viscoplastic modeling of soft biological tissues using a mixed finite element formulation based on the relative deformation gradient. *International Journal for Numerical Methods in Biomedical Engineering*, 30:1238–1262, 2014.
- [14] S. Göktepe et al. A multiscale model for eccentric and concentric cardiac growth through sarcomerogenesis. *Journal of Theoretical Biology*, 265:433–442, 2010.
- [15] A. Menzel and E. Kuhl. Frontiers in growth and remodeling. *Mechanics Research Communications*, 42:1–14, 2012.
- [16] J. D. Humphrey. *Cardiovascular tissue mechanics: Cells, tissues and organs*. Springer, 2002.
- [17] L. A. Taber. Biomechanics of growth, remodelling and morphogenesis. *Applied Mechanics Reviews*, 48:487–545, 1995.
- [18] G. Krishnamurthy et al. Material properties of the ovine mitral valve anterior leaflet in vivo from inverse finite element analysis. *American Journal of Physiology - Heart and Circulatory Physiology*, 295:H1141–H1149, 2008.
- [19] V. Alastrue et al. Modelling adaptative volumetric finite growth in patient-specific residually stressed arteries. *Journal of Biomechanics*, 41(1773-1781), 2009.
- [20] V. Alastrue et al. Anisotropic microsphere-based finite elasticity applied to blood vessel modelling. *Journal of the Mechanics and Physics of Solids*, 57:178–203, 2009.
- [21] L. A. Taber and J. D. Humphrey. Stress-modulated growth, residual stress and vascular heterogeneity. *Journal of Biomechanical Engineering*, 123:528–535, 2001.
- [22] N. Famaey et al. A three-constituent damage model for arterial clamping in computer-assisted surgery. *Biomechanics and Modeling in Mechanobiology*, 2012.
- [23] S. I. Murtada, M. Kroon, and G. A. Holzapfel. A calcium-driven mechanochemical model for prediction of force generation in smooth muscle. *Biomechanics and Modeling in Mechanobiology*, 9:749–762, 2010.
- [24] Y. C. Fung. *Biomechanics: Mechanical Properties of Living Tissues*. Springer-Verlag, New York, 2 edition, 1993.
- [25] J. E. Bischoff et al. A rheological network model for the continuum anisotropic and viscoelastic behaviour of soft tissue. *Biomechanics and Modeling in Mechanobiology*, 3:56–65, 2004.

- [26] J. A. Fozard et al. Continuum approximations of individual-based models for epithelial monolayers. *Mathematical Medicine and Biology*, 21(1):39–74, 2010.
- [27] R. W. Ogden. *Non-Linear Elastic Deformations*. Ellis Horwood Ltd., 1984.
- [28] M. Chaplain A. R. A. Anderson and K. Rejniak. *A hybrid multiscale model of tumour invasion: evolution and the microenvironment, Ch I.1*. Basel: Birkhäuser, 2007.
- [29] Y. Lanir and Y. C. Fung. Two-dimensional mechanical properties of rabbit skin - ii: experimental results. *Journal of Biomechanics*, 7:171–182, 1974.
- [30] P. Tong and Y-C. Fung. The stress-strain relationship for the skin. *Journal of Biomechanics*, 9:649–657, 1976.
- [31] W. Li. Modelling methods for in vitro biomechanical properties of the skin: a review. *Biomedical Engineering Letters*, 5:241–250, 2015.
- [32] J. W. Y. Jor et al. Computational and experimental characterization of skin mechanics: identifying current challenges and future directions. *Wiley Interdisciplinary Reviews: Systems Biology and Medicine*, 5:539–556, 2013.
- [33] Y. C. Fung. Microrheology and constitutive equation of soft tissue. *Biorheology*, 26(1-2):261–270, 1988.
- [34] J. D. Humphrey. Continuum biomechanics of soft biological tissues. *Proceedings of the Royal Society A*, 459:3–46, 2002.
- [35] Y. Lanir. Multi-scale structural modeling of soft tissues mechanics and mechanobiology. *Journal of Elasticity*, pages 1–42, 2017.
- [36] F. J. Vermolen et al. In vitro wound healing: experimentally based phenomenological modelling. *Advanced Engineering Materials*, 14:76–88, 2012.
- [37] J. A. Sherratt and J. C. Dallon. Theoretical models of wound healing: past successes and future challenges. *Comptes Rendus Biologies*, 325:557–564, 2002.
- [38] G. A. Holzapfel, T. C. Gasser, and R. W. Ogden. A new constitutive framework for arterial wall mechanics and a comparative study of material models. *Journal of Elasticity*, 61:1–48, 2000.
- [39] R. W. Ogden. Large deformation isotropic elasticity - on the correlation of theory and experiment for incompressible rubberlike solids. *Proceedings of the Royal Society of London. Series A: Mathematical and Physical Sciences*, 326(1567):565–584, 1972.

- [40] C. J. Chuong and Y-C. Fung. Three-dimensional stress distribution in arteries. *Journal of Biomechanical Engineering*, 105:268–274, 1983.
- [41] G. A. Holzapfel, T. C. Gasser, and M. Stadler. A structural model for the viscoelastic behaviour of arterial walls: Continuum formulation and finite element analysis. *European Journal of Mechanics A: Solids*, 21:441–463, 2002.
- [42] P. N. Watton, N. A. Hill, and M. Heil. A mathematical model for the growth of the abdominal aortic aneurysm. *Biomechanics and Modeling in Mechanobiology*, 3:98–113, 2004.
- [43] Y. Miyahara et al. Monolayered mesenchymal stem cells repair scarred myocardium after myocardial infarction. *Nature Medicine*, 12:459–465, 2006.
- [44] A. V. Hill. The heat of shortening and the dynamic constants of muscle. *Proceedings of the Royal Society of London Series B: Biological Sciences*, 126(843):136–195, 1938.
- [45] A. V. Hill. The abrupt transition from rest to activity in muscle. *Proceedings of the Royal Society of London Series B: Biological Sciences*, 136:399–420, 1949.
- [46] S. A. Niederer, K. S. Campbell, and S. G. Campbell. A short history of the development of mathematical models of cardiac mechanics. *Journal of Molecular and Cellular Cardiology*, 127:11–19, 2019.
- [47] T. Arts et al. A model of the mechanics of the left ventricle. *Annals of Biomedical Engineering*, 7(3):299–318, 1979.
- [48] J. M. Guccione et al. Passive material properties of intact ventricular myocardium determined from a cylindrical model. *Journal of Biomechanical Engineering*, 113(1):42–55, 1991.
- [49] P. J. Hunter et al. Modelling the mechanical properties of cardiac muscle. *Progress in Biophysics and Molecular Biology*, 69(289-331), 1998.
- [50] J. D. Humphrey and F. C. Yin. Constitutive relations and finite deformations of passive cardiac tissue ii: Stress analysis in the left ventricle. *Circulation Research*, 65:805–817, 1989.
- [51] G. A. Holzapfel and R. W. Ogden. Constitutive modelling of passive myocardium: a structurally based framework for material characterization. *Philosophical Transactions of the Royal Society A*, 367:3445–3475, 2009.
- [52] S. A. Niederer, P. J. Hunter, and N. P. Smith. A quantitative analysis of cardiac myocyte relaxation: A simulation study. *Biophysical Journal*, 90:1697–1722, 2006.

- [53] L. Cai et al. A mathematical model for active contraction in healthy and failing myocytes and left ventricles. *PLoS ONE*, 12(4), 2017.
- [54] V. Leeuwen et al. An integrative computational model for intestinal tissue renewal. *Cell Proliferation*, 45:617–636, 2009.
- [55] I. Ramis-Conde, M. A. J. Chaplain, and A. R. A. Anderson. Mathematical modelling of cancer cell invasion of tissue. *Mathematical and Computer Modelling*, 47:533–545, 2008.
- [56] A. G. Fletcher et al. Vertex models of epithelial morphogenesis. *Biophysical Journal*, 106(11):2291–2304, 2014.
- [57] J. Moreira and A. Deutsch. Cellular automaton models of tumor development: a critical review. *Advances in Complex Systems*, 5:247–67, 2002.
- [58] W. Düchting and T. Vogelsaenger. Recent progress in modelling and simulation of three-dimensional tumour growth and treatment. *BioSystems*, 18:79–91, 1985.
- [59] A-S. Qi et al. A cellular automaton model of cancerous growth. *Journal of Theoretical Biology*, 161:1–12, 1993.
- [60] F. Graner and J. A. Glazier. Simulation of biological cell sorting using a two-dimensional extended potts model. *Physical Review Letters*, 69:2013–2016, 1992.
- [61] P. Pathmanathan et al. A computational study of discrete mechanical tissue models. *Physical Biology*, 6(3):036001, 2009.
- [62] E. Pallson. A three-dimensional model of cell movement in multicellular systems. *Future Generation Computer Systems*, 17:835–852, 2001.
- [63] R. Farhadifar et al. The influence of cell mechanics, cell-cell interactions and proliferation on epithelial packing. *Current Biology*, 17:2095–2104, 2007.
- [64] M. Marder. Soap-bubble growth. *Physical Review A*, 36:438–440, 1987.
- [65] T. Okuzono and K. Kawasaki. Intermittent flow behaviour of random foams: a computer experiment on foam rheology. *Physical Review E Statistical physics, plasmas, fluids, and related interdisciplinary topics*, 51:1246–1253, 1995.
- [66] K. Kawasaki et al. Vertex models for two-dimensional grain growth. *Philosophical Magazine B*, 60(399-421), 1989.
- [67] P. J. Murray et al. From a discrete to a continuum model of cell dynamics in one dimension. *Physical Review E*, 80:031912, 2009.

- [68] P. J. Murray et al. Classifying general nonlinear force laws in cell-based models via the continuum limit. *Physical Review E*, 85:021921, 2012.
- [69] C. Raufaste et al. Discrete rearranging disordered patterns: prediction of elastic and plastic behaviour, and application to two-dimensional foams. *Physical Review E*, 81(3):031404, 2010.
- [70] H. Honda and G. Egnuchi. How much does the cell boundary contract in a monolayered cell sheet? *Journal of Theoretical Biology*, 84:575–588, 1980.
- [71] A. Nestor-Bergmann et al. Relating cell shape and mechanical stress in a spatially disordered epithelium using a vertex-based model. *Mathematical Medicine and Biology*, 35:1–27, 2018.
- [72] G. M. Odell et al. The mechanical basis of morphogenesis. i. epithelial folding and invagination. *Developmental Biology*, 85:446–462, 1981.
- [73] H. H. Chen and G. W. Brodland. Cell-level finite-element studies of viscous cells in planar aggregates. *Journal of Biomechanical Engineering*, 122:394–401, 2000.
- [74] F. A. Meineke et al. Cell migration and organization in the intestinal crypt using a lattice-free model. *Cell Proliferation*, 34:253–266, 2001.
- [75] T. Nagai and H. Honda. A dynamic cell model for the formation of epithelial tissues. *Philosophical Magazine B*, 81(7):699–719, 2001.
- [76] D. C. Walker et al. Agent-based computational modeling of wounded epithelial cell monolayers. *IEEE Transactions on Nanobioscience*, 3:153–163, 2004.
- [77] P. Pathmanathan et al. Computational modelling of cardiac electro-physiology: explanation of the variability of results from different numerical solvers. *International Journal for Numerical Methods in Biomedical Engineering*, 28(8):890–903, 2012.
- [78] J. Cooper et al. Considerations for the use of cellular electrophysiology models within cardiac tissue simulations. *Progress in Biophysics and Molecular Biology*, 107(1):74–80, 2011.
- [79] D. Drasdo et al. On the role of physics in the growth and pattern formation of multicellular systems: What can we learn from individual-cell based models? *Journal of Statistical Physics*, 128:287–345, 2007.
- [80] J. Galle et al. Individual cell-based models of the spatial-temporal organization of multicellular systems - achievements and limitations. *International Society for Analytical Cytology: Cytometry Part A*, 69:A:704–710, 2006.

- [81] Y. Davit et al. Homogenization via formal multiscale asymptotics and volume averaging: How do the two techniques compare? *Advances in Water Resources*, 62:178–206, 2013.
- [82] R. D. O’Dea and J. R. King. Continuum limits of pattern formation in hexagonal-cell monolayers. *Journal of Mathematical Biology*, 64(3):579–610, 2012.
- [83] R. J. Shipley and S. J. Chapman. Multiscale modelling of fluid and drug transport in vascular tumours. *Bulletin of Mathematical Medicine and Biology*, 72(6):1464–1491, 2010.
- [84] Geir Hasle, Knut-Andreas Lie, and Ewald Quack, editors. *Geometric Modelling, Numerical Simulation and Optimisation: Applied Mathematics at SINTEF*. Springer Science and Business Media, 2007.
- [85] J. A. Oliveira et al. Asymptotic homogenisation in linear elasticity. part ii: Finite element procedures and multiscale applications. *Computational Materials Science*, 45:1081–1096, 2009.
- [86] D. Moulton et al. Multilevel upscaling in heterogeneous porous media. *Research Highlights LA-UR 99-4754, Centre for Nonlinear Studies, LA National Lab*, 1999.
- [87] N. S. Bakhvalov and G. Panasenko. *Homogenisation: Averaging Processes in Periodic Media: Mathematical Problems in the Mechanics of Composite Materials*. Springer Science and Business Media, 2012.
- [88] A. Gerisch, R. Penta, and J. Lang, editors. *Multiscale Models in Mechano and Tumor Biology*. Springer, Cham, 2017.
- [89] R. Penta et al. Can a continuous mineral foam explain the stiffening of aged bone tissue? a micromechanical approach to mineral fusion in musculoskeletal tissues. *Bioinspiration and Biomimetics*, 11(3), 2016.
- [90] H. Byrne and L. Preziosi. Modelling solid tumour growth using the theory of mixtures. *Mathematical Medicine and Biology*, 20:341–366, 2003.
- [91] G. E. Lang et al. Is the donnan effect sufficient to explain swelling in brain tissue slices? *Journal of the Royal Society Interface*, 11, 2014.
- [92] S. Whitaker. Diffusion and dispersion in porous media. *American Institute of Chemical Engineers Journal*, 13:420–427, 1967.
- [93] J. C. Slattery. Flow of viscoelastic fluids through porous media. *American Institute of Chemical Engineers Journal*, 13:1066–71, 1967.

- [94] B. D. Wood et al. Volume averaging for determining the effective dispersion tensor. *Water Resources Research*, 39(8), 2003.
- [95] S. Whitaker. *The Method of Volume Averaging*. Kluwer Academic Publishers, Dordrecht, The Netherlands, 1999.
- [96] R. R. Rosales. Discrete to continuum modelling. MIT Lecture Notes, 2001.
- [97] N. Bogoliubov and Y. Mitropolsky. *Asymptotic Methods in the Theory of Nonlinear Oscillations*. Gordon and Breach, New York, 1961.
- [98] J. Cole. Uniformly valid approximations for certain nonlinear differential equations. In S. Lefschetz J. P. La Salle, editor, *Proceedings of the 1961 international symposium on nonlinear differential equations and nonlinear mechanics*, pages 113–120, New York, 1963. Academic Press.
- [99] M. D. Kruskal and N. J. Zabusky. Stoboscopic-perturbation procedure for treating a class of nonlinear wave equations. *Journal of Mathematical Physics*, 5(2):231–244, 1964.
- [100] M. D. Kruskal and N. J. Zabusky. Interaction of “solitons” in a collisionless plasma and the recurrence of initial states. *Physical Review Letters*, 15:240–243, 1965.
- [101] A. Goriely et al. Elastic growth models. RUMMBA, University of Arizona, Tucson, 2008.
- [102] A. Goriely and D. Moulton. Morphoelasticity - a theory of elastic growth. Mathematical Institute, University of Oxford, 2011.
- [103] J. A. Sherratt and M. A. J. Chaplain. A new mathematical model for avascular tumour growth. *Journal of Mathematical Biology*, 43(291-312), 2001.
- [104] I-E. Lin and L. A. Taber. A model for stress-induced growth in the developing heart. *Journal of Biomechanical Engineering*, 117(3):343–349, 1955.
- [105] T. S. E. Eriksson et al. Modelling volumetric growth in a thick walled fibre reinforced artery. *Journal of the Mechanics and Physics of Solids*, 73:134–150, 2014.
- [106] D. Ambrosi and F. Mollica. On the mechanics of a growing tumor. *International Journal of Engineering Science*, 40:1297–1316, 2002.
- [107] E. K. Rodriguez et al. Stress-dependent finite growth in soft elastic tissue. *Journal of Biomechanics*, 27:455–467, 1994.
- [108] J. D. Humphrey. A constrained mixture model for growth and remodeling of soft tissues. *Mathematical Models and Methods in Applied Sciences*, 12(3):404–430, 2002.

- [109] G. A. Holzapfel and R. W. Ogden, editors. *Mechanics of Biological Tissue*, chapter Growth in soft biological tissue and residual stress development, pages 47–62. Springer, 2006.
- [110] S. M. Klisch et al. A theory of volumetric growth for compressible elastic biological materials. *Mathematics and Mechanics of Solids*, 6(6):551–575, 2001.
- [111] N. Kida and Y. Morishita. Continuum mechanical modeling of developing epithelial tissues with isotropic surface growth. *Finite Elements in Analysis and Design*, 144:49–60, 2018.
- [112] G. A. Ateshian et al. Continuum modeling of biological tissue growth by cell division, and alteration of intracellular osmolytes and extracellular fixed charge density. *Journal of Biomechanical Engineering*, 131(10):101001, 2009.
- [113] W. Freijtag et al. An increase in surface area is not required for cell division in early sea urchin development. *Developmental Biology*, 259(1):62–70, 2003.
- [114] J. D. Hywood et al. Modeling biological tissue growth: Discrete to continuum representations. *Physical Review E*, 88(3):032704, 2013.
- [115] R. D. O’Dea and J. R. King. The isolation of spatial patterning modes in a mathematical model of juxtacrine cell signalling. *Mathematical Medicine and Biology*, 30(2):95–113, 2011.
- [116] A. Goriely and M. Tabor. Biomechanical models of hyphal growth in actinomycetes. *Journal of Theoretical Biology*, 222(22):211–218, 2003.
- [117] M. Gracheva and H. Othmer. A continuum model of motility in ameboid cells. *Bulletin of Mathematical Biology*, 66:167–193, 2004.
- [118] G. A. Holzapfel, M. J. Unterberger, and R. W. Ogden. An affine continuum mechanical model for cross-linked f-actin networks with compliant linker proteins. *Journal of the Mechanical Behaviour of Biomedical Materials*, 38:78–90, 2014.
- [119] K. Miller. How to test very soft tissues in extension. *Journal of Biomechanics*, 34(5):651–657, 2001.
- [120] K. Miller. Method of testing very soft biological tissues in compression. *Journal of Biomechanics*, 38:153–158, 2005.
- [121] G. Schaller and M. Meyer-Hermann. Multicellular tumor spheroid in an off-lattice voronoi-delaunay cell model. *Physical Review E*, 71(5), 2005.

- [122] D. Drasdo, R. Kree, and J. S. McCaskill. Monte carlo approach to tissue-cell populations. *Physical Review E*, 52(6), 1995.
- [123] L. F. Shampine et al. Solving index-1 daes in matlab and simulink. *Society for Industrial and Applied Mathematics Review*, 41(3):538–552, 1999.
- [124] P. Howell, G. Kozyreff, and J. Ockendon. *Applied Solid Mechanics*. Cambridge University Press, 2008.
- [125] K. B. Gupta et al. Changes in passive mechanical stiffness of myocardial tissue with aneurysm formation. *Circulation*, 89(5):2315–26, 1994.
- [126] H. P. Greenspan. Models for the growth of a solid tumour by diffusion. *Studies in Applied Mathematics*, 51:317–340, 1972.
- [127] E. A. López-Guerra and S. D. Soares. Modeling viscoelasticity through spring–dashpot models in intermittent-contact atomic force microscopy. *Beilstein Journal of Nanotechnology*, 5:2149–2163, 2014.
- [128] H. M. Zhang et al. Modeling ramp-hold indentation measurements based on kelvin-voigt fractional derivative model. *Measurement Science and Technology*, 29(3), 2018.